FAILURE MECHANISMS IN PRESSURISED FIBRE WOUND TUBES

by

BRIAN SPENCER

A THESIS SUBMITTED TO THE
UNIVERSITY OF ASTON IN BIRMINGHAM
FOR THE DEGREE OF
DOCTOR OF PHILOSOPHY

JANUARY 1976

'Responsibility is a unique concept. It can only reside and inhere in a single individual. You may share it with others, but your portion is not diminished. You may delegate it, but it is still with you. You may disclaim it, but you cannot divest yourself of it. Even if you do not recognize it or admit its presence, you cannot escape it. If responsibility is rightfully yours, no evasion or ignorance, or passing the blame can shift the burden on someone else. Unless you can point your finger at the man who is responsible when something goes wrong, then you never had anyone really responsible.'

Admiral Hyman G. Rickover, July 23rd. 1963.

I certify that to the best of my knowledge no part of the work described in this thesis was done in collaboration, unless specifically so described, and that the work has not been submitted for any other award.

Brian Spencer

B. Spencer

December 1975.

Summary.

An investigation into the effects of artificially induced defects on the failure mechanisms of glass fibre reinforced plastic tubes has been carried out. A fracture mechanics approach was used in the analysis of the results. The failure pressures of the tubes were found to obey equations in existence for isotropic materials. The failure mechanisms of the combined tube and defect types are discussed. The mechanisms were found to vary according to these variations.

The values of Young's modulus and Poisson's ratio determined for the compliance analysis were compared to the predictions of two theories. This indicated that the theories were reasonable for the predictions of Young's modulus, but of little use for the prediction of Poisson's ratio. The defect sizes were too small to obtain an accurate compliance analysis to be compared to those of isotropic materials.

Nomenclature.

$\|A\|$	coefficient matrix
a	radius of circular plate
C	contiguity factor, or compliance where applicable
c	$\frac{1}{2}$ surface crack length, or critical where used as a subscript
D	inside diameter of thin walled tube
$\|D\|$	coefficient matrix
E	Young's modulus limited by subscript
F	load on circular plate
f	subscript fibre
G	shear modulus, limited by subscript, or elastic strain energy release rate, limited by subscript where applicable
H	subscript for hoop
h	thickness of a circular plate, or $\frac{1}{2}$ thickness of composite layer, where applicable
h_o	individual thickness of composite layer
K	fibre misalignment factor, or stress intensity factor limited by subscript
L	length of tube subjected to internal pressure
l	length of individual fibre
M	Young's modulus of matrix
$\|M\|$	coefficient matrix
m	subscript for matrix
P	pressure
P^*	critical pressure
R	inside radius of thin walled tube

S	constant included in the Folias correction factor = $0.49(12(1-v^2))^{\frac{1}{2}}$
T	subscript for transverse
t	tube wall thickness
v	volume fraction limited by subscript
W	width of tensile specimen
w	subscript for working stress
x	direction along axis of tube
y	hoop direction in tube
z	radial direction in tube
γ	Shear strain limited by subscript
δ	deflection in a circular plate
ε	strain limited by subscript
θ	angle of fibres in tube axis and direction subscript
θ_1	$\cos^2\theta$
θ_2	$\sin^2\theta$
θ_3	$\sin\theta\cos\theta$
ν	Poisson's ratio limited by subscript
σ	normal stress limited by subscript
σ^*_H	critical hoop stress
τ	shear stress limited by subscript

Acknowledgements.

My thanks are due to Professor W. Alexander for the provision of laboratory facilities and for financial support during the final year of the research work; to Mr. F. R. Wallis for providing access to his report; to Mr. M. Jones and I. M. I. Ltd. (Kynoch) for the provision of the tubes for testing, without which the work could not have been carried out; to Dr. R. Popley for his efforts in the construction of the tubes; to the technicians of the Department of Metallurgy for their industry and help; to the technicians of the Department of Mechanical Engineering Workshop; to the Science Research Council for their financial support during the first two years of the research work; to Miss. L. M. Morton for her help in the correction of errors; and ultimately to Dr. J. T. Barnby (Terry), my supervisor throughout this work, for his patience, understanding, guidance and, above all, friendship.

Contents

Chapter 1

Chapter 2

Chapter 3

Chapter 4

Chapter 5

Chapter 6

Chapter 1.

1. Introduction.

In recent years man has made many great steps forward in the fields of supersonic flight and manned space exploration. Complementing these advances has been the need for high strength/weight ratio and/or high modulus materials for structural members in the craft for these. Interest has been aroused in composite materials consisting of stiff fibres in a relatively soft and weak matrix. Work has been carried out to obtain a knowledge of the stiffening and strengthening mechanisms in such composites, but little is known about the fracture characteristics of many systems.

Difficulties are experienced, when manufacturing fibre reinforced materials, in obtaining a defect free composite. Defects, such as voids, fibre/fibre contact, inhomogeniety and debonding of the fibre/matrix interface, are not uncommon. Catastrophic failure of such composites will often be initiated at one, or more, of these defects. For homogenous and isotropic materials, such as many metals, failure stresses and critical sizes of defect can be predicted, with accuracy, from well tried and tested fracture mechanics approaches. Composite materials are, at best, orthotropic and often anisotropic and the application of linear elastic fracture mechanics to these systems has not been fully determined. Clearly there is a need to establish the response of these systems to this approach.

An important application of these materials is the filament wound, cylindrical pressure vessel. When a cylindrical pressure vessel, containing an axial defect, is subjected to internal pressure the combined effect of the hoop stress and the radial stress causes bulging of the mouth of the crack. This causes fracture to initiate at a lower hoop stress than the axial stress in a flat plate,with a similar defect, subjected to pure tension. For isotropic materials this has been rigourously analysed(1,2,3,28,29,30,31,32,33) and factors have been evaluated to correct for this bulging. It does not necessarily follow that these analyses will apply to the systems which are the subject of this work.

In this investigation a number of filament wound, glass fibre reinforced plastic tubes have been subjected to internal pressure. The tubes were tested with and without artificially produced, axial defects. Tubes of two different winding configurations were used. These were:

1) Helical ± 30° angle of wind and
2)50% helical ± 30° and ± 90° angle of wind.

Three depths of defect were investigated, each of five axial lengths.

It was found that, in general, the behaviour of the tubes agreed well with the analyses of the above workers. Interesting failure mechanisms for each tube system were observed and photographs of the history of the failures are presented. For the fracture mechanics analysis, Young's modulus and Poisson's ratio measurements had to be made. Comparisons of theoretical and observed measurements of these were drawn for two theories. Comparisons of two methods of compliance measurement for the different tube categories were also made.

Chapter 2.

2. Literature Survey.

2. 1. The properties and response of fibre reinforced composites.

2. 1. 1. Basic considerations of the strengthening mechanisms of fibre reinforced composites.

In recent years we have seen the advent of many new materials for use in aerospace applications where a high strength and /or modulus to weight ratio is essential. One such material is the fibre reinforced composite consisting mainly of two components - strong, stiff fibres in a relatively weak matrix, but containing voids and defects due manufacturing process. Clearly theories are needed which will predict composite strengths and physical properties accurately from the basic properties of matrix and fibre.

The simplest fibre composite consists of discontinuous fibres embedded in a resin matrix. The load is transferred to the fibres by means of shear stresses set up as the resin attempts to flow around the fibres. In the fibre the stress varies as shown in Fig. 1. The shear stresses are greatest at the ends of the fibre and are zero at the mid point. If the fibre is longer than the critical elastic aspect ratio $(l/d)_{crit}$ the tensile stress σ_y is constant along the length of the fibre. More rigourous solutions to the simple model illustrated in Fig. 1 have been given(5,6,7,8,9) amongst others (see Fig. 2.).

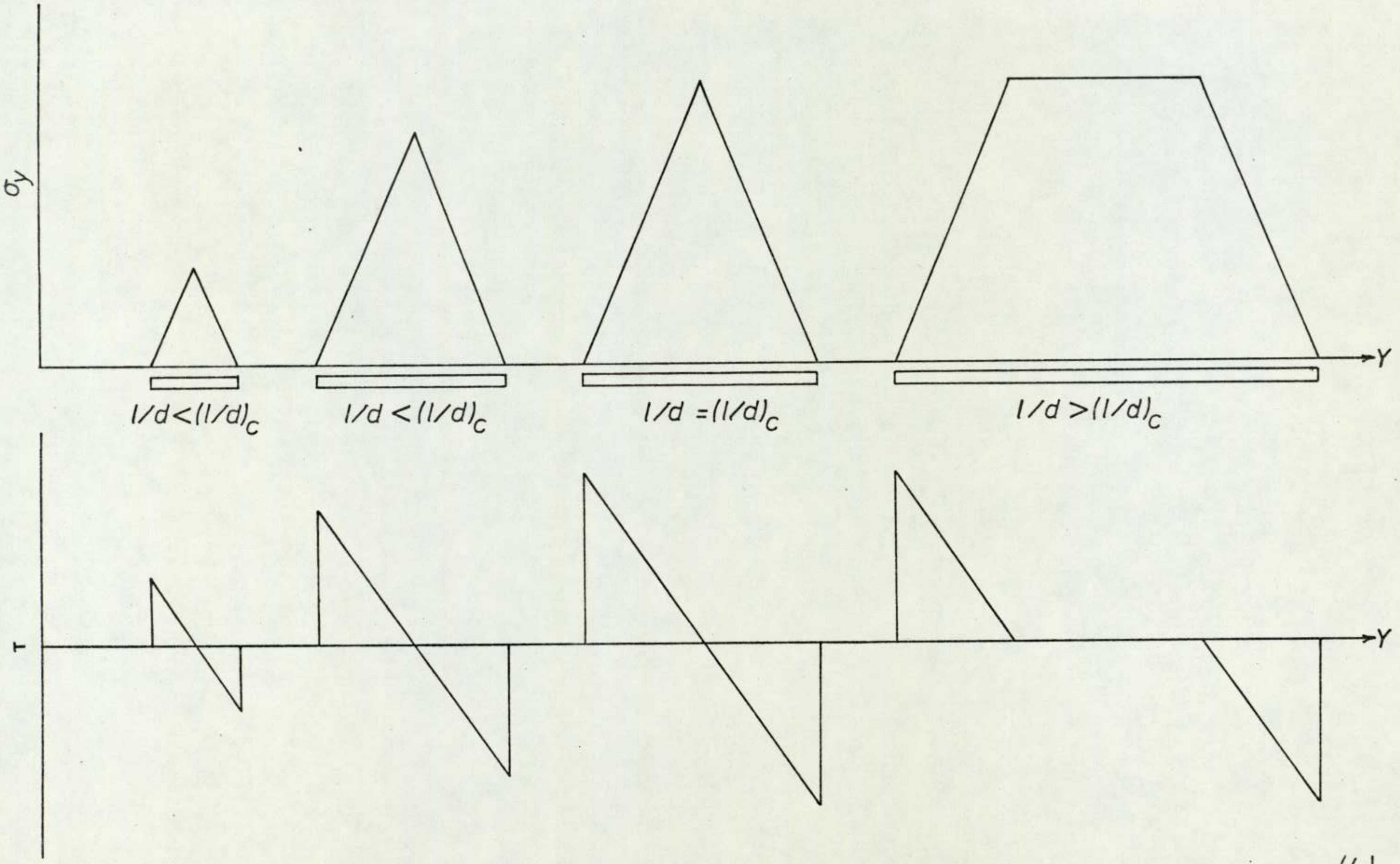

Fig. 1. Stress distribution and interfacial shear stress in discontinuous fibres (Schuster and Scala(4)).

As illustrated in Fig. 1 the longer the fibre the greater the load carrying capabilities of it and hence the better the properties of the composite. Also the presence of shear stresses at the ends of the fibres will favour crack initiation. Continuous fibres are therefore more desirable. For continuous fibres and elastic behaviour the nominal stress obeys the rule of mixtures:

$$\sigma = (E_f v_f + E_m(1 - v_f))$$

At higher stresses the matrix deforms plastically and:

$$\sigma = E_f v_f + (1 - v_f)\sigma_m(\varepsilon)$$

where $\sigma_m(\varepsilon)$ is the true flow strength of the matrix at strain Most continuous fibre composites usually contain some discontinuous fibres prior to fracture. These arise due to:

1) Fracture of fibres during fabrication,

2) Fracture of individual fibres during loading.

Thus the criteria for failure in discontinuous fibre composites can not be neglected since these are nearly always present and may effect the initial crack propogation.

The fibre models illustrated in Fig. 2 are useful for prediction of behaviour when the applied stress is parallel to the main fibre direction. Many applications exist when the applied stress is at an angle to the fibre direction. The most notable example of this is the filament wound component. Many theories are available for prediction of behaviour in this more complex case. Two of these are examined and discussed in 2. 1. 2.

H. L. Cox, 1952$^{(5)}$

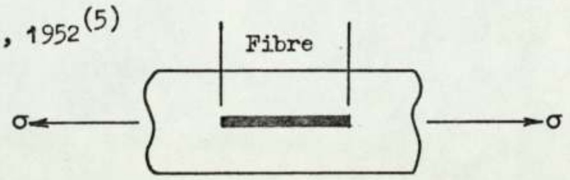

Elastic fibre completely bonded into an extensive elastic matrix. Results derived for two and three dimensions.

J. O. Outwater, 1956$^{(6)}$

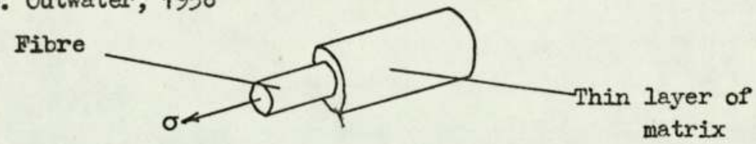

Assumes that the maximum interface shear stresses are a function of the interface pressure developed by the differential shrinkage of the matrix on to the fibre.

N. F. Dow, 1963$^{(7)}$

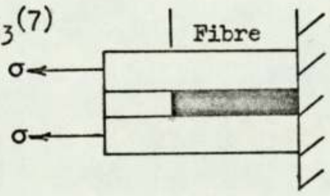

Considers cylindrical matrix with fully bonded elastic fibre. Implication is that straight lines remain straight after deformation and two or three dimensions can be analysed.

W. B. Rosen, 1964$^{(8)}$

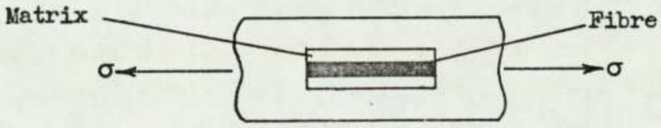

Perfect bonding is assumed at the interface of fibre and matrix subjected to tensile stress only. The matrix only carries shear stress.

A. Kelly and W. R. Tyson, 1965$^{(9)}$

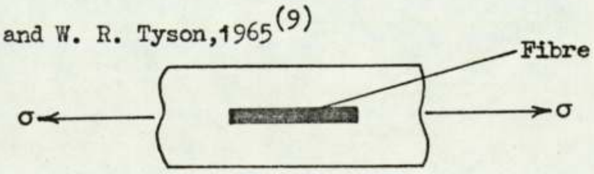

Elastic fibre in a plastic matrix yielding according to the Tresca criterion.

Fig. 2. Fibre models used for developing approximate analyses (Allison and Holloway$^{(10)}$)

2. 1. 2. Prediction of the properties of angle-ply fibre reinforced composites by two workers, Wallis(11) and Tsai(13).

In this section the prediction of the properties of helically wound glass fibre reinforced tubes is investigated. The work of Wallis(11) and Tsai(13) is examined and compared.

2. 1. 2. 1. Wallis.

Wallis utilises the Cutler(12) model and Fig. 3 shows the element for an orthotropic fibre. From the properties of fibre and matrix ($E_1, E_2, \nu_1, \nu_2, \nu_3, E_m, \nu_m, v_f$) a stiffness matrix M is obtained where:

$$\left|\begin{matrix}\sigma_\theta \\ \sigma_t \\ \tau_{\theta t}\end{matrix}\right| = \left|\begin{matrix}M_{11} & M_{12} & M_{13} \\ M_{21} & M_{22} & M_{23} \\ M_{31} & M_{32} & M_{33}\end{matrix}\right| \quad \left|\begin{matrix}\varepsilon_\theta \\ \varepsilon_t \\ \gamma_{\theta t}\end{matrix}\right|$$

It is necessary to transform the equation from the θ and t directions to the X and Y directions. The stress transformation is:

$$\left|\begin{matrix}\sigma_x \\ \sigma_y \\ \tau_{xy}\end{matrix}\right| = \left|\begin{matrix} \\ A \\ \\ \end{matrix}\right| \quad \left|\begin{matrix}\sigma_0 \\ \sigma_t \\ \tau_{\theta t}\end{matrix}\right|$$

where:

$$\left|\begin{matrix} \\ A \\ \\ \end{matrix}\right| = \left|\begin{matrix}\theta_1 & \theta_2 & -2\theta_3 \\ \theta_2 & \theta_1 & 2\theta_3 \\ \theta_3 & -\theta_3 & (\theta_1 - \theta_2)\end{matrix}\right|$$

The reverse transformation for the strains is:

$$\left|\begin{matrix}\varepsilon_\theta \\ \varepsilon_t \\ \gamma_{\theta t}\end{matrix}\right| = \left|\begin{matrix} \\ A \\ \\ \end{matrix}\right|^T \quad \left|\begin{matrix}\varepsilon_x \\ \varepsilon_y \\ \gamma_{xy}\end{matrix}\right|$$

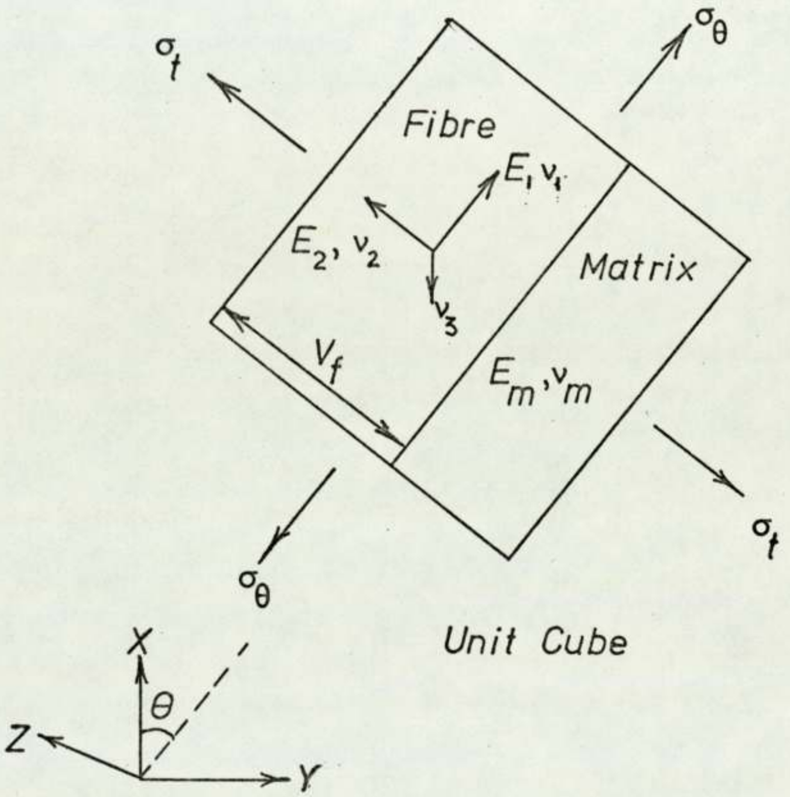

Fig. 3. Cutler element with orthotropic fibre.

This yields:

$$\begin{vmatrix} \sigma_x \\ \sigma_y \\ \tau_{xy} \end{vmatrix} = \begin{vmatrix} A \end{vmatrix} \begin{vmatrix} M \end{vmatrix} \begin{vmatrix} A \end{vmatrix}^T \begin{vmatrix} \varepsilon_x \\ \varepsilon_y \\ \gamma_{xy} \end{vmatrix}$$

Defining $|M'| = |A|\,|M|\,|A|^T$

we can obtain M' and

$$\nu_x = \frac{M'_{12}}{M'_{22}}$$

$$\nu_y = \frac{M'_{12}}{M'_{22}}$$

$$E_x = M'_{11} - \nu_x M'_{12}$$

and $$E_y = M'_{22} - \nu_y M'_{12}$$

2. 1. 2. 2. Tsai.

Tsai first calculates properties in the fibre direction and transverse to it then transforms to the required axis. By the law of mixtures:

$$E_L = (v_f E_f + (1 - v_f)E_m)K \qquad (1)$$

where K is a fibre misalignment factor.

$$\nu_L = (1-C)\,\frac{K_f\,\nu_f(2K_m+G_m)v_f + K_m\nu_m(2K_f+G_m)(1-v_f)}{K_f(2K_m+G_m) - G_m(K_f - K_m)(1 - v_f)}$$

$$+ C\,\frac{K_m\nu_m(2K_f+G_f)(1-v_f) + K_f\nu_f(2K_m+G_f)v_f}{K_f(2K_m+G_f) + G_f(K_m - K_f)v_f} \qquad (2)$$

where:

$$G_f = \frac{E_f}{2(1+\nu_f)}, \quad G_m = \frac{E_m}{2(1+\nu_m)}, \quad K_f = \frac{E_f}{2(1-\nu_f)}, \quad K_m = \frac{E_m}{2(1-\nu_m)}.$$

C is a contiguity factor of the order of 0.2.

Tsai found that in most cases the law of mixtures equation:

$$\nu_L = \nu_f v_f + (1 - v_f)\nu_m$$

was accurate to ± 5% of the values computed from the more complex equation (2). For computing values of E_T the following equation was used:

$$E_T = 2\left[1 - \nu_f + (\nu_f - \nu_m)(1 - v_f)\right] \left[(1 - C)\,\frac{K_f(2K_m + G_m) - G_m(K_f - K_m)(1 - v_f)}{(2K_m + G_m) + 2(K_f - K_m)(1 - v_f)} + C\,\frac{K_f(2K_m + G_f) + G_f(K_m - K_f)(1 - v_f)}{(2K_m + G_f) - 2(K_m - K_f)(1 - v_f)}\right] \quad (3)$$

ν_T can then be obtained from the well known reciprocal relationship:

$$\nu_T = E_T\,\frac{\nu_L}{E_L} \quad (4)$$

The shearing modulus is given by:

$$G_{LT} = (1 - C)G_m\,\frac{2G_f - (G_f - G_m)(1 - v_f)}{2G_m + (G_f - G_m)(1 - v_f)} + CG_f\,\frac{(G_f + G_m) - (G_f - G_m)(1 - v_f)}{(G_f + G_m) + (G_f - G_m)(1 - v_f)} \quad (5)$$

The transformation equations(14) are:

$$\frac{1}{E_x} = \frac{\cos^4\theta}{E_L} + \left[\frac{1}{G_{LT}} - \frac{2\nu_L}{E_L}\right]\sin^2\theta\cos^2\theta + \frac{\sin^4\theta}{E_T}$$

$$\frac{1}{E_y} = \frac{\sin^4\theta}{E_L} + \left[\frac{1}{G_{LT}} - \frac{2\nu_L}{E_L}\right]\sin^2\theta\cos^2\theta + \frac{\cos^4\theta}{E_T}$$

$$\frac{\nu_x}{E_x} = \frac{\nu_y}{E_y} = \frac{\nu_L}{E_L} - \frac{1}{4}\left[\frac{1 + \nu_L}{E_L} + \frac{1 + \nu_T}{E_T} - \frac{1}{G_{LT}}\right]\sin^2 2\theta$$

2. 1. 3. Comparison of the predictions of Young's modulus and Poisson's ratio for a filament wound glass reinforced epoxy resin tube.

The material constants used for the computations are typical of a glass fibre / epoxy resin system and were:

$E_f = 75800 \text{ MN/m}^2$

$E_m = 2900 \text{ MN/m}^2$

$\nu_f = 0.200$

$\nu_m = 0.380$

$v_f = 0.650.$

Since Wallis assumes contiguity of fibre and good alignment the contiguity factor was 0.0 and the fibre misalignment factor was 1.0. An ICL series 1905 computer was used for the computations.

Fig. 4 shows the variation with helix angle of Young's modulus and Poisson's ratio in the longitudinal and hoop directions for the Wallis equations. As expected the curves are mirror images about the helix angle of 45°. The longitudinal modulus decreases rapidly from helix angles of 10° to 30° and small changes in helix angle can have a large effect on the modulus. After about 40° there is little change in modulus, but the minimum modulus does not occur at 90°. The Poisson's ratio increase from a helix angle of 90° to 50° (more than four times) more than counterbalances the improving alignment which results in the minimum modulus occurring at about 50°.

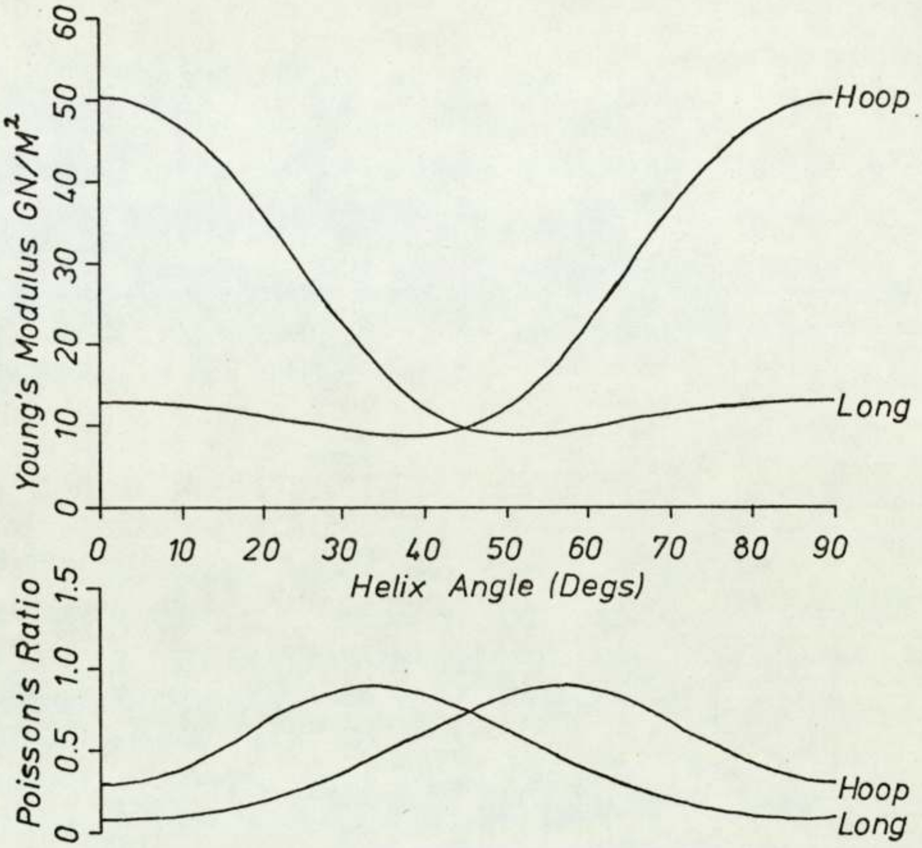

Fig. 4. Theory of Wallis.

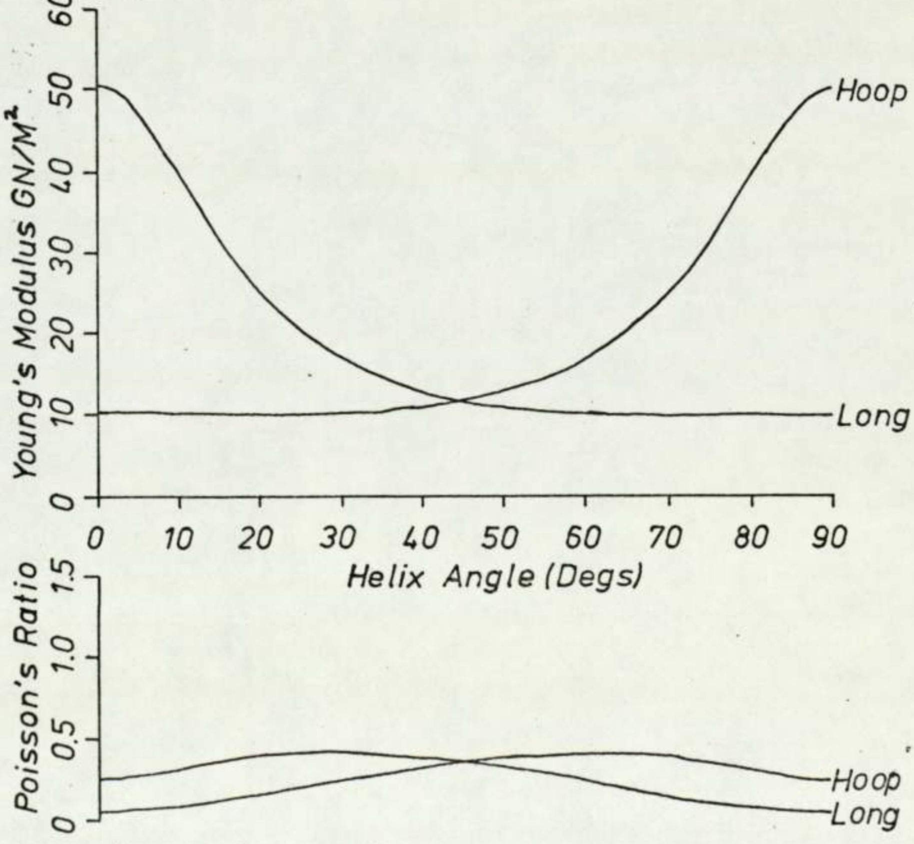

Fig. 5. Theory of Tsai.

Fig. 5 shows the variation of Young's modulus and Poisson's ratio in the longitudinal and hoop directions for the Tsai equations. Again, as is expected, the curves are mirror images about a helix angle of 45°. The curves of modulus against helix angle are similar to those of Wallis, but show no minimum. The decrease in Young's modulus is also more rapid than that of Wallis between helix angles of 10° and 30°. Between helix angles of 60° and 90° the curve is reasonably flat corresponding to the minimum value of Young's modulus that was reached in the Wallis predictions. The Poisson's ratio increase between 90° and 60° is not as pronounced and this results in the Tsai predictions showing no minimum in the Young's modulus curves.

Fig. 6 shows the variation of Young's modulus and Poisson's ratio with volume fraction of fibres at a fixed helix angle of 30° for the Wallis equations. The Young's modululii increase rapidly for volume fractions greater than 0.75. At a volume fraction of about 0.5 the Poisson's ratio in the longitudinal direction goes through a maximum. The Poisson's ratio in the hoop direction increases with addition of fibres and in order to satisfy the reciprocal relationship:

$$\frac{\nu_x}{\nu_y} = \frac{E_x}{E_y}$$

the Poisson's ratio in the longitudinal direction must also increase. This results in the high values of Poisson's ratio in the predictions.

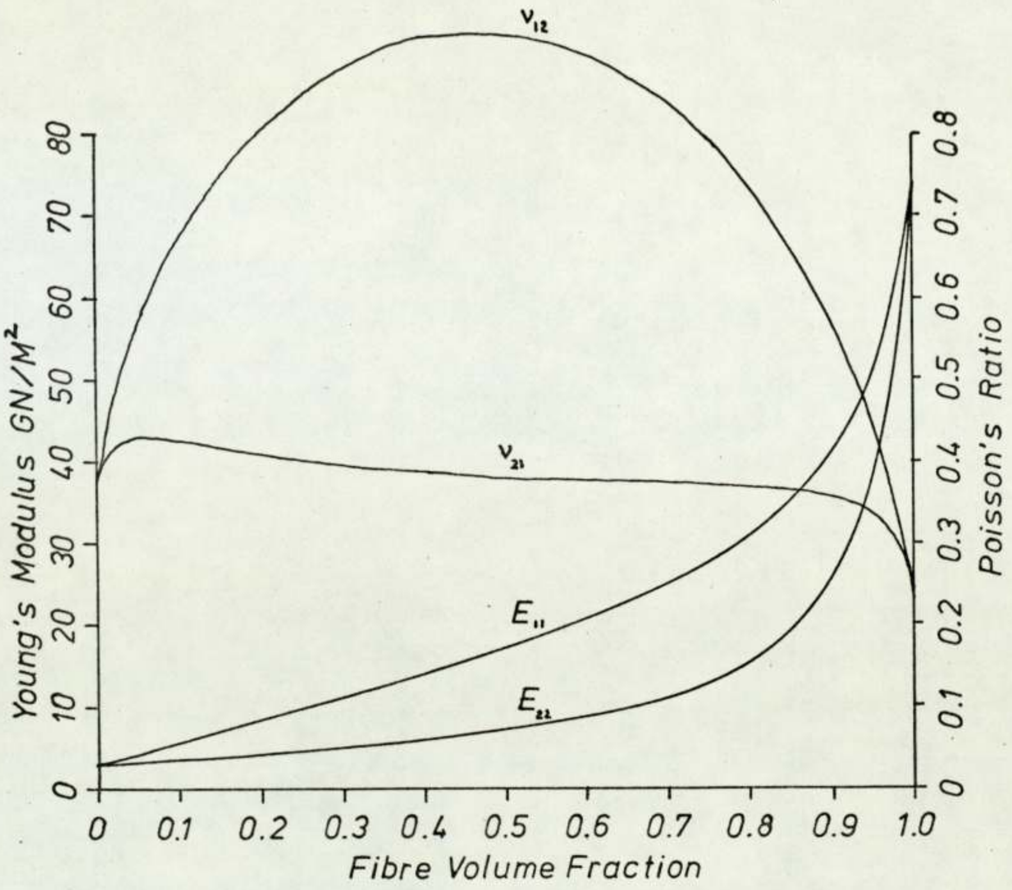

Fig.6. Theory of Wallis.

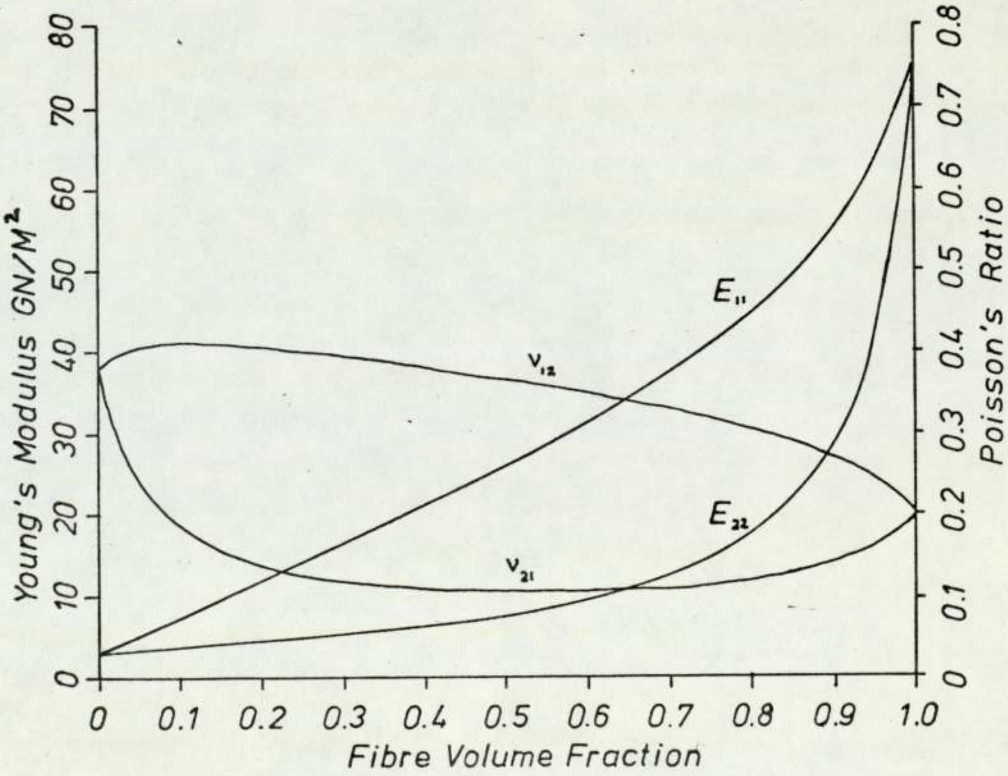

Fig. 7. Theory of Tsai.

Fig. 7 shows the variation of Young's modulus and Poisson's ratio with volume fraction of fibres at a fixed helix angle of 30° for the Tsai equations. The predictions of Young's modulus are lower than those predicted by Wallis, but the curves show a similar shape. The predictions of Poisson's ratio are very different and ν_y decreases with fibre addition in the predictions by Tsai. This results in much lower values of ν_x than the values obtained from the Wallis equations.

In order to compare the predictions for multilayered tubes containing different angles of wind the following procedure is necessary:

2. 1. 3. 1. Wallis.

A matrix D is computed where:

$$D_{pq} = \sum_{i=1}^{n} \frac{(h_o)_i}{t} M'_{pqi}$$

i is the number of strata of each winding angle and
n is the total number of strata in the tube.

It is not valid to add the modulii by superposition due to coupling effects. It is necessary to compute a value of ν_x where:

$$\nu_x = \frac{\sum_{i=1}^{n} n_i E_{yi} \nu_{xi}}{\sum_{i=1}^{n} n_i E_{yi}}$$

E_x, E_y and ν_y are obtained from:

$$E_x = D_{11} - \nu_x D_{12}$$

$$E_y = \frac{E_x D_{22}}{E_x + {}_x D_{12}}$$

$$\nu_y = \frac{\nu_x E_y}{E_x}$$

2. 1. 3. 2. Tsai.

The equations for computation of the Young's modulii and Poisson's ratios for a tube with two different winding angles are quite complex by Tsai's theory. The equations therefore need not be quoted here and are available in Appendix 2.

Figs. 8 and 9 show the predictions by Wallis and Tsai for a tube comprising 50% of hoop winding and 50% of ± 30° helix angle winding. The predictions are of the variation of Young's modulus and Poisson's ratio with fibre volume fraction. Again the predictions of Young's modulus from Tsai's equations are lower than those of Wallis, but the curves are similar. Poisson's ratio values are also similar, but in this case the values predicted by Tsai are higher than those by Wallis.

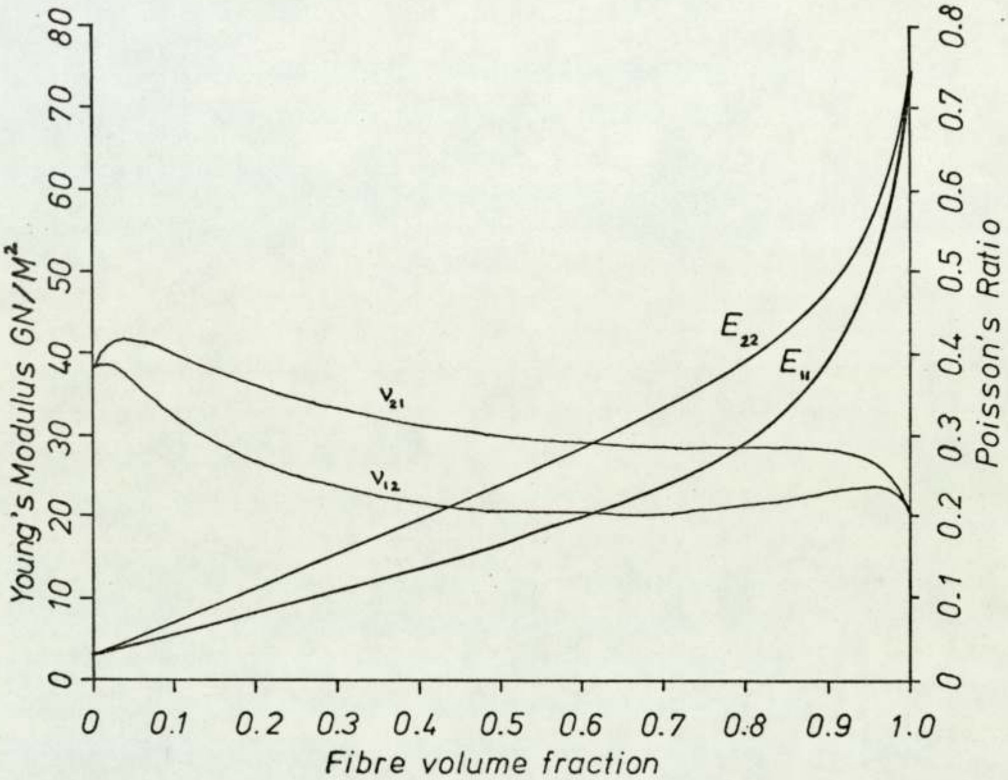

Fig. 8. Theory of Wallis.

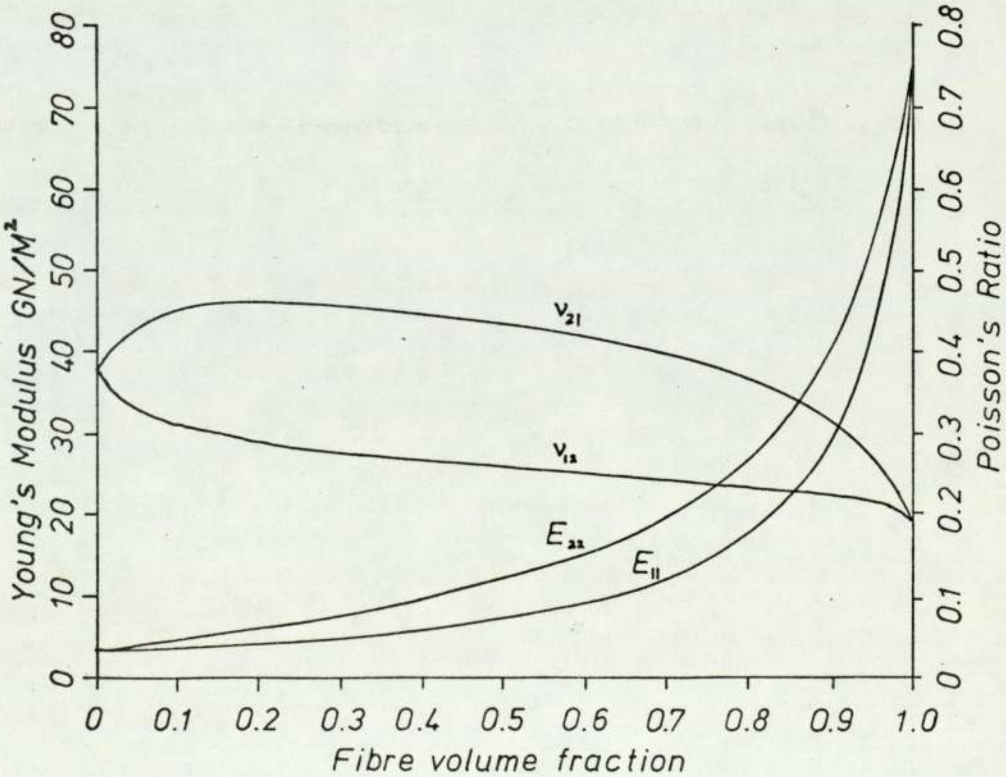

Fig. 9. Theory of Tsai.

2. 1. 4. The influence of Interlaminar stresses on the failure of fibre reinforced composites.

It is of great importance to consider the effect of interlaminar stresses on fibre reinforced composite materials. This arises because the interfacial surfaces between layers in a laminated composite represent planes of minimum strength.

Puppo and Evenson(15) have shown that a finite width specimen of a laminate in a generalised state of plane stress can have finite values of interlaminar shear stress at the edge of the specimen. If these stresses become high enough then the strip can fail prematurely by delamination initiated at the edge of the strip. This would give misleading values of strength data from uniaxial tests. If the data were subsequently used for the design of a tubular structural member, which is an infinite width body, the member may be overdesigned. For aircraft and spacecraft, where weight saving is of paramount importance, this would be undesirable.

Pipes and Pagano(16) calculated, by finite differences, a solution of the elasticity equations governing the behaviour of a four layer, symmetric angle ply laminate. The interlaminar shear stress was also found to be an edge effect, restricted to a region approximately equal to the laminate thickness. Such stresses can be expected to cause failure of the laminate by delamination.

Pagano and Pipes(17) observed this unusual failure mechanism in a carbon fibre / epoxy system. The distribution of σ_z is of the form shown in Fig. 10. The maximum value of interlaminar stress occurs at the edge of the laminate. The interlaminar stress is low compared with other stresses in the system, but can result in failure, represented schematically in Fig. 11. Pagano and Pipes showed that the stress can be maximised by using a specimen with a stacking sequence of (25°,-25°,25°,-25°,90°,90°,-25°,25°,-25°,25°). They constructed specimens of carbon fibre / epoxy with this lay up. The specimens they constructed failed by delamination, initiated at the edge of the specimens.

Clearly it is necessary to calculate the interlaminar normal stresses in composite laminates for design purposes. Pagano(18) has presented an approximate method of calculation of these stresses. The calculations are based on recent theory developed by Whitney and Sun(19) and compare favourably with existing elasticity solutions.

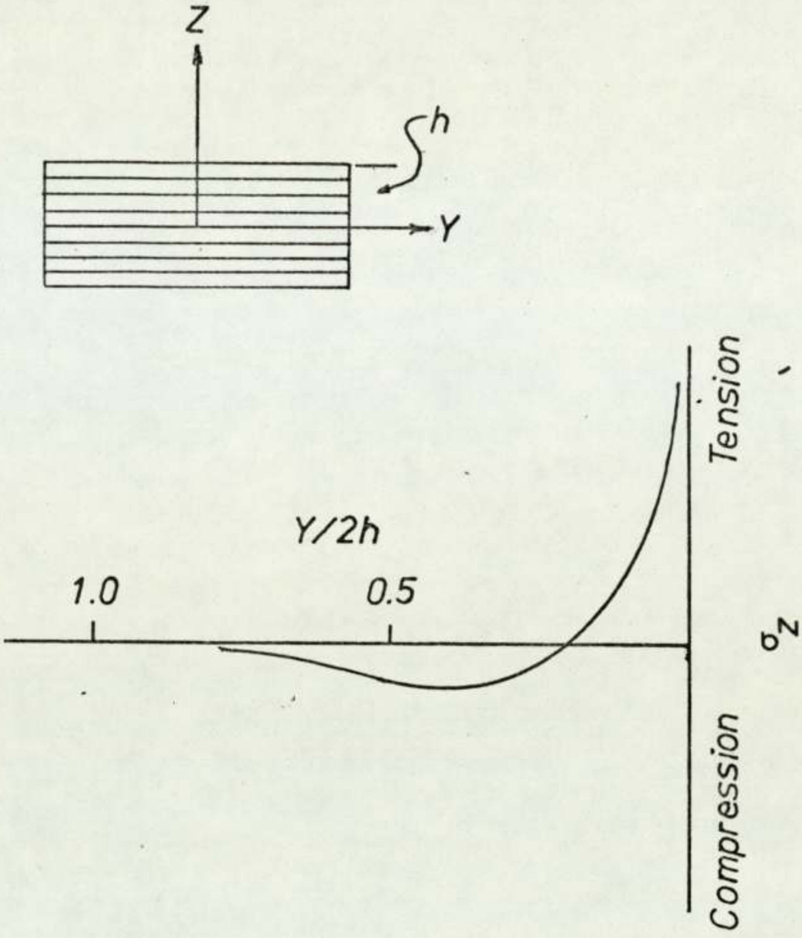

Fig. 10. Distribution of interlaminar normal stress v. Y.

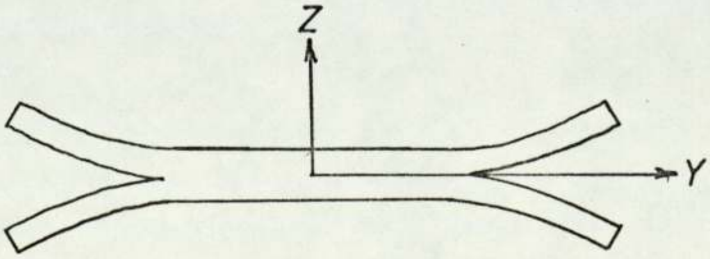

Fig. 11. Schematic representation of failure of fibre composite by delamination.

2. 1. 5. The effect of stacking sequence on the properties of fibre reinforced composites.

Section 2. 1. 3. showed that the interlaminar stresses which may exist in composite laminates must be minimised to protect against failure, by delamination, under axial loadings. Recent work has shown that the strength of composite laminates, which contain identical ply orientations, can be dependent on the stacking sequence.

Pagano and Pipes(20) have presented an approach to predict how the layers of specific orientations should be arranged in order to minimise the effects of interlaminar stresses. They present an example of a boron/epoxy ±15°,±45° laminate with layers of equal thickness. Fig. 12 shows how the change of stacking sequence can reduce the interlaminar normal stress in this system. The calculations help to explain the pronounced difference in strength of these laminates which was observed by Foye and Baker(21). Clearly the arrangement of the layers and orientations must be considered when designing fibre reinforced composite components.

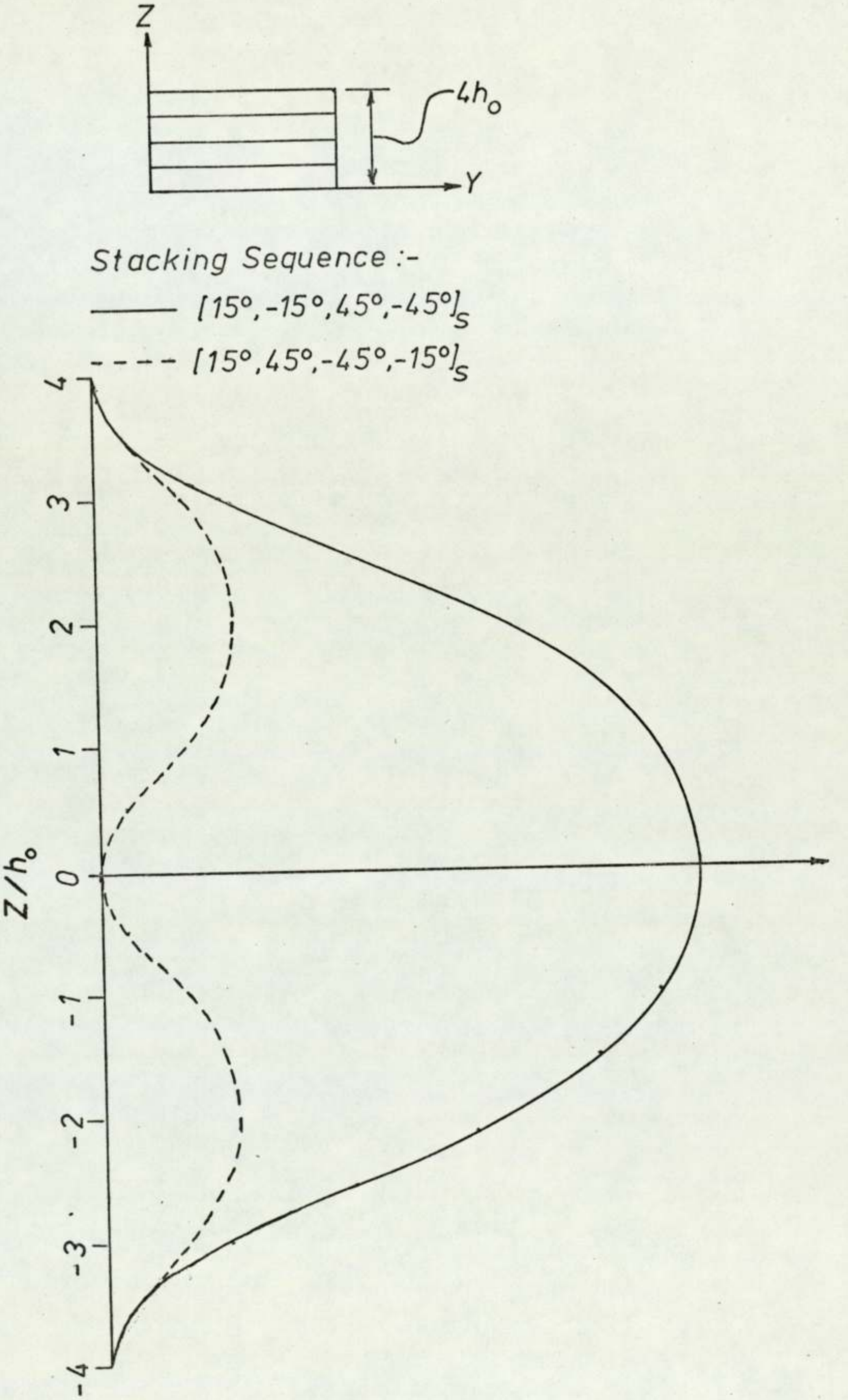

Fig. 12. Distribution of interlaminar normal stress in boundary layer region v. Z.

2. 1. 6. Stress gradients which may exist in helically wound, fibre reinforced composite tubes.

When an anisotropic cylinder is subjected to simple loading conditions the stress field may be far from uniform. It has been shown by Pagano et Al(22) that the stress field approaches uniformity in such a cylinder when the wall thickness approaches zero. Since this is not acceptable from a practical standpoint it is necessary to re-define the term 'thin walled cylinder' for anisotropic materials. Pagano and Whitney(23) have made calculations of the distributions of stress in the walls of typical glass / epoxy and carbon / epoxy unidirectional cylinders for three basic loadings - axial,torsion and internal pressure. Figs. 13, 14 and 15 show the normalised stress gradients for axial loading, torsion and internal pressure repectively. These figures show the severity of the stress gradients and the high R/t ratio necessary to approximate a state of uniform stress for the highly anisotropic carbon system. Pagano and Whitney also studied the variation of the three normalised stresses with helix angle in a carbon / epoxy cylinder with R/t = 20. Fig. 16 shows these variations. The maximum normalised shear and hoop stresses occur in a tube with a helix angle of about 60° and the maximum normalised axial stress in a tube with a helix angle of about 30°. They also show that the gradients are drastically reduced for the same system but with cross ply lay ups.

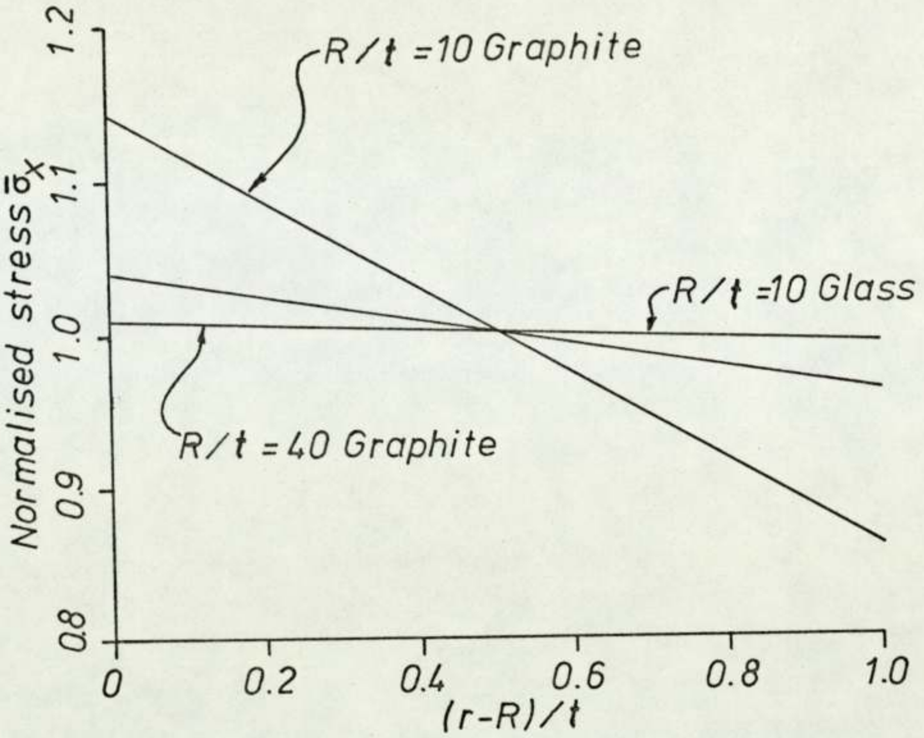

Fig.13. Axial normalised stress in wall section, axial loading, $\theta = 30°$.

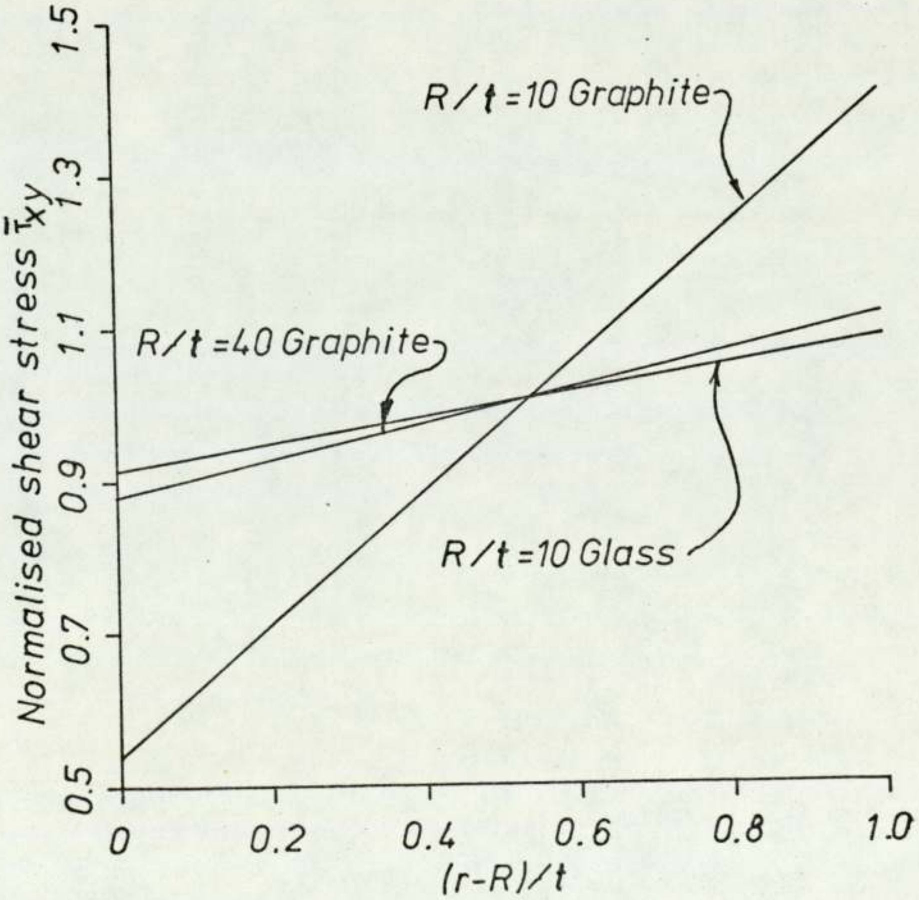

Fig.14. Normalised shear stress in wall section, $\theta = 60°$.

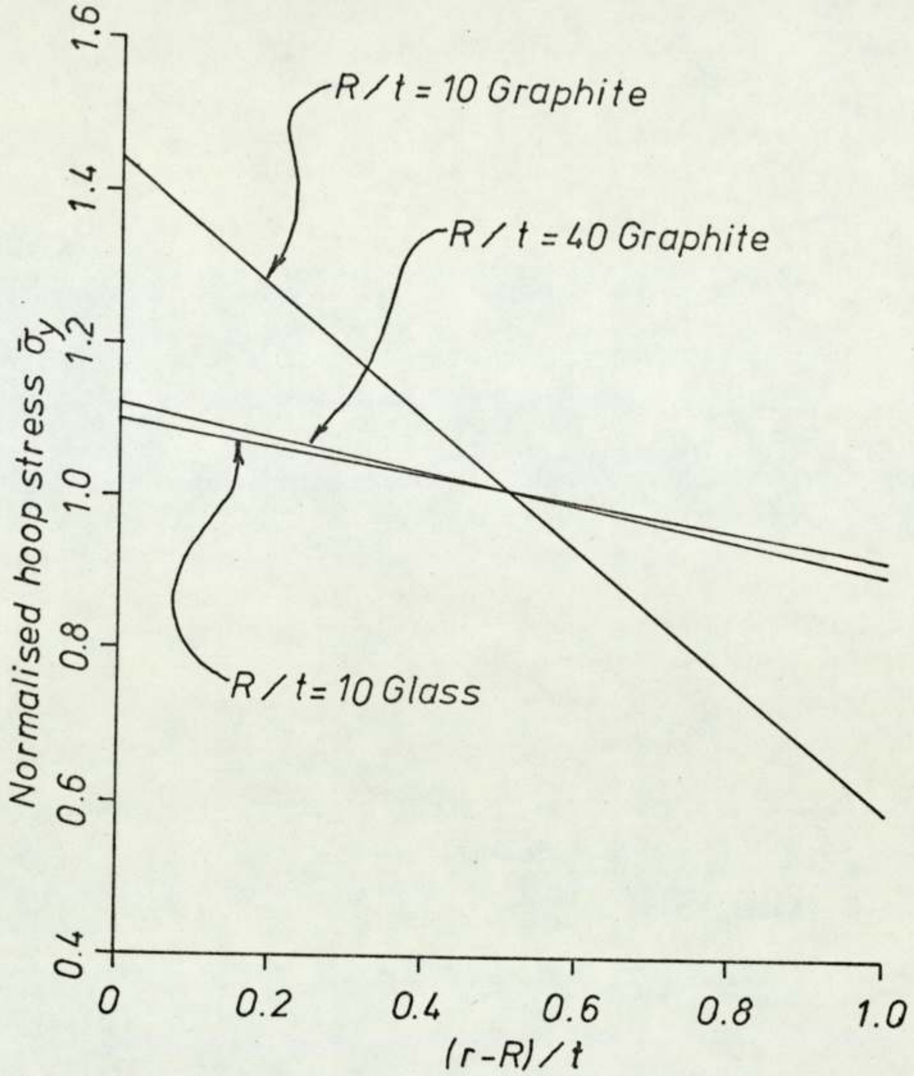

Fig. 15. Normalised hoop stress in wall section, internal pressure, $\theta = 60°$.

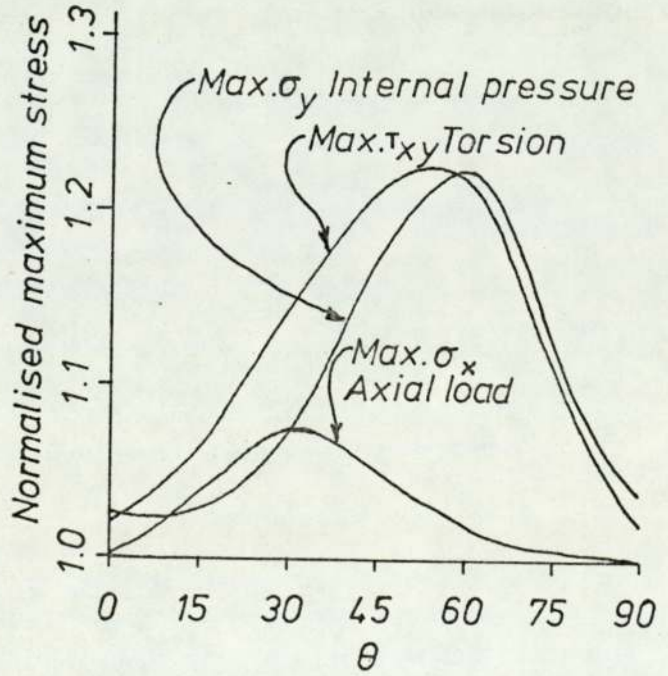

Fig. 16. Maximum stresses in wall section, carbon, $R/t = 20$.

2. 2. Fracture mechanics of isotropic and anisotropic materials.

2. 2. 1. Brief historical review of the application of fracture mechanics to isotropic materials.

Griffith(24) satisfactorily explained the brittle fracture of glass as early as 1920. Using the Inglis(25) solution for the stresses and strains around the crack tip he said that the crack would extend when the release of elastic stored energy became equal to the energy required to form a new crack surface. Using the fracture surface energy, to be a measure of the initiation of the fracture process, he derived the equation:

$$\sigma = \left(\frac{2E\gamma}{\pi c}\right)^{\frac{1}{2}}$$

which was later modified to:

$$\sigma = \left(\frac{2E\gamma}{\pi c(1 - \nu^2)}\right)^{\frac{1}{2}} \quad \text{for plane strain conditions.}$$

When he tested these equations experimentally for validity he found good correlation for the fracture behaviour of glass, but application to most metals was unsatisfactory. This is due to the formation of plastically deformed material, close to and ahead of the crack tip which absorbs work during crack propogation. Since glass has little or no plasticity this discrepancy was not shown.

Orowan(26) suggested a plastic work factor but, to overcome the difficulties associated with this Irwin(27) introduced a factor, G, known as the strain energy release rate. The critical value of G is known as the 'Fracture Toughness', G_c or G_{Ic}, for plane stress and plane strain conditions, respectively.

Fig. 17 shows the three ~~opening~~ modes of crack behaviour, designated modes I,II and III, combinations of which will describe all situations encountered.

The critical value of G in the mode I opening and for plane strain conditions is denoted G_{Ic}. This is related to the critical stress intensity factor, K_{Ic}, by the equation:

$$K_{Ic} = \left[\frac{G_{Ic} E}{(1 - \nu^2)}\right]^{\frac{1}{2}}$$

The magnitude of K_{Ic} is of particular importance when designing against brittle fracture. The relationship:

$$c_{crit} = \frac{K_{Ic}^2}{Y^2 \sigma_w^{\,2}}$$

can be used to determine the critical defect size, c_{crit}, which would initiate fracture at a working stress of σ_w. Y is a geometrical factor and is available, from tables, for most situations. Should geometrical factors be unavailable from tables for a particular situation it is possible to obtain Y calibration curves both experimentally and theoretically.

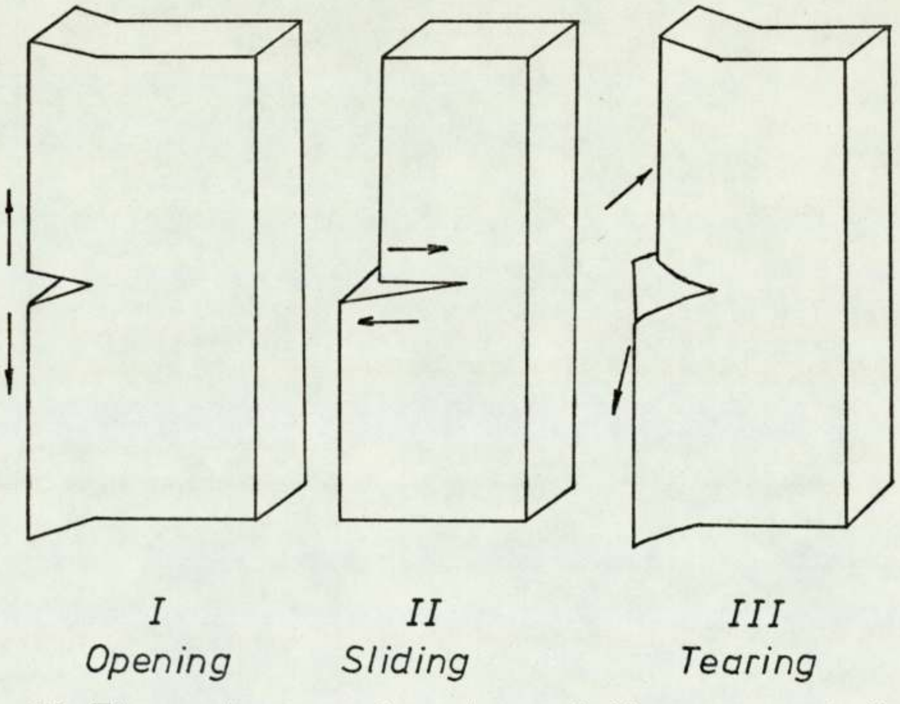

Fig. 17. Elementary modes of crack tip movement displacement.

2. 2. 2. Fracture mechanics applied to cylindrical pressure vessels.

If a cylindrical pressure vessel containing an axial crack is subjected to internal pressure both the hoop stress and the radial stress will tend to propagate the crack. The radial stress will tend to cause bulging of the mouth of the crack and coupled with the hoop stress will tend to cause propogation. The critical propagation hoop stress will be a lower than the equivalent stress for a simple axially loaded specimen. It is of practical value to correlate flat plate behaviour with behaviour in pressure vessels.

It is found that the pressure vessel can be treated like a flat plate if the nominal stress, σ, is taken as a multiple of the hoop stress in the wall, σ_H, i.e.

$$\sigma \quad = \quad \sigma_H \, f(c,R,t)$$

A summary of the form of f(c,R,t) is given in Table 1 for various workers. The critical hoop stress $\overset{*}{\sigma}_H$ can be related to the nominal stress $\overset{*}{\sigma}$ which is critical for crack propagation in a flat plate. In particular Duffy et Al(33) combined the Folias theoretical treatment form with the fracture mechanics approach and included a correction for crack tip plasticity. The latter correction was derived from the Dugdale crack model. Hahn et Al(3) present other approaches and two which are important here are shown in Table 2, which is a shortened form of their table. There appears to be some confusion about the plasticity correction factor ϕ_3 in their table since the function:

$$\phi_3 \quad = \left(\frac{\pi \overset{*}{\sigma}_H M}{2\bar{\sigma}}\right) \quad \ln\left(\sec \frac{\pi \overset{*}{\sigma}_H M}{2\bar{\sigma}}\right)$$

Failure criterion	M	ϕ	Investigators
$\sigma_H^* = \sigma^* M^{-1}$	$(1+9.2\,\frac{c}{R})$	-	Peters and Kuhn, 1957(28)
$\sigma_H^* = \sigma^* M^{-1}$	$(1+1.61\,\frac{c^2}{Rt})^{\frac{1}{2}}$	-	Folias, 1965(2)
$\sigma_H^* = \frac{K_c}{(\underline{\pi}c\underline{\phi})^{\frac{1}{2}}} M^{-1}$	$(1+\frac{\beta c}{R})$	$(1+\frac{(M\sigma_H^*)^2}{2\sigma_y^2})$	Anderson and Sullivan, 1966(29)
$\sigma_H^* = (\sigma_y^e \sigma_U^f (g+hW))^{\frac{1}{3}} M^{-1}$	$(c^{\frac{1}{3}})$	-	Nichols et Al, 1965(30)
$\sigma_H^* = \sigma^* M^{-1}$	$(1+\frac{c^2}{4Rt})$	-	Kihara et Al, 1966(31)
$\sigma_H^* = \sigma^* M^{-1}$	$(1+0.81\frac{c}{(Rt)^{\frac{1}{2}}})^{\frac{3}{4}}$	-	Chrichlow and Wells, 1967(32)
$\sigma_H^* = \frac{K_c}{(\pi c\phi)^{\frac{1}{2}}}$	$(1+1.61\,\frac{c^2}{Rt})^{\frac{1}{2}}$	$\sec\frac{\sigma_H^*}{(\sigma_y+\sigma_U)}$	Duffy et Al, 1967(33)

Table 1. Criteria for crack extension in unstiffened cylindrical pressure vessels with axial through cracks (after Hahn, Sarrate and Rosenfield(3)).

(In the table e, f, g, h and β are coefficients depending on the geometry of the vessel and W is the Charpy V notch energy)

Category	Specifications		Criterion	M	Applications
	R/t	$\frac{K_c^2}{\sigma_y}\frac{1}{c}$			
1. Intermediate wall thickness, low to medium toughness vessels with relatively long cracks.	5-50	<7,	$\overset{*}{\sigma}_H = \frac{K_c}{(\pi c\phi_3)^{\frac{1}{2}}} M^{-1}$	$(1+1.61 \frac{c^2}{Rt})^{\frac{1}{2}}$	Steel pipe lines and pressure vessels operating below the shear to cleavage fracture transition temperature.
2. Very thin wall, low and medium toughness vessels with relatively long cracks.	>50	>7	$\overset{*}{\sigma}_H = \frac{K_c}{(\pi c\phi_3)^{\frac{1}{2}}} M^{-1}$	$(1+1.61\frac{c^2}{R^2}\ 50\tanh\frac{R}{50t})^{\frac{1}{2}}$	Thin walled rocket propellant tanks.

$\phi_3 = (\frac{\overset{*}{\sigma}_H M}{2\bar{\sigma}}) \ln(\sec \frac{\overset{*}{\sigma}_H M}{2\bar{\sigma}})$ $\sigma_y < \bar{\sigma} < \sigma_U$

Table 2. Criteria for extension of axial through cracks in unstiffened pressure vessels(after Hahn et Al$^{(3)}$).

does not approach unity as $\sigma_H^* / \bar{\sigma}$ approaches zero as Fig. 1 in (3) suggests. Hahn et Al show that inspection of the equation in the first category reveals that $(\sigma_H^2 \pi c \phi_3)^{-1}$ is a function of c^2/Rt with K_c^{-2} and $1.61K_c^{-2}$ the intercept and slope respectively. Using data relevent to category 1 supplied from (29,30,31,33 and 34) they represent the data graphically on plots of $(\sigma_H^{*2} \pi c \phi_3)^{-1}$ versus c^2/Rt. In all cases the points could be approximated to a linear relationship with slope and intercept consistent with a single K_c value. Also it was shown that the K_c values agreed very well with those derived from flat plate tests. Hahn et Al also used data for thin walled vessels and plotted $(\sigma_H^{*2} \pi c \phi_3)^{-1}$ against $c^2/Rt(50tahnR/50t)$. The scatter in this case was worse than the former, but still conformed roughly with the equation for category 2 and with the K_c values obtained for flat plate tests.

The methods of dealing with data from flat plate tests and correlating it to behaviour in cylindrical pressure vessels is quite well established for isotropic materials such as metals. Little material, if any, is available in the literature of the behaviour of helically wound fibre reinforced pressure vessels containing defects. At present the state of the science is that methods of obtaining K_c values for normal tensile and bend conditions in fibre reinforced materials are not fully established and a review of the present position follows in the next section.

2. 2. 3. The present situation in the determination and utilisation of K_c values for fibre reinforced composites.

The possibility of failure of composite materials by brittle fracture has brought about the need to classify the notch sensitivity of these materials in some way. The linear elastic fracture mechanics approach, which is widely used for metals, is the logical choice. If it could be found that this approach is applicable it would be possible to utilise the large amount of information, both theoretical and experimental, which has been obtained for isotropic materials, particularly metals. The linear elastic fracture mechanics approach may not be applicable to composite materials due to the difference in nature of the crack tips of composites and isotropic materials such as metals. It is hoped that other factors will be more important and outweigh these discrepancies and the approach will be applicable.

Sanford and Stonesifer(36) have shown that it is possible to obtain reproducable fracture toughness parameters (K_c and G_c) for a glass reinforced composite system. They used both single edged and double edged notched specimens with longitudinal fibres. An important conclusion reached was that the test method was sensitive to variations in the material and could be used to evaluate the material on the basis of fracture toughness. Attention is drawn to the fact that measurement of fracture toughness parameters in the forward shear mode of failure (K_{II}) is difficult and has been largely ignored for isotropic materials.

linear elastic fracture mechanics and theoretical stress concentration factors were found to underestimate the strengths of the notch sensitive composites. The strengths tended towards the theoretical predictions as the crack sharpness was increased.

Zimmer(39) found that for a particular carbon fibre composite lay up ($0^\circ, 90^\circ, 0^\circ$) the analysis for the fracture mechanics of isotropic materials could be applied with accuracy. Linear elastic fracture mechanics were applied by Owen and Bishop(40) to various composites, including chopped strand mat and balanced weave fabric glass reinforced polyester resin. K_c values were found to be dependent on crack length; by the use of a suitable correction factor, based on an equivalent yield strength and suggested by Irwin(41), a constant K_c could be calculated. Using the constant value of K_c it was possible to be able to predict with accuracy the failure of a plate specimen containing a central hole. Confirmation of this was given by Holdsworth, Owen and Morris(47) who obtained constant K_c values for similar materials after correcting using Irwin's crack tip zone correction factor. Using the K_c value, prediction of failure stresses in both plate and box section beams containing holes, were in good agreement with observed values.

The above indicates that , in general, the linear elastic fracture mechanics approach to failure in composite materials is reasonably acceptable. It must be remembered that composite variables can invalidate the application and clearly more data

The composite material fails in this mode frequently. By use of specimens containing angled notches they showed that it was possible to relate the K_{IIc} values to K_{Ic} values by a simple relationship. This means that only fracture toughness tests for the opening mode need be carried out since the forward shear mode values can be deduced from these.

Waddups et Al(37) showed that for a graphite / epoxy system containing a circular hole, fracture mechanics analysis was applicable. The material was subjected to fatigue prior to testing for static strength. The theoretical values of static strengths agreed very well with those observed in practice. Applying the analysis to narrow slits in the same specimens it was found that the material had a slightly higher static strength than the predictions. This was probably due to material damage at the end of the slit improving the material geometry. It appears that, unlike metals, the geometry of the specimen does not alter substantially with repetitive loading.

Further illustration of the underestimation of the strengths of composites was provided by Beaumont and Phillips(38). The materials which were investigated were carbon and glass fibre composites containing either surface untreated or surface treated fibres. It was found that the composites containing untreated fibres exhibited notch insensitivity and those with treated fibres exhibited notch sensitivity. The lower shear strengths of the fibre interfacial bond with the untreated fibres caused effective crack blunting at the tip of the notch. Both

are
~~is~~ needed before the widespread use of the approach can be made. In particular, it has been shown by Barnby and Spencer(35) that K calibration curves for itotropic materials, such as those provided by Brown and Srawley(42), can be significantly different from those found for composites. The use of the isotropic calibration curves can produce similar K_c values in some ranges of c/W, but in others can overestimate failure stresses of components by as much as 50%.

2. 2. 4. Applications of fracture mechanics to anisotropic plates.

Wu$^{(48)}$ has shown that the magnitude of the stress intensity factors in anisotropic plates can be dependent on the normal stresses in the system and functions of the material constants and orientation of the crack. Mode 1 stress intensity factors for isotropic materials have been shown to be dependent on the normal stresses only. The dependence of the stress intensity factor on the material and orientation functions will not exist if the crack has an orientation along a plane of symmetry. When this situation exists the stress intensity factor can be defined as:

$$K_I = \sigma (c)^{\frac{1}{2}}$$

The equation can be written:

$$\log(K_{Ic}) = \log(\sigma^*) + \log(c)$$

at criticality. Wu plotted values of $\log(\sigma^*)$ against $\log(c)$ for tests on orthotropic tension test pieces. They were tested in pure tension, pure shear and a mixture of both. The graphs showed that within experimental error the slopes of the graphs were 0.5.

The most deleterious orientation of a crack in a cylindrical pressure vessel is the axial orientation. This is a principal axis of symmetry for the tubes which are the subject of this work. There is justification in attempting to apply linear elastic fracture mechanics, normally used for isotropic materials, to these tubes if the defects which are introduced have an axial orientation.

Chapter 3.

3. Design of equipment to pressurise the tubes.

3. 1. Pressure testing cubicle and pumping systems.

Plate 1 shows the pressure testing cubicle with the high pressure pump taken out for clarity. A close-up of the tie bars and end plates to hold the tube are shown in plate 2. The empty cubicle normally houses the main pump to pressurise the tubes and an isostatic press.

The cubicle was made of 6mm. mild steel plate and angle. The top left, left front, right front and right back sections were removable. Provision was made to incorporate two removable laminated glass windows in the front and back of the tube testing cubicle. The windows could be replaced with mild steel sheets, if required.

Fig. 18 shows a line diagram of the pumping system. A small pump was added to recirculate any water from the tube side back to the main pump reservoir. The isostatic press could be used as a pressure sink to obtain slower pumping rates and could be isolated for slightly higher rates. The high pressure pump was supplied by Stanstead Filtration Fluid Power Products and was Model TC/10 with the following specification:

Model	Rated Pressure	Output	Outlet
512	2800 K_g/cm^2	0.125 l/min.	$\frac{1}{4}$" O/D H. P.

Plates 3, 4, 5 and 6 show the pump from all sides.

3. 2. End caps and clamps.

When subjecting steel tubes to internal pressure there are no problems in sealing the ends since end caps can be simply welded into place, thus effecting a seal. This technique is not possible with glass reinforced plastic tubes and a problem encountered was one of sealing the ends of the tube satisfactorily. Wilson(43), who was working on high vaccuum systems, encountered the problem of sliding rods in and out of a high vaccuum system without breaking the seal. He produced a sliding seal and it was possible by careful design to utilise his ideas and to make an end cap capable of sealing the pressure in the tube.

Fig. 19 shows a cross section of this end cap and plates 7 and 8 show the assembled cap and its individual components. The internal pressure forces the rubber gasket against the wall of the tube; the greater the pressure the more effective is the seal. At high pressures it is possible for the tube wall to expand sufficiently to allow the rubber sealing ring to bend back and release the pressure. To minimise the risk of this occurring, mild steel clamps were designed. Plate 9 shows the assembled clamps.

The end seals were constructed of stainless steel (EN58J) and the rubber seals were a stiff neoprene. A compromise must be made between the need for a stiff rubber to minimise extrusion of the seal and an easily deformed rubber for flexibility when fitting. To hold the caps in position it is necessary to have

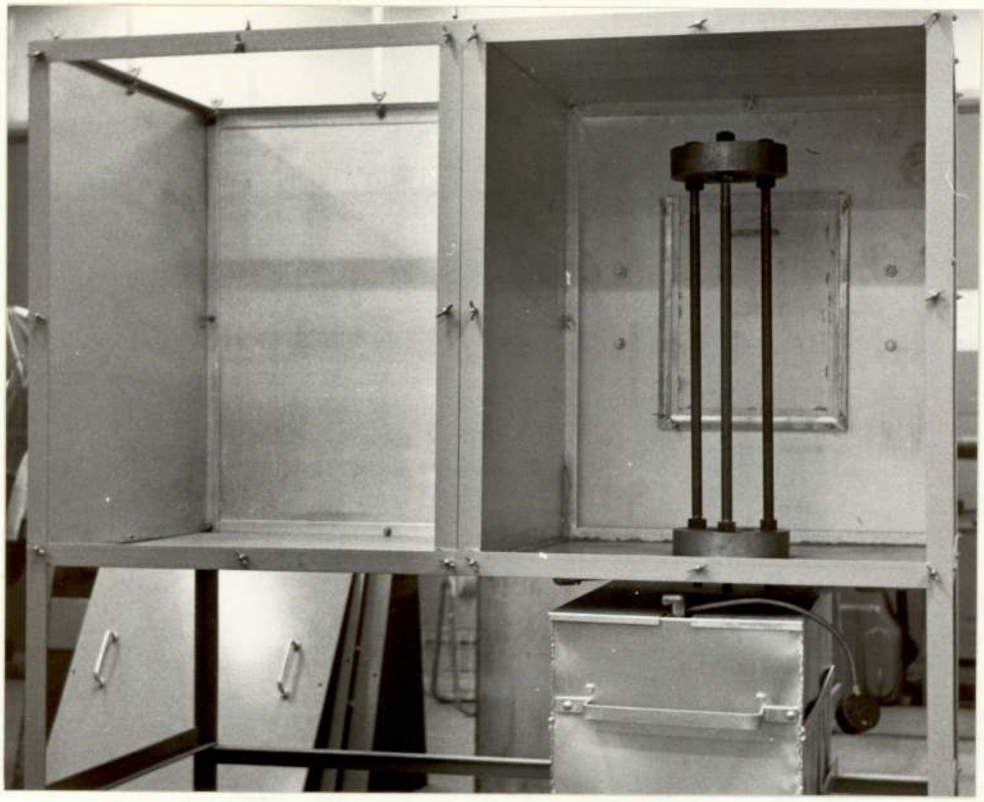

Plate 1.

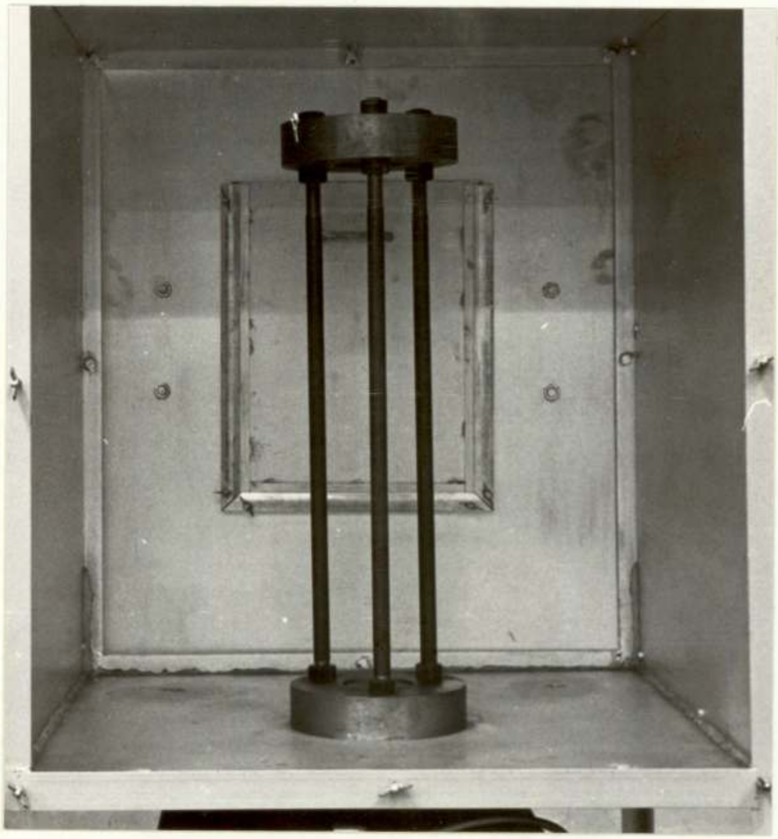

Plate 2.

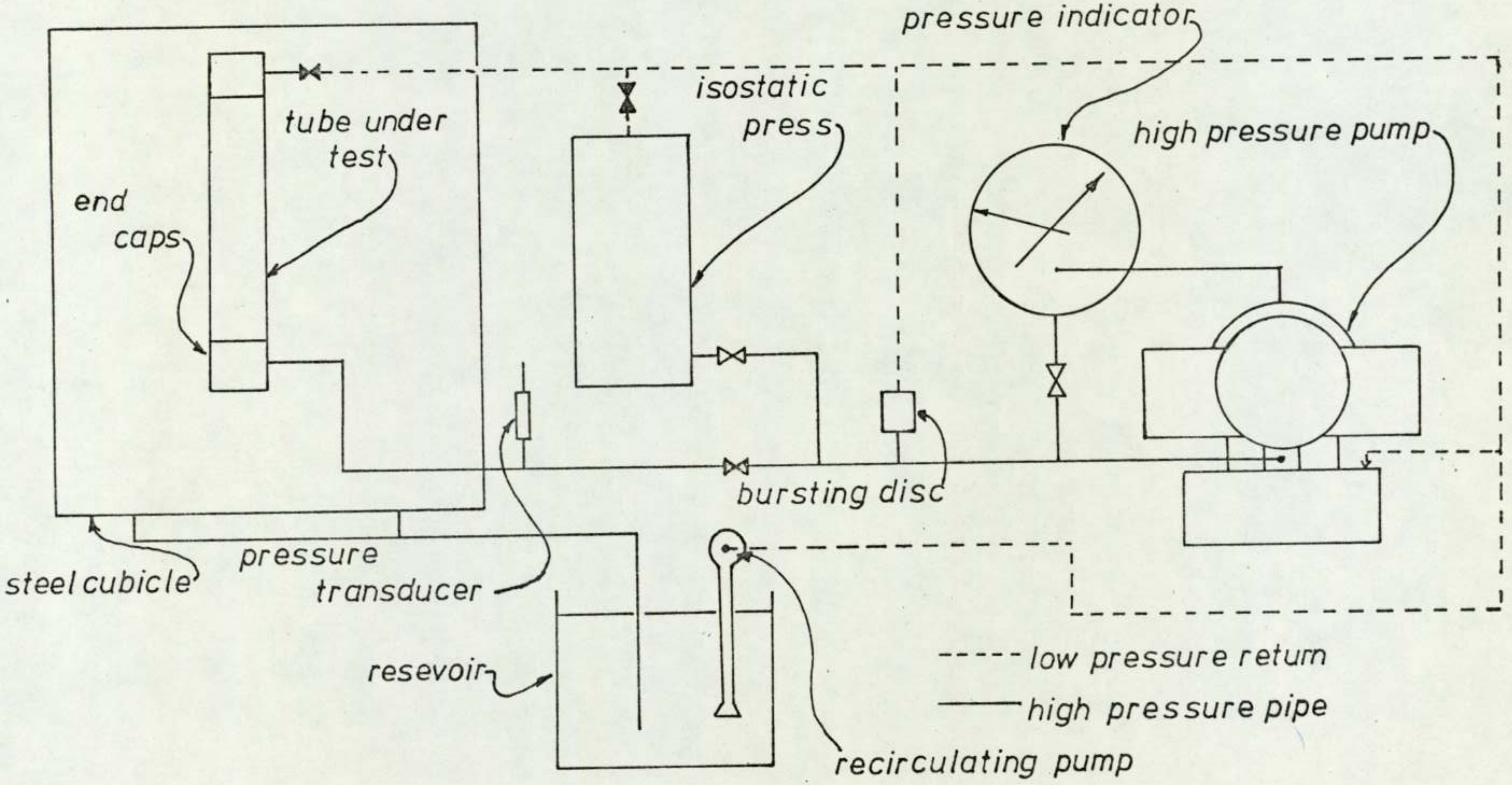

Fig. 18. Line diagram of the pumping system.

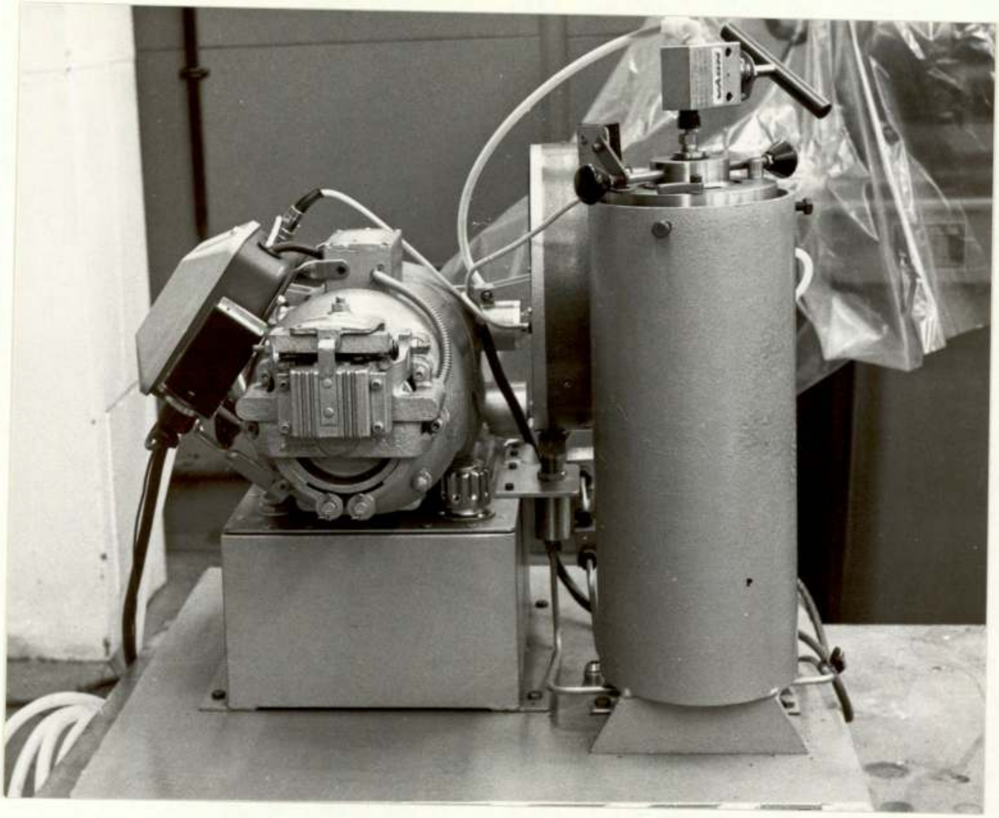

Plate 3.

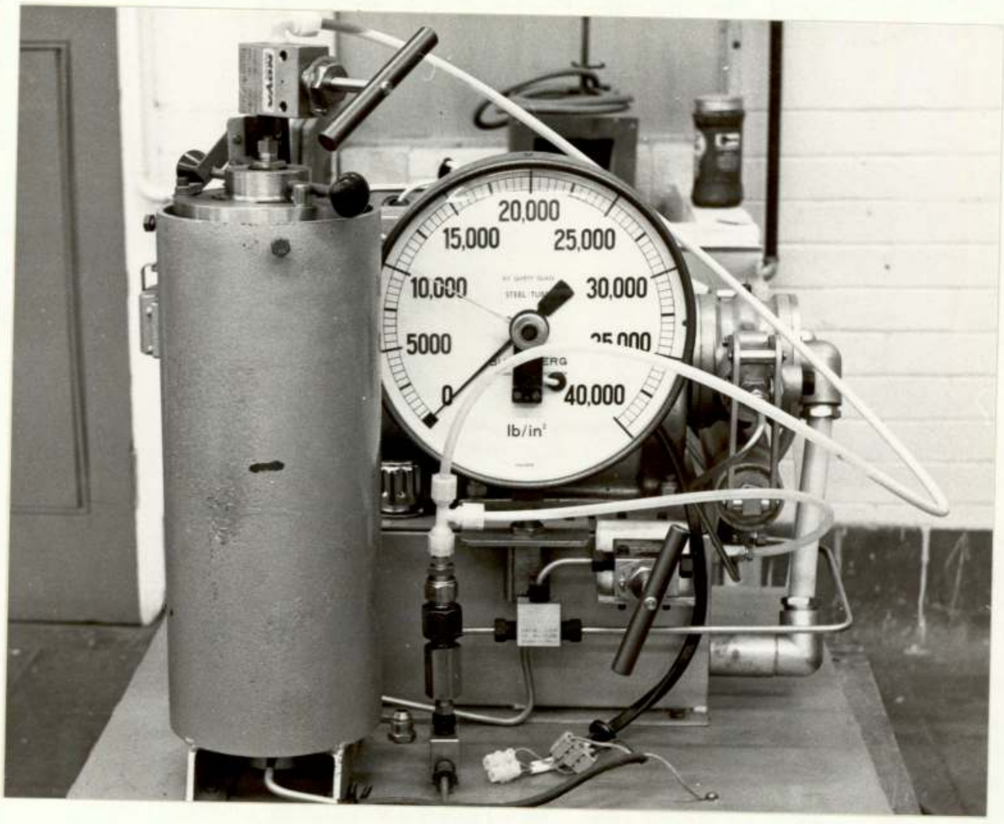

Plate 4.

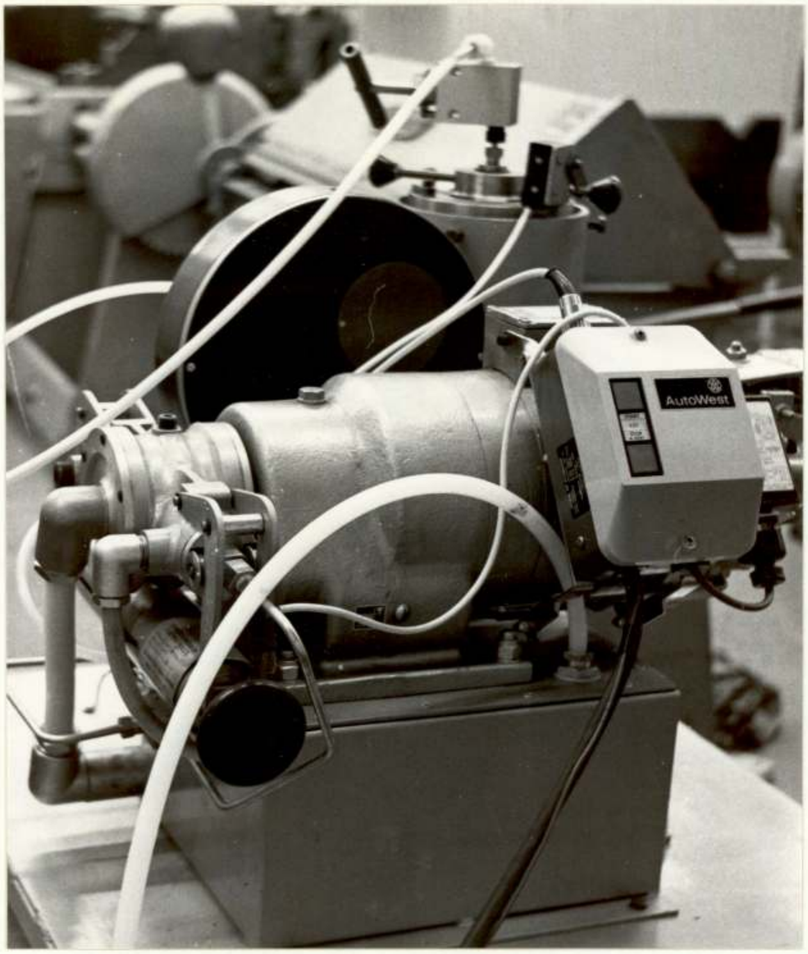

Plate 5.

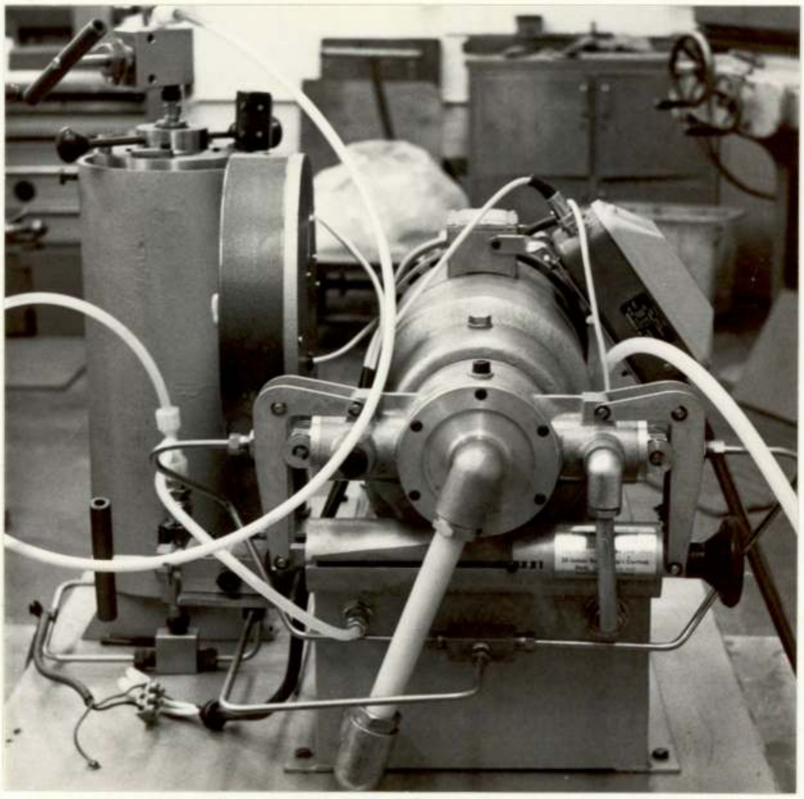

Plate 6.

Superfluous

3. 2. End caps and clamps.

When subjecting steel tubes to internal pressure there are no problems in sealing the ends since end caps can be simply welded into place, thus effecting a seal. This technique is not possible with glass reinforced plastic tubes and a problem encountered was one of sealing the ends of the tube satisfactorily. Wilson(43), who was working on high vaccuum systems, encountered the problem of sliding rods in and out of a high vaccuum system without breaking the seal. He produced a sliding seal and it was possible by careful design to utilise his ideas and to make an end cap capable of sealing the pressure in the tube.

Fig. 19 shows a cross section of this end cap and plates 7 and 8 show the assembled cap and its individual components. The internal pressure forces the rubber gasket against the wall of the tube; the greater the pressure the more effective is the seal. At high pressures it is possible for the tube wall to expand sufficiently to allow the rubber sealing ring to bend back and release the pressure. To minimise the risk of this occurring, mild steel clamps were designed. Plate 9 shows the assembled clamps.

The end seals were constructed of stainless steel (EN58J) and the rubber seals were a stiff neoprene. A compromise must be made between the need for a stiff rubber to minimise extrusion of the seal and an easily deformed rubber for flexibility when fitting. To hold the caps in position it is necessary to have

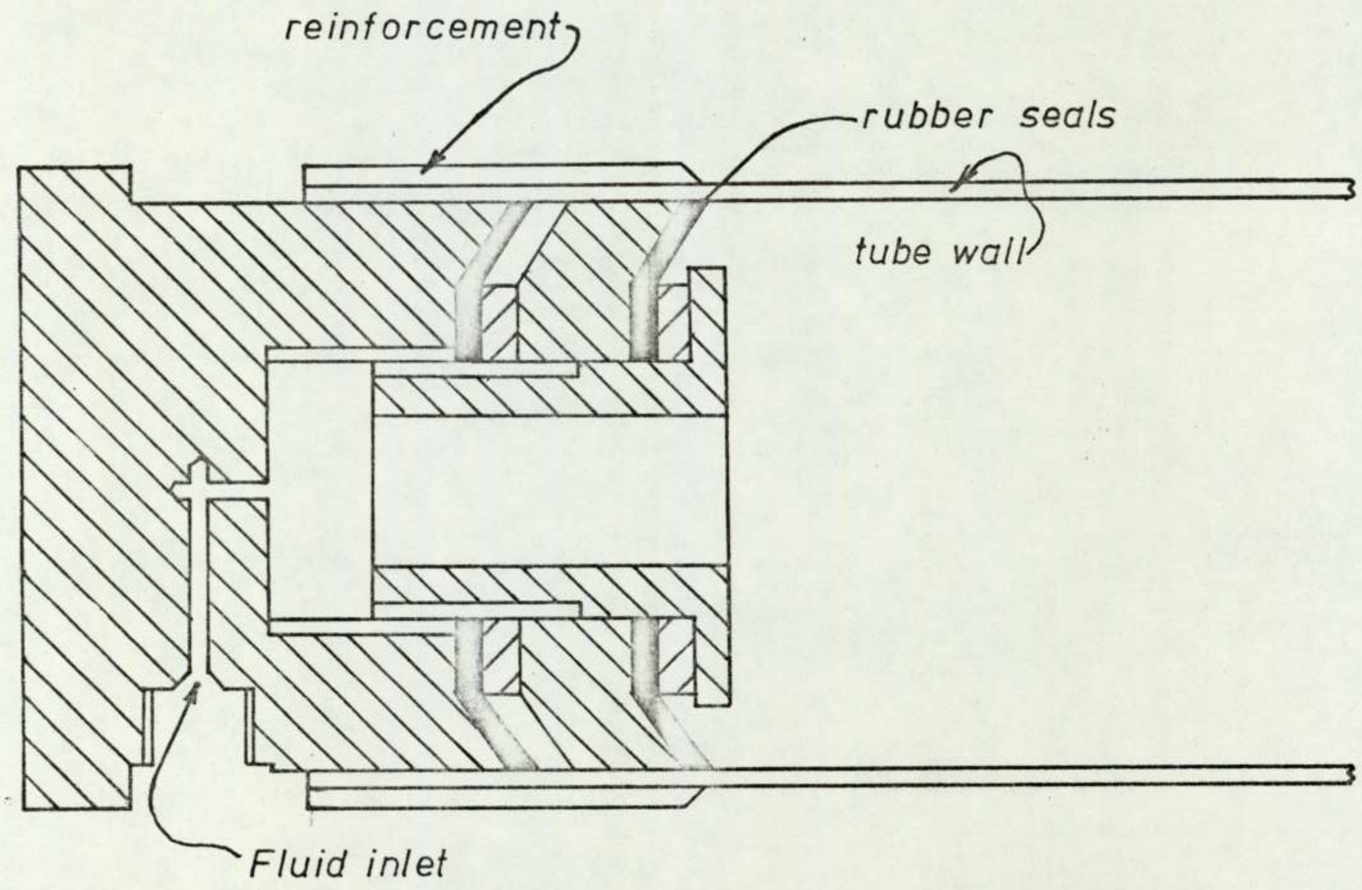

Fig.19. Cross section of end cap.

Plate 7.

Plate 8.

Plate 9.

tie bars and plates on the outside of the tube. Due to the presence of the tie bars the tube is not subjected to any longitudinal stress.

3. 3. Tie bars.

Plate 2 shows the tie bars and plates which retained the end caps in the tube. The working pressure for designing the bars and plates was 138 MNS/M^2. This pressure acting on the area of the end cap was equivalent to a force of 357 KNS. Sinc there were three tie bars each had to sustain a loading of 119 KNS. The material used for the bars was EN24Z, which has a yield strength of 1312 MNS/M^2. Designing at half yield strength the bars had to have a minimum diameter of 1.52 cms. (In fact 1.90 cms. diameter bar was used.)

3. 4. Steel end plates.

It was necessary to determine the minimum thickness of plate necessary such that the maximum stress in the plate was equal to half the yield strength of the material used. Since there are no readily available formulae to apply to the bending of a circular plate restrained by three bolts an approximation was necessary. An assumption was made that the plate behaves in a similar way to a three point supported plate, with a uniformly distributed load acting over a circular area in the centre. Formulae were not available for this case and a correction factor to convert the simply supported case to the three point supported case had first to be calculated.

From Raork(44):

1) Three point supported uniformly distributed load on a circular plate

$$\delta_{max} = \frac{0.307\ F\ a^2}{E\ h^3}$$

Where F = 178.26 KNS

a = 7.62 cms

$E = 206.85\ GNS/M^2$

$\text{ie } \delta_{max} = 1.54 \times 10^{-9}/h^3\ M^4$

2) Simply supported uniformly distributed load on a circular plate.

$$\delta_{max} = \frac{3\ F\ (m - 1)(5m + 1)\ a^2}{16\pi E\ m^2\ h^3}$$

Where m = 3

F, a and E as above

$\text{ie } \delta_{max} = 1.06 \times 10^{-9}/h^3\ M^4$

For the above figures the deflection for the three point supported plate is 1.54/1.06 times as great as the simply supported plate (i. e. 1.453). Within the sizes of plate to be used this correction factor will be accurate enough.

3) σ_{max} for simply supported uniform load over an area of 7.62 cms diameter in the centre of 15.24 cms diameter plate is given by:

$$\sigma_{max} = \frac{3F}{2\pi m h^2} \left(m + (m+1)\log(a/r_o) - \frac{(m-1)(r_o)^2}{4a^2} \right)$$

Correction factor for three point supported is 1.453

where F = 178.26 KNS

a = 7.62 cms

r_o = 3.81 cms

σ_{max} = 139 mns/m^2 at half yield strength (EN 3 B)

i. e. Thickness of plate must be a minimum of 3.56 cms.

(In fact 5 cms thick plates were used.)

Chapter 4.

4. Experimental Procedure.

The tubes were wound by Imperial Metals Industries, Ltd. Two glass types, 'E' glass and 'S' glass, were used for this, the properties of which were:

	density(gm/cc)	Roving	E_1 MN.M.$^{-2}$	ν_1
'E' glass	2.55	20 end	75800	0.20
'S' glass	2.54	30 end	97895	0.22

The resin types were:

	Supplier	Cure	E_m	ν_m
MY705/H906/DY062	CIBA GEIGY Ltd.	4hrs@180°C	2900	0.38
828/MNA/BDMA	SHELL Ltd.	4hrs@150°C	3100	0.34

The final densities of the resins were 1.31 and 1.22 gms/cc, respectively.

The continuous fibres were passed through a resin bath and wound on a Royalene covered mandrel, 7.5cms in diameter. Excess resin was brushed off continuously during the winding process. Woven glass fibre ribbon was wound around the ends of the tubes for reinforcement. Each tube was held on a lathe, by tapered metal blocks, and the reinforcement machined down to 8.5cms diameter ± 0.001cms.

The final tube was 55cms long and had a nominal wall thickness of 3mms. This resulted in tubes of about 8.3cms outside diameter due to the presence of the Royalene.

4. 1. Preparation of the tubes for testing.

4. 1. 1. Full through wall slots.

A hole 2mm in diameter was drilled half way along the tube. By use of a specially prepared hacksaw blade and guide a full through slot was cut to the necessary length. The slot was sharpened by a jeweller's saw blade. The dimensions of the slots are shown in Fig. 20. A thin sheet of annealed copper was bonded over the slot, on the inside of the tube, by means of epoxy resin to hold the pressure during testing. The copper membrane was held in position while the resin hardened by means of an inflatable rubber bag.

4. 1. 2. Part through wall slots.

The tube was held in a lathe by tapered metal blocks and a 0.75mm thick tool brought up to bear against it. The tool was wound in 0.1mm and scratched along the tube, thus forming a slot. This was repeated until a defect of the required depth was obtained. The dimensions of the slot are shown in Fig. 21. Since the process did not damage the Royalene lining, copper sheet was not needed to hold the pressure.

4. 1. 3. Knife edges.

These were made by machining a mild steel ring 8.9 cms outside diameter, 8.5 cms inside diameter and 4mm thick. Short lengths were cut out of the band and were filed to form the knife edge with a fine file. They were bonded on to the tube, a standard distance apart(3mm), by means of epoxy resin. Fig. 22 shows an isometric drawing of the knife edges in position on the tube.

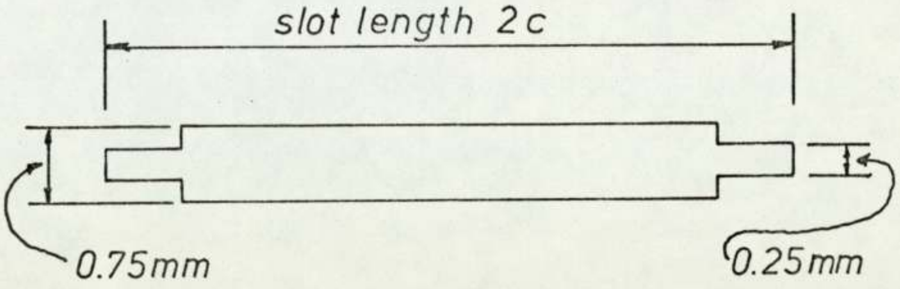

Fig. 20. Dimensions of full through slot.

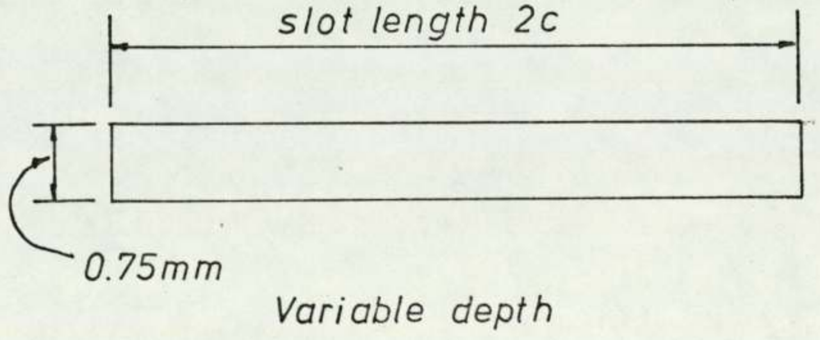

Fig. 21. Dimensions of part through slot.

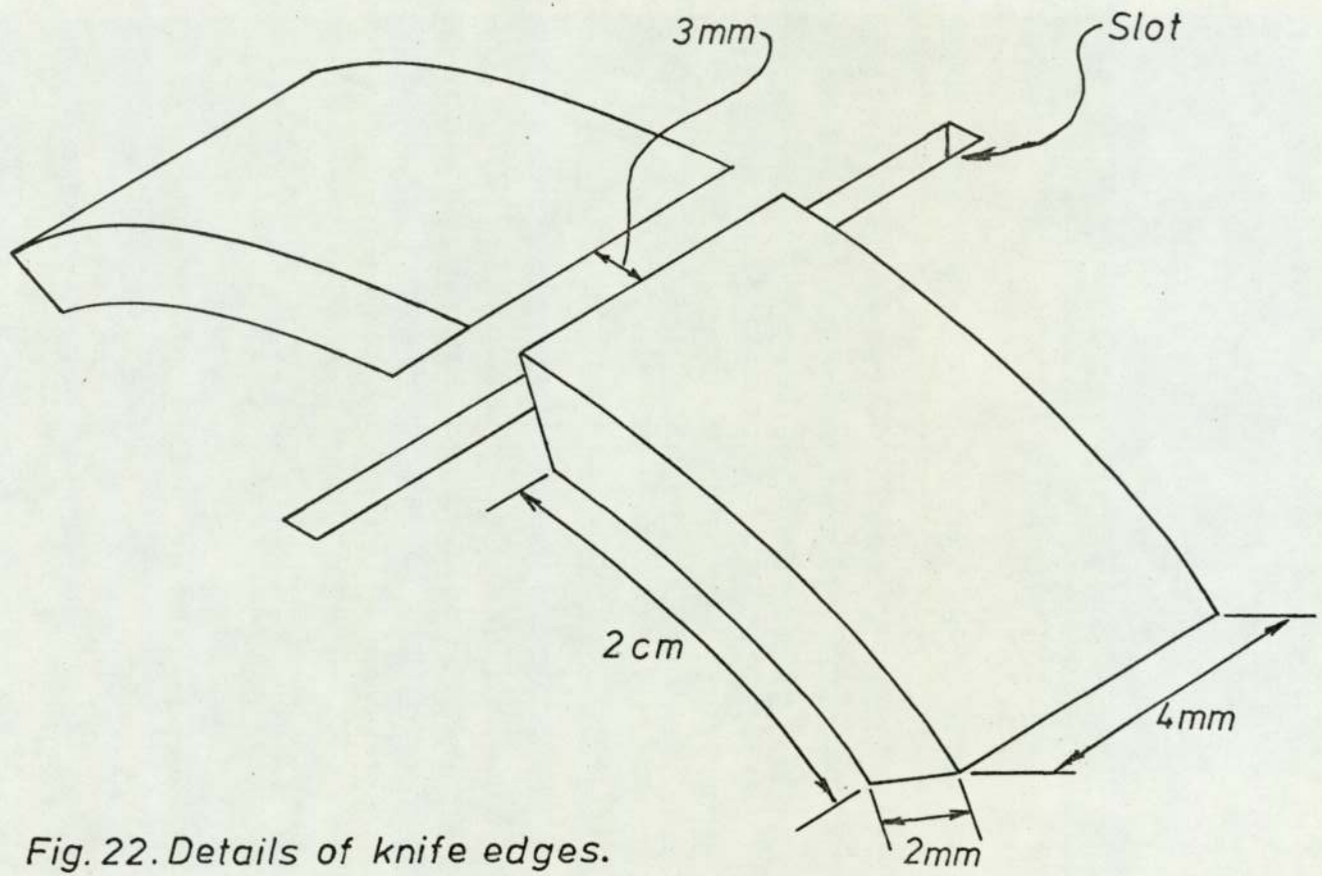

Fig. 22. Details of knife edges.

4. 1. 4. Measurement of tube dimensions.

Pieces were cut from the ends of each tube and the faces were polished by normal metallurgical techniques, finishing with metal polish. The metal polish etched the composite clearly defining the various layers. Using a travelling microscope the average inside and outside diameters, wall thicknesses and hoop layer thicknesses were determined.

4. 1. 5. Strain gauges.

Strain gauges were bonded to the tubes in the longitudinal and hoop directions by means of epoxy resin. For the tubes containing no defects an extra gauge 45° to the tube axis was also included to form a rectangular strain gauge rosette. Fine wires were soldered to each gauge and secured, by adhesive tape, to the walls of the tubes.

4. 1. 6. Measurement of volume fraction of fibres.

Samples of the tubes were cleaned and dried in an oven at $90^{\circ}C$ for 2 hours. They were weighed in air and weighed suspended in water. After subjecting them to $550^{\circ}C$ for 2 hours the resulting glass fibres were weighed to constant weight. From a knowledge of the glass and resin densities the volume fraction of fibres was determined.

4. 2. Calibration of the clip gauge.

The clip gauge was held by a points micrometer, whose jaws were separated by 2mm. Fig. 23 shows the clip gauge and the micrometer jaws. The output from the clip gauge and amplifier was fed into a digital voltmeter. A calibration chart was prepared by opening the micrometer by pre-set amounts and reading the out of balance e. m. f.'s on the digital voltmeter. Care was necessary to ensure the clip gauge did not slip out of the jaws. Calibration charts were obtained for all ranges of the amplifier. The most sensitive range was able to detect jaw openings of 0.02mm. The charts showed that the clip gauge was linear for all of the ranges used.

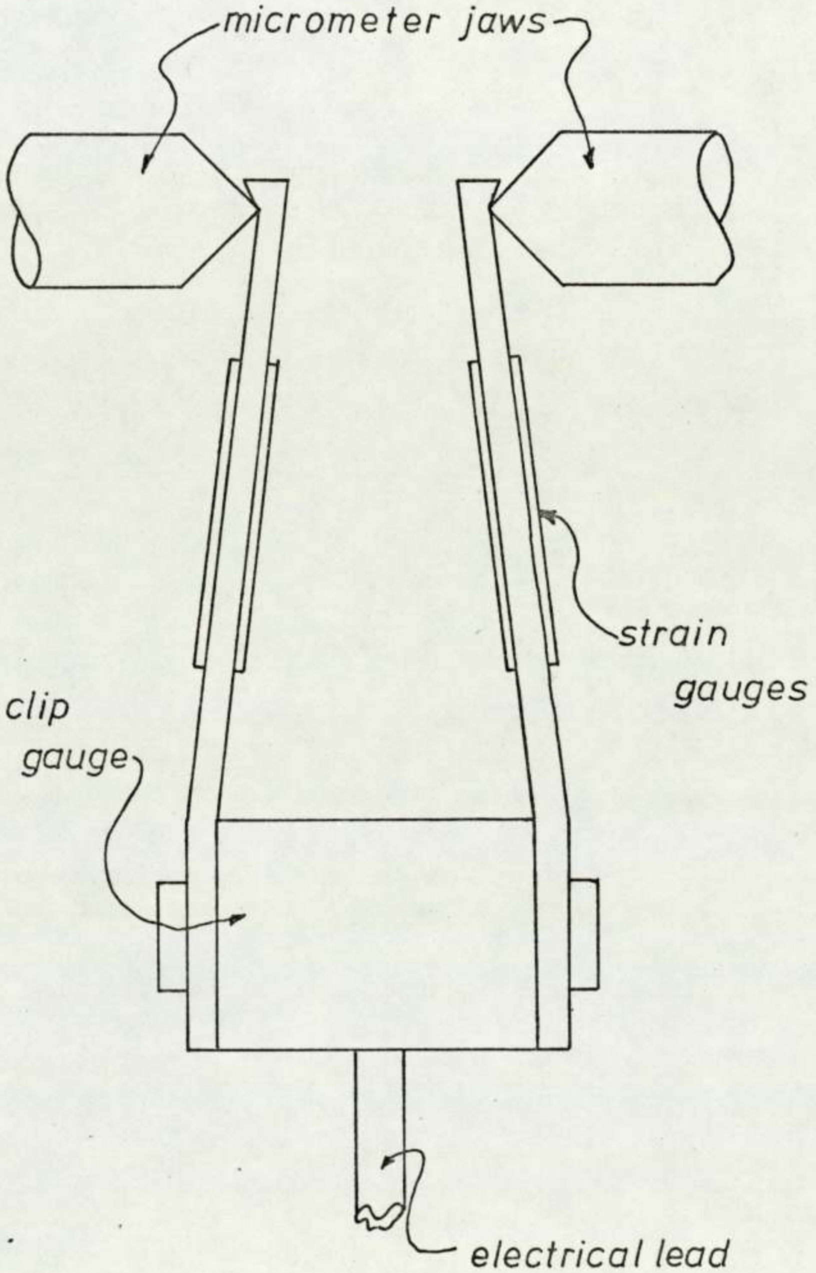

Fig. 23. Calibration of clip gauge.

4. 3. Determination of the longitudinal Young's modulii and Poisson's ratios.

A number of tubes were subjected to determine the longitudinal Young's modulii and Poisson's ratios. The base and top of each tube were machined flat and parallel and the tube subjected to axial compression on a 5 Ton Instron testing machine. The longitudinal and hoop strains were plotted, versus stress, on two Bryans X - Y recorders. The test was repeated three times to obtain average modulii and Poisson's ratios.

X

X

X

4. 4. Pressurisation of the tubes.

The end caps were carefully fitted into place in the ends of each tube and the whole stood in position on the end plate. The inlet and outlet lines were connected and tightened. Clamps were placed in position around the tube reinforcement and their bolts tightened. The six tie bar nuts were tightened using a torque wrench to minimise bending moments on the tube whilst it was under pressure. A camera, with flash attached, was assembled in front of the armour plated glass windows to photograph any interesting developments as the tube was pressurised.

4. 4. 1. Tubes without artificial defects.

The three strain gauges, forming the rosette, were each connected to the appropriate amplifier and the outputs from the strain gauges and the pressure transducer were fed into three Bryans X - Y recorders. The tubes were pressurised slowly and photographs were taken at known pressures.

4. 4. 2. Tubes with artificial defects.

The three Bryans recorders in this case recorded hoop strain, longitudinal strain and crack opening displacement on their X - axes and pressure on their Y - axes. The tubes were pressurised slowly and photographs were taken similarly to the tubes with defects absent.

4. 5. Compliance Testing.

The determination of K-calibration charts relies on some means of measuring the change in compliance of a system, with crack length. This compliance change was estimated in two ways:

1) The measurement of crack opening displacement, and

2) The measurement of volume change.

When pressurising the tubes graphs of crack opening displacement versus hoop stress were obtained. The slopes of these graphs were taken as the compliance of the tubes. For the crack opening displacement measurements the following assumptions were made:

1) That the tubes had similar elastic moduli,

2) That the tubes deformed evenly around the perimeter.

A strain gauge was attached opposite the slot on each pipe. The strain in this region was so obtained and used to estimate the volume change with pressure. The assumptions for this were:

1) That the strain in this region was the same as the strain would be for an uncracked tube,

2) That the tube deformed from and to a true circular cross section.

The increase in circumference was calculated from the strain observed and from a knowledge of the initial circumference. At the same pressure the crack opening displacement was known and added to this so that the final circumference was:

Final circumference = Initial circumference + elastic strain + C. O. D.

From this a new radius, R_2 could be calculated, i.e.

New radius R_2 = final circumference/2π

The volume change per unit length was taken as the difference between the volume calculated using R_2 and the initial volume of the tube. The volume changes were plotted against pressure and the slope $\Delta V/P$ obtained as another compliance measurement.

Chapter 5.

5. Results.

5. 1. Measurement of Young's modulus and Poisson's ratio.

Tube No.		Lay up	Fibre volume fraction	E_{11}	ν_{12}
WGE/33	1	± 20°	0.613	50440	0.481
	2	± 20°		56970	0.528
WGE/35	1	± 20°	0.608	45300	0.445
	2	± 20°		50390	0.502
WGE/36	1	± 20°	0.604	44270	0.483
	2	± 20°		45390	0.526
WGE/41	1	± 40°	0.641	21760	0.616
	2	± 40°		20200	0.635
WGE/42	1	± 40°	0.644	20160	0.716
	2	± 40°		25570	0.543
WGE/43	1	± 40°	0.636	18460	0.533
	2	± 40°		21910	0.640
WGE/37		± 20°	0.609	55080	0.513
WGE/38		± 20°	0.613	70110	0.623
WGE/39		± 20°	0.616	65250	0.561
WGE/40		± 20°	0.606	57310	0.571
WGE/44		± 40°	0.622	20970	0.531
WGE/45		± 40°	0.652	28110	0.575
WGE/3B		7/9 ± 20° 2/9 ± 90°	0.623	42190	0.266
WGE/5B		7/9 ± 20° 2/9 ± 90°	0.626	41750	0.275

Table 3. Longitudinal Young's modulii and Poisson's ratios for tubes with 20° and 40° helix angle.

(Modulii values are in MNS/M^2)

Tube No.	Fibre volume fraction	E_{11}	ν_{12}
A 1	0.683	23250	0.271
2		35220	0.198
3		33900	0.216
4		33380	0.200
5		26000	0.223
B 1	0.681	34310	0.247
2		24150	0.187
3		20050	0.117
4		E. F.	E. F.
5		29650	0.218
C 1	0.673	20350	0.157
2		28820	0.223
3		36780	0.241
4		31760	E. F.
5		30600	0.176
D 1	0.689	38670	0.223
2		35910	0.215
3		42050	0.241
4		36370	0.208
5		33880	0.180
E 1	0.687	25200	0.323
2		24860	0.240
3		26900	0.198
4		26060	0.181
5		24210	0.185
F 1	0.698	37320	0.210
2		38610	0.226
3		38080	0.323
4		37830	0.170
5		37070	0.200
G 1	0.722	37040	0.230
2		38300	0.250
3		43020	0.242
4		35380	0.265
5		45540	0.212

Table 4. Hoop Young's modulii and Poisson's ratios for tubes with 50% ± 30° and 50% ± 90° lay up. (Modulii values are in MNS/M^2)

Tube No.	Fibre volume fraction	E_{11}	ν_{12}
H 1	0.650	19030	0.233
2		20550	0.286
3		21770	0.273
4		21510	0.279
5		31470	0.396
J 1	0.649	17650	0.228
2		23740	0.259
3		20980	0.232
4		20020	0.191
5		20780	0.200
K 1	0.672	27400	0.421
2		21620	0.305
3		21620	0.277
4		18450	0.240
5		20690	0.406
L 1	0.649	20380	0.295
2		17070	0.198
3		18450	0.231
4		20420	0.249
5		18780	0.214
M 1	0.627	19420	0.273
2		19580	0.302
3		17060	0.247
4		19280	0.305
5		18710	0.259

Table 5. Hoop Young's modulii and Poisson's ratios for tubes with ± 30° helix angle.

(Modulii values are in MNS/M^2)

5. 2. Defect types.

Table 6 shows the types of defect and the tube numbers for the results which follow in 5. 3. The distance between the pressure seals was 0.495M in all cases.

Lay up	No defect	Full through wall defect	$\frac{1}{2}$ through wall defect	$\frac{1}{4}$ through wall defect
± 30°	H1 - H5	J1 - J5 L1 - L5	K1 - K5 M1 - M5	N/A
50% ± 30° 50% ± 90°	A1 E1 - E5	A2 - A5 D1 - D5	B1 - B5 F1 - F5	C1 - C5 G1 - G5

Table 6. Defect types for the tubes subjected to failure by internal pressure.

5. 3. Compliance and failure measurements.

Tube No.	c (cms)	$\frac{C.O.D.}{\sigma_H} \times 10^6$ $M/MN/M^2$	$\frac{\Delta V}{P} \times 10^6$ $M^3/MN/M^2$	P^* MN/M^2	σ_H^* MN/M^2
A 1	-	-	-	48.91	682.23
2	1.198	3.95	6.47	2.89	40.33
3	0.821	1.71	5.33	E. F.	E. F.
4	1.802	6.29	8.08	1.61	22.41
5	2.232	6.83	9.63	0.68	9.52
B 1	0.612	1.10	4.70	4.02	51.87
2	1.154	2.15	7.03	2.01	26.57
3	2.291	3.08	8.75	1.48	19.56
4	1.701	3.46	6.70	1.65	21.47
5	2.240	9.02	9.74	2.19	28.91
C 1	1.945	1.58	7.66	E. F.	E. F.
2	1.378	1.27	5.44	3.09	40.15
3	3.084	2.32	4.98	2.25	29.20
4	0.552	1.14	4.95	6.43	83.43
5	0.913	1.33	5.22	3.53	45.47
D 1	1.027	3.11	6.05	2.17	32.36
2	0.711	1.81	5.56	3.53	52.73
3	2.113	10.35	10.06	1.37	19.01
4	1.852	9.57	10.37	1.2	17.98
5	1.437	5.58	8.18	2.81	29.96
E 1	-	-	-	50.23	721.97
2	-	-	-	47.59	683.97
3	-	-	-	52.21	750.47
4.	-	-	-	47.32	680.17
5	-	-	-	50.23	721.97
F 1	0.617	0.473	4.38	3.29	47.54
2	1.017	2.12	5.22	2.41	34.79
3	1.432	2.50	5.51	1.57	22.61
4	1.687	2.77	5.70	1.41	20.29
5	2.194	3.46	6.20	1.00	14.50

Table 7. Compliance and failure measurement for the A to M series of tubes. (E. F. is equipment failure)

Table 7. continued

G 1	0.655	1.03	4.75	4.50	65.31
2	1.027	1.01	4.60	4.58	66.48
3	1.372	0.87	4.08	2.61	37.90
4	1.979	1.03	4.89	4.18	60.65
5	2.436	1.27	4.12	2.61	37.90
H 1	-	-	-	4.98	66.42
2	-	-	-	4.86	64.82
3	-	-	-	5.10	68.03
4	-	-	-	5.10	68.03
5	-	-	-	5.06	67.49
J 1	0.539	1.81	9.78	2.17	30.86
2	1.019	3.36	8.41	1.37	19.43
3	1.441	5.92	10.81	0.95	13.49
4	1.93	7.51	12.13	0.42	5.94
5	2.475	10.87	13.88	0.45	6.40
K 1	0.659	2.23	6.92	2.01	28.72
2	0.959	1.75	8.14	1.61	22.97
3	1.619	2.74	8.73	1.31	18.72
4	2.248	2.22	9.66	1.49	21.25
5	2.819	2.46	8.89	1.08	15.39
L 1	0.503	1.61	8.09	2.17	29.47
2	0.748	1.96	9.70	1.49	20.19
3	1.233	2.92	9.60	0.68	9.17
4	1.732	3.15	8.96	0.48	6.55
5	3.010	7.06	11.84	0.37	5.02
M 1	0.49	1.22	7.95	2.73	35.64
2	1.305	2.28	8.47	1.57	20.44
3	1.942	2.06	9.43	1.37	17.82
4	2.439	3.15	9.06	1.29	16.77
5	3.207	2.34	10.64	1.16	15.09

Chapter 6.

6. Discussion of the results.

6. 1. Young's modulus and Poisson's ratio.

6. 1. 1. Predictions of compressive E_{11} and ν_{12} for 'S' glass in a resin matrix of 828/MNA/BDMA (Shell Ltd.) using the theories of Wallis(11) and Tsai(13).

Appropriate values of Young's modulus and Poisson's ratio were calculated using the theories of Wallis and Tsai. The following physical constants were used for this:

	'S' glass	Resin 828/MNA/BDMA
Young's modulus	97895 MN/M^2	3100 MN/M^2
Poisson's ratio	0.22	0.34

For the theory of Tsai the contiguity factor, C was taken as 0.2 as suggested by Tsai for this type of tube. Twenty tubes were subjected to axial compression and the values of E_{11} and ν_{12} so obtained were compared to the theoretical ones obtained from the two theories. The observed and calculated values were subjected to statistical analysis to obtain the variance, standard deviation and mean of the differences between the observed and calculated figures.

6. 1. 1. 1. Longitudinal Young's modulus, E_{11}.

Table 8 shows the observed and calculated values of longitudinal Young's modulus and Fig. 24 illustrates a comparison of these for the two theories. The line at 45°, passing through the origin of each graph, is the line which would exist if there

Tube No.	E_{11} (observed)	E_{11} (after Wallis)	E_{11} (after Tsai)
WGE/33 1	50440	43450	36710
2	56970	43450	36710
WGE/35 1	45300	43090	36330
2	50390	43090	36330
WGE/36 1	44270	42800	36030
2	45390	42800	36030
WGE/41 1	21760	13700	21510
2	20200	13700	21510
WGE/42 1	20160	13800	21670
2	25570	13800	21670
WGE/43 1	18460	13550	21240
2	21910	13550	21240
WGE/37	55080	43160	36410
WGE/38	70110	43450	36710
WGE/39	65250	43670	36940
WGE/40	57310	42940	36180
WGE/44	20970	13130	20510
WGE/45	28110	14060	22110
WGE/3B	42190	39970	49830
WGE/5B	41750	40160	50090

Table 8. Variation of observed and calculated values of E_{11} for 'S' glass in a resin matrix of 828/MNA/BDMA (Shell Ltd.)

(Modulii values are in MN/M^2)

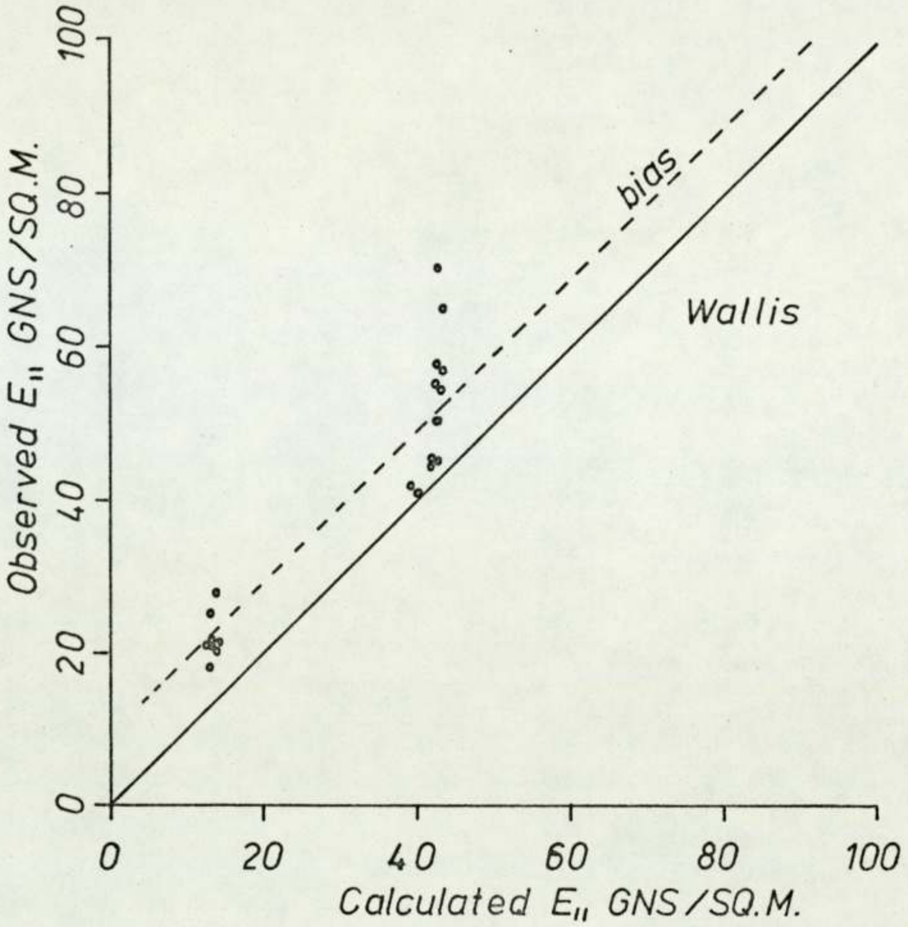

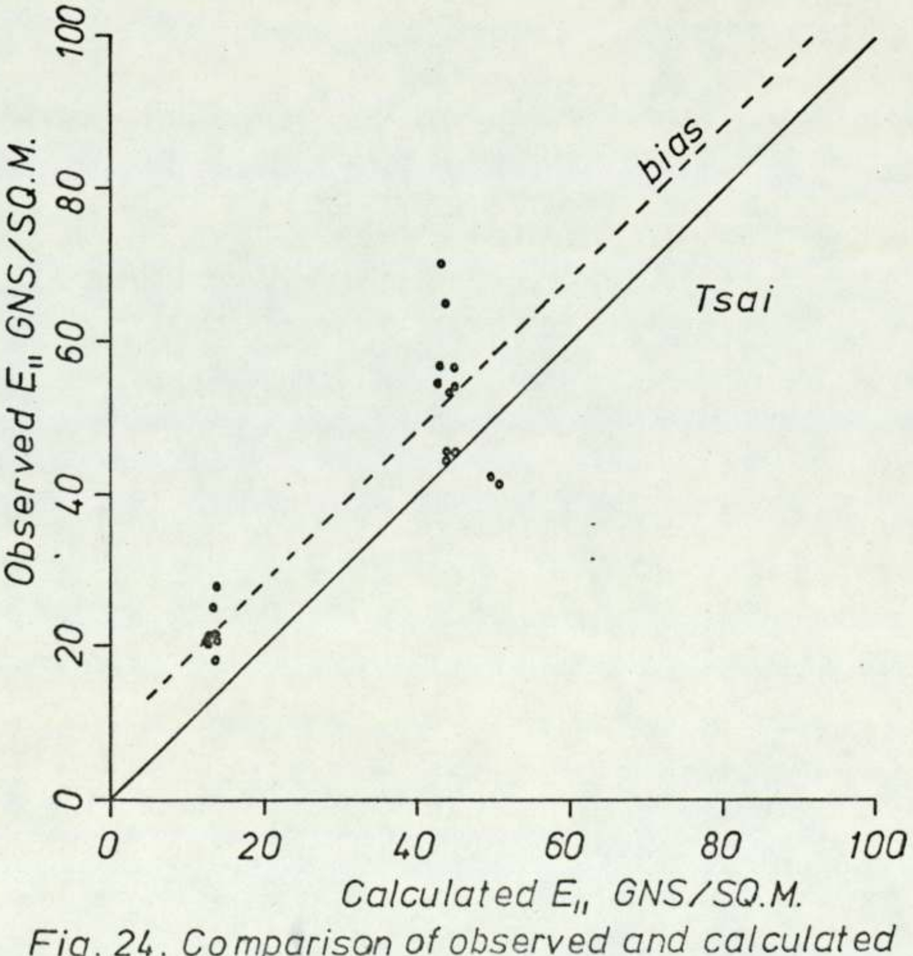

Fig. 24. Comparison of observed and calculated values of E_{11} for 'S' Glass in 828IMNAIBDMA resin.

were no difference between observed and calculated E_{11}. The results of the statistical analysis are as follows:

	Variance of differences	Standard deviation of differences	Mean of differences
Theory of Wallis	1.30×10^8	1.14×10^4	9005
Theory of Tsai	2.07×10^8	1.44×10^4	8290

Ratio of the variances = 1.60

'F' ratio at the 95% confidence level = 2.51

The 'F' test is a test for the equality of population variances. The ratio of the variances was the ratio of the larger to the smaller sample variances. The 'F' test was used to determine whether there was a significant difference between the predictions from the two theories. In this case since two theories are being compared it is necessary to obtain the 2.5% significance 'F' ratio from tables for 95% confidence.

Since the ratio of the variances was less than the 'F' ratio obtained from tables there was no significant difference between each theory at the 95% confidence level. The means of the differences gave an indication of the 'bias' of the observed results. This is shown by the broken line on the graphs and indicates that the observed values were, in general, higher than the calculated values by about 8-9000MN/m^2 for both theories. To obtain the most accurate estimate of E_{11} it is necessary to add the mean of the differences to the predicted value. The quantity so obtained is subject to 95% confidence limit of about ± 22000MN/m^2 for Wallis and ± 28000 MN/m^2 for Tsai. The results show that the theories, though reasonable, are not exact and neither is significantly better than the other for the prediction of E_{11}.

6. 1. 1. 2. Longitudinal Poisson's ratio, ν_{12}.

Table 9 shows the observed and calculated values of Poisson's ratio and Fig. 25 illustrates a comparison of these for the two theories. The 45^0 lines on each graph are the lines which would exist for no differences between observed and calculated ν_{12}.

Tube No.		ν_{12} (observed)	ν_{12} (after Wallis)	ν_{12} (after Tsai)
WGE/33	1	0.481	0.783	0.307
	2	0.528	0.783	0.307
WGE/35	1	0.445	0.785	0.307
	2	0.502	0.785	0.307
WGE/36	1	0.483	0.787	0.308
	2	0.526	0.787	0.308
WGE/41	1	0.616	0.878	0.282
	2	0.635	0.878	0.282
WGE/42	1	0.716	0.877	0.282
	2	0.543	0.877	0.282
WGE/43	1	0.533	0.880	0.282
	2	0.640	0.880	0.282
WGE/37		0.513	0.785	0.307
WGE/38		0.623	0.783	0.307
WGE/39		0.561	0.781	0.307
WGE/40		0.571	0.786	0.308
WGE/44		0.531	0.884	0.282
WGE/45		0.575	0.874	0.283
WGE/3B		0.266	0.316	0.281
WGE/5B		0.275	0.316	0.281

Table 9. Variation of observed and calculated values of ν_{12} for 'S' glass in a resin matrix of 828/MNA/BDMA (Shell Ltd.)

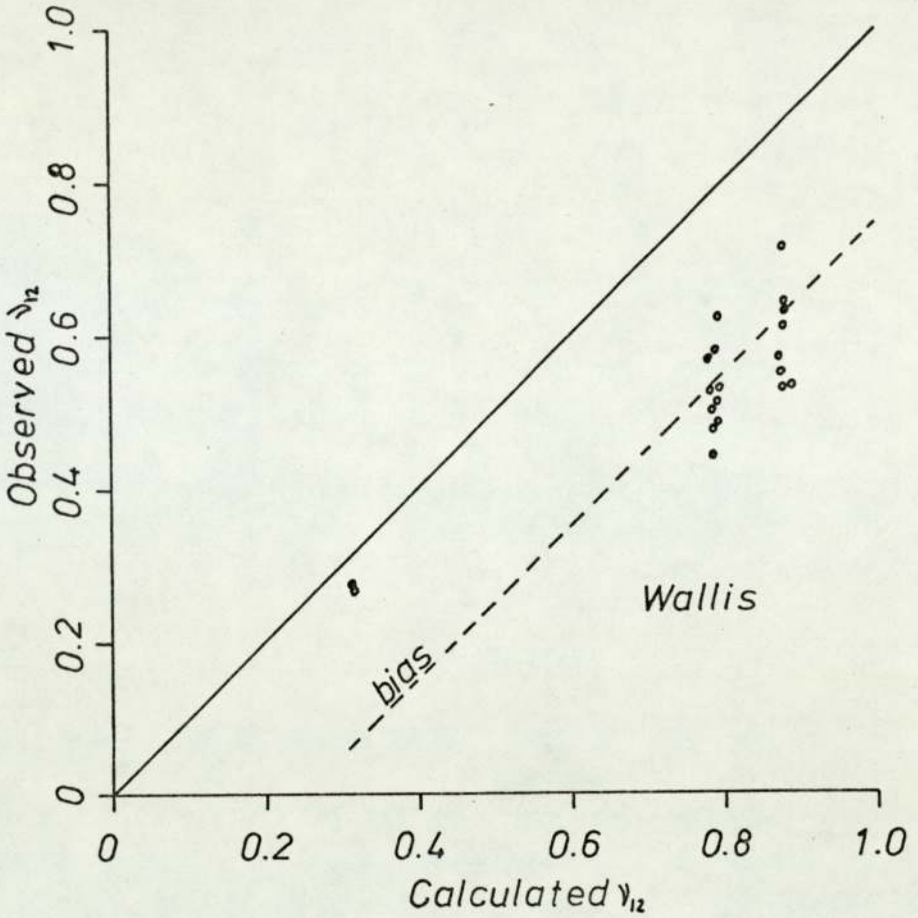

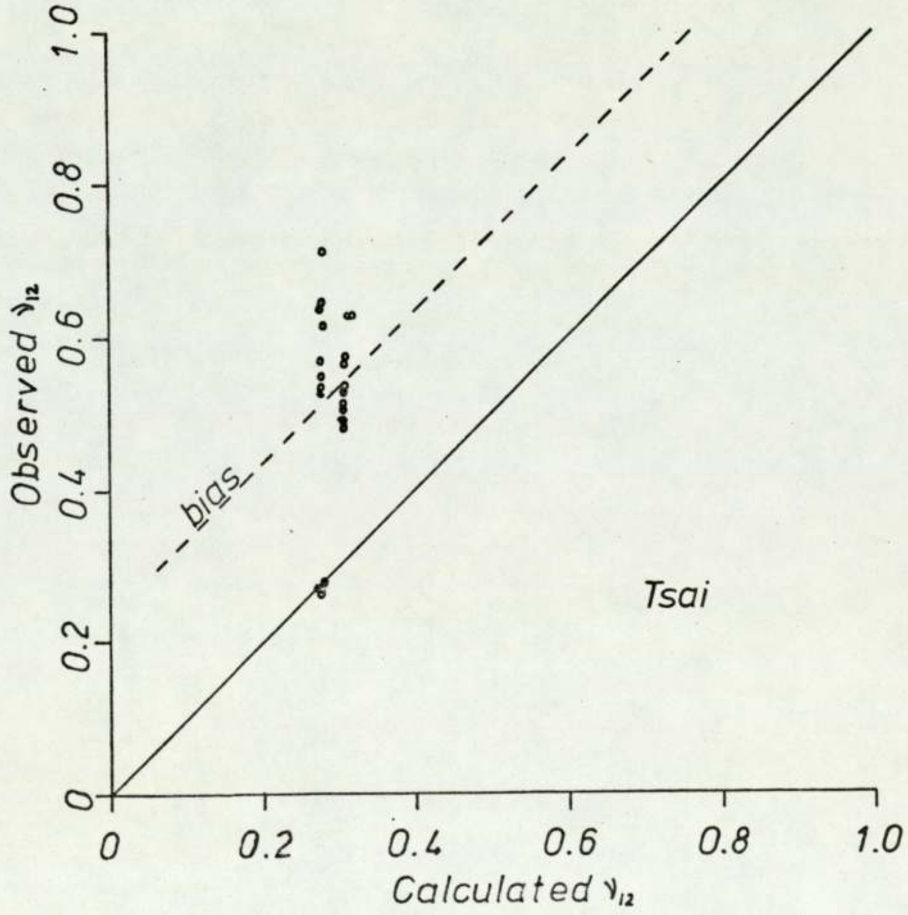

Fig. 25. Comparison of observed and calculated values of ν_{12} for 'S' glass in 828IMNAIBDMA resin.

The results of the statistical analysis are as follows:

	Variance of differences	Standard deviation of differences	Mean of differences
Theory of Wallis	0.07	0.27	- 0.247
Theory of Tsai	0.07	0.26	0.234

Ratio of the variances = 1.03

'F' ratio at the 95% confidence level = 2.51

Since the ratio of the variances was less than the 'F' ratio obtained from the tables, there was no significant difference between each theory at the 95% confidence level. The means of differences gave an indication of the 'bias' of the observed results. It is seen that the Wallis predictions had a higher 'bias' and the Tsai predictions a lower one. To obtain the most accurate estimate of ν_{12} it is necessary to add the mean of the differences to the predicted value. The quantity so obtained is subject to 95% confidence limits of about ± 0.5 for both theories. Such estimates are unacceptable and it is clear that the theories are not very useful for the prediction of ν_{12} for these types of tube.

6. 1. 2. Prediction of E_{22} and ν_{21} for 'E' glass in a resin matrix of MY705/HY906/DY062 (CIBA-GEIGY) using the theories of Wallis(11) and Tsai(13).

Appropriate values of Young's modulus and Poisson's ratio were calculated using the theories of Wallis and Tsai. The following physical constants were used for this:

	'E' glass	Resin MY705/HY906/DY062
Young's modulus	75800 MN/M^2	2900 MN/M^2
Poisson's ratio	0.20	0.38

For the theory of Tsai the contiguity factor, C was taken as 0.2 as suggested by Tsai for this type of tube. Sixty tubes were subjected to internal pressure and the values of E_{22} and ν_{21}, so obtained, were compared to the theoretical ones obtained from the two theories. The sixty results were reduced to twelve lots of five and average values used for the comparisons. The observed and calculated values were subjected to statistical analysis to obtain the variance, standard deviation and mean of the differences between the observed and calculated figures.

6. 1. 2. 1. Hoop Young's modulus, E_{22}.

Table 10 shows the observed and calculated values of hoop Young's modulus and Fig. 26 illustrates a comparison of these for the two theories. The 45° lines, on each graph, are the lines which would exist for no differences between observed and calculated E_{22}. The results of the statistical analysis are as follows:

	Variance of differences	Standard deviation of differences	Mean of differences
Theory of Wallis	7.16×10^8	8.46×10^3	4400
Theory of Tsai	6.89×10^8	8.30×10^3	- 1700

Tube No.	E_{22} (observed)	E_{22} (after Wallis)	E_{22} (after Tsai)
A 1-5	28350	32180	39160
B 1-5	27040	32080	39030
C 1-5	29600	31680	38500
D 1-5	37380	32490	39560
E 1-5	25450	32390	39430
F 1-5	37780	32950	40170
G 1-5	39860	34230	41840
H 1-5	22870	9645	14355
J 1-5	20630	9620	15240
K 1-5	21960	10210	15240
L 1-5	19020	9620	14320
M 1-5	18810	9120	13500

Table 10. Variation of observed and calculated values of E_{22} for 'E' glass in a resin matrix of MY705/HY906/DY062 (CIBA-GEIGY) (Modulii values are in MNS/M^2)

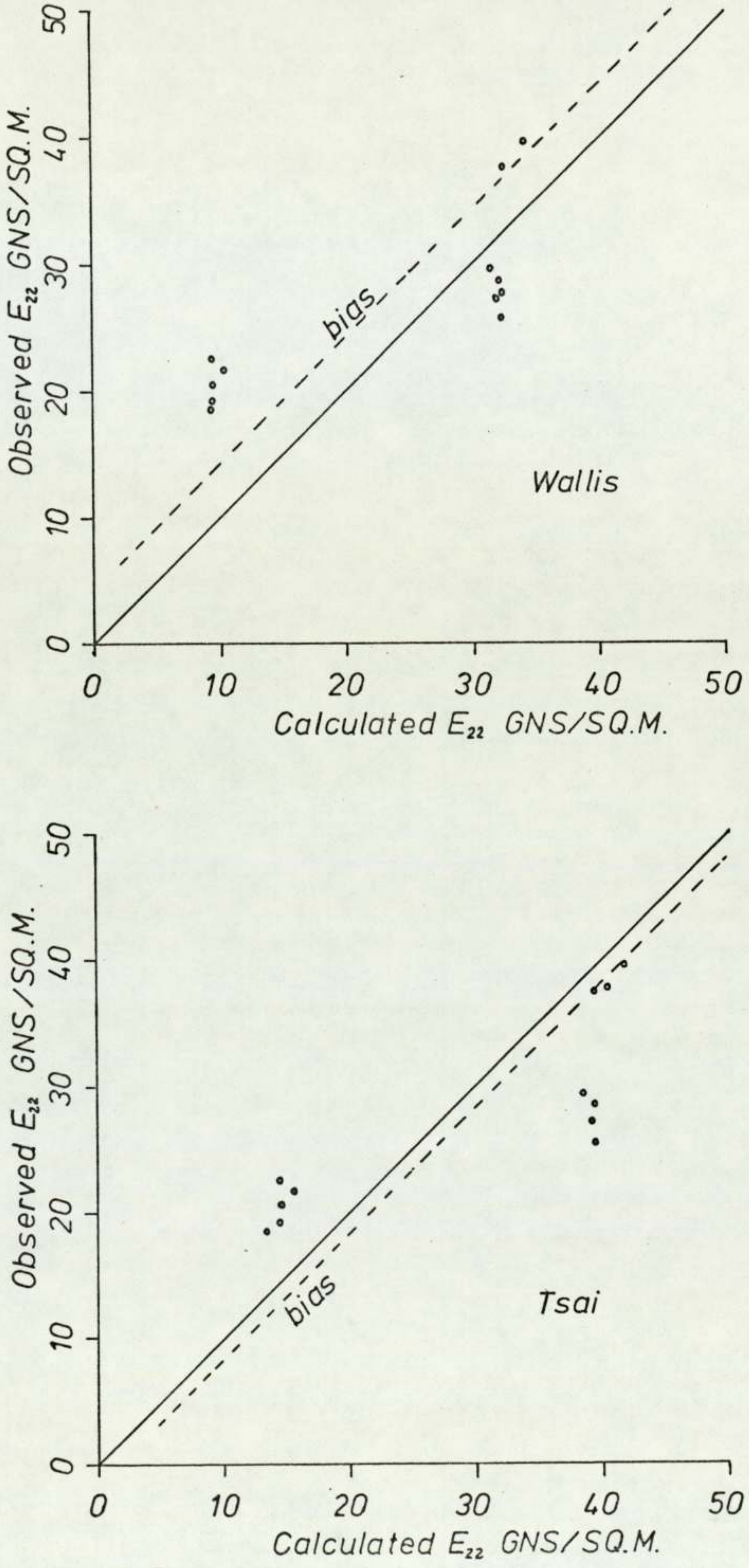

Fig. 26. Comparison of observed and calculated values of E_{22} for 'E' glass in MY705/HY906/DY062 resin.

Ratio of the variances = 1.04

'F' ratio at the 95% confidence level = 3.48

Since the ratio of the variances was less than the 'F' ratio obtained from tables, there was no significant difference between the two theories at the 95% confidence level. In general, the predictions for tubes containing hoop windings were more accurate than those without. The means of the differences gave an indication of the 'bias' of the observed values. It is seen that the predictions by Wallis were lower than the observed results and vice versa for the predictions of Tsai. The means of the differences and the standard deviations indicated that the predictions of E_{22} for this system were more accurate than the predictions of E_{11} for the 'S' glass system.

To obtain the most accurate estimate of E_{22} it is necessary to add the means of differences to the predicted value. The quantity so obtained is subject to 95% confidence limits of about $\pm$ 16000 MN/M^2 for the two theories. The predictions of E_{22} for the plain tubes appeared to be worse than the predictions for tubes containing hoop windings.

6. 1. 2. 2. Hoop Poisson's ratio, ν_{21}.

Table 11 shows the observed and calculated values of hoop Poisson's ratio and Fig. 27 illustrates a comparison of these for the two theories. The 45° lines on each graph are the lines which would exist for no differences between observed and calculated values of ν_{21}. The results of the statistical analysis were as follows:

Tube No.	ν_{21} (observed)	ν_{21} (after Wallis)	ν_{21} (after Tsai)
A 1-5	0.222	0.289	0.283
B 1-5	0.192	0.289	0.283
C 1-5	0.199	0.289	0.284
D 1-5	0.213	0.289	0.282
E 1-5	0.225	0.289	0.282
F 1-5	0.226	0.289	0.281
G 1-5	0.240	0.288	0.279
H 1-5	0.293	0.375	0.194
J 1-5	0.222	0.375	0.194
K 1-5	0.330	0.374	0.195
L 1-5	0.239	0.375	0.194
M 1-5	0.277	0.376	0.193

Table 11. Variation of observed and calculated values of ν_{21} for 'E' glass in a resin matrix of MY 705/HY906/DY062 (CIBA-GEIGY)

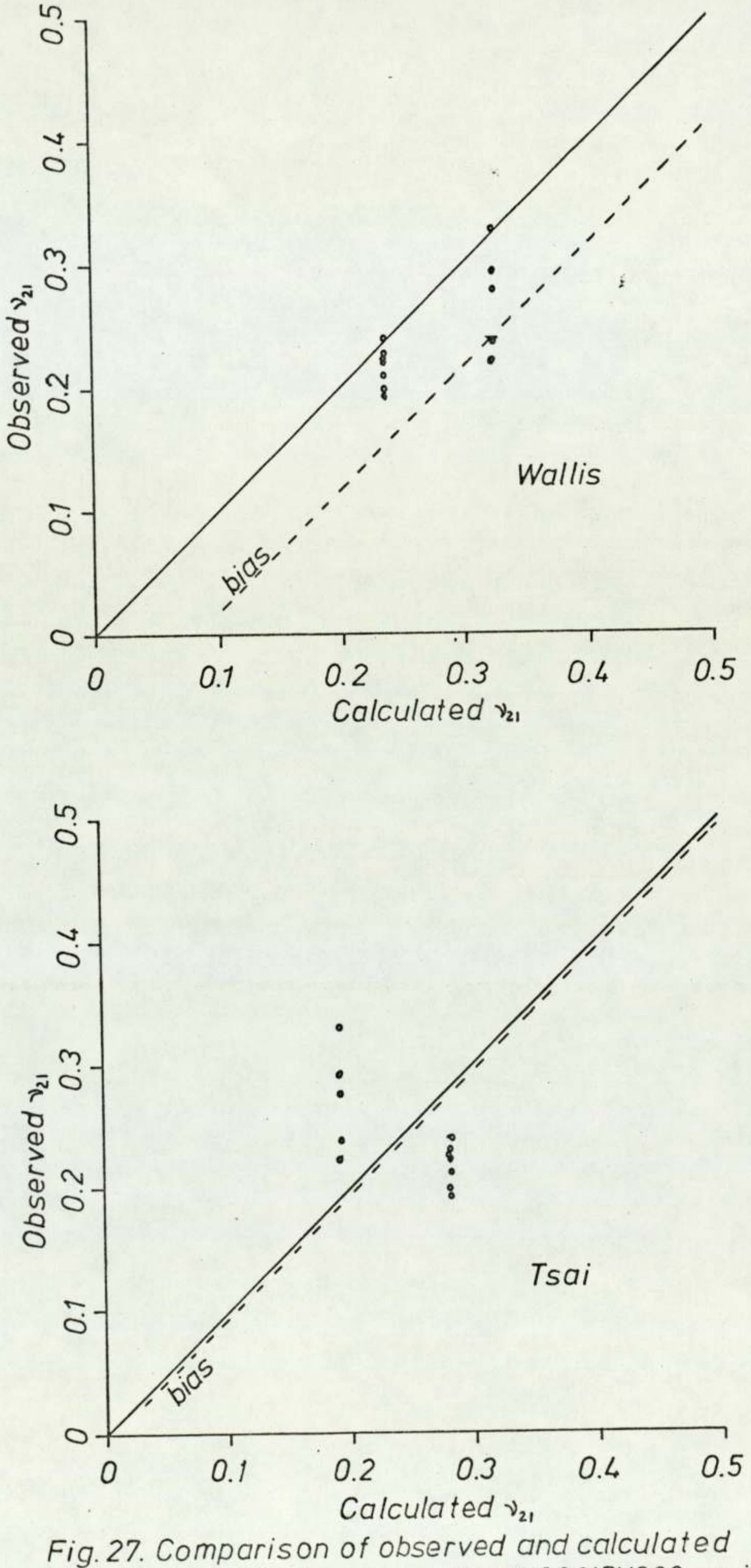

Fig. 27. Comparison of observed and calculated values of ν_{21} for 'E' glass in MY705/HY906/DY062 resin.

	Variance of differences	Standard deviation of differences	Mean of differences
Theory of Wallis	0.009	0.095	- 0.085
Theory of Tsai	0.006	0.080	- 0.005

Ratio of the variances = 1.50

'F' ratio at the 95% confidence level = 3.48

Since the ratio of the variances was less than the 'F' ratio obtained from tables, there was no significant difference between the two theories at the 95% confidence level. The means of the differences gave an indication of the 'bias' of the observed results. The 'bias' indicates that the observed results were, in general, lower than the calculated ones, for both theories. To obtain the most accurate estimate of ν_{21} it is necessary to add the mean of the differences to the predicted value. The quantity so obtained is subject to 95% confidence limits of about ± 0.16 - 0.19 for the two theories. In general, predictions of ν_{21}, although higher than the observed values were more reasonable than predictions of ν_{12}.

6. 2. Compliance measurements.

When determining fracture toughness data for isotropic and elastically homogenous materials, it is necessary to have a knowledge of the change of compliance with crack length for a given geometry. For such a material the compliance increases with crack length for most geometries. The compliance versus crack length curves are analysed to obtain geometrical factors for use in computing values of K_c. These calibration curves are applicable to a wide range of isotropic materials, but Barnby and Spencer (35) have shown that they are not necessarily applicable to fibre reinforced materials. Further it is possible, by careful choice of specimen, to observe compliance decreasing with increasing crack length. It was necessary to carry out compliance tests, on the material which was the subject of this work, to establish the premise that compliance would increase with increase in crack length. Intuitively this was expected, but the material was so anisotropic and subject to micro-geometrical effects that it could not be assumed.

Two methods of compliance measurement were investigated for this material. The first was a crack opening displacement measurement which was determined from first principles. The measurement of compliance was the slope of the graph of hoop stress versus crack opening displacement of the crack when the tube was pressurised. The other compliance measurement was the slope of the graph of pressure versus the volume change per unit length of the tube obtained during pressurising. A similar measurement of compliance as a volume change was made by Underwood et Al and is described in reference 45. The method used here is an analogous approach based on the same principles and the details of this can be found on page 37.

6. 2. 1. Crack opening displacement measurements.

The absolute value of crack opening displacement was measured by means of a calibrated clip gauge. The compliance was taken as the slope of the line obtained by plotting hoop stress against crack opening displacement for initial pressurising of the tube, i. e. C.O.D./σ_H. Figs. 28,29,30,31 and 32 show graphs of compliance versus half axial crack length for each tube type and defect depth. For isotropic materials, graphs of compliance versus crack length take the form of a curve. These curves usually cover the c/L range of 0.0 to 0.6. The first part of the curve, in the range of c/L = 0 to c/L = 0.1, is normally quite flat and only after about c/L = 0.2 are rapid increases of compliance with crack length shown. The range of c/L which this work covers is limited to a maximum c/L of 0.1. The points were considered to be representative of the straight line section of the compliance curve and the data subjected to linear regression analysis to obtain the lines of best fit. The results of this were as follows:

	Intercept	Slope	Regression coefficient	Degrees of freedom
K and M tubes	1.65×10^{-6}	3.35×10^{-5}	0.592	9
J and L tubes	8.07×10^{-8}	3.10×10^{-4}	0.837	9
C and G tubes	7.38×10^{-7}	3.57×10^{-5}	0.701	9
B and F tubes	-8.95×10^{-7}	2.62×10^{-4}	0.718	9
A and D tubes	-1.92×10^{-6}	5.04×10^{-4}	0.902	8

In all cases the regression coefficient was significant at the 95% level.

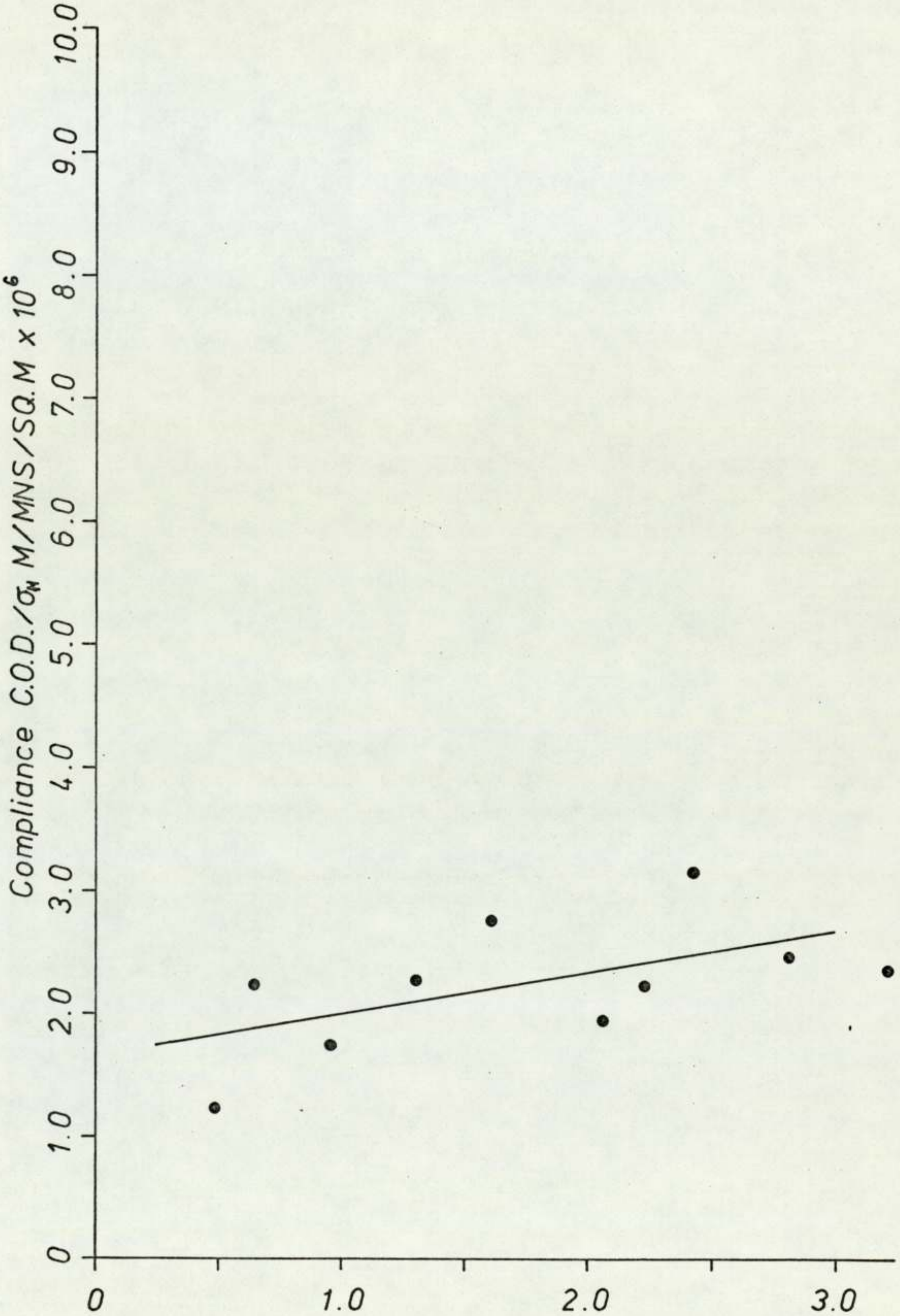

Fig. 28. Compliance v. crack length for K and M tubes.

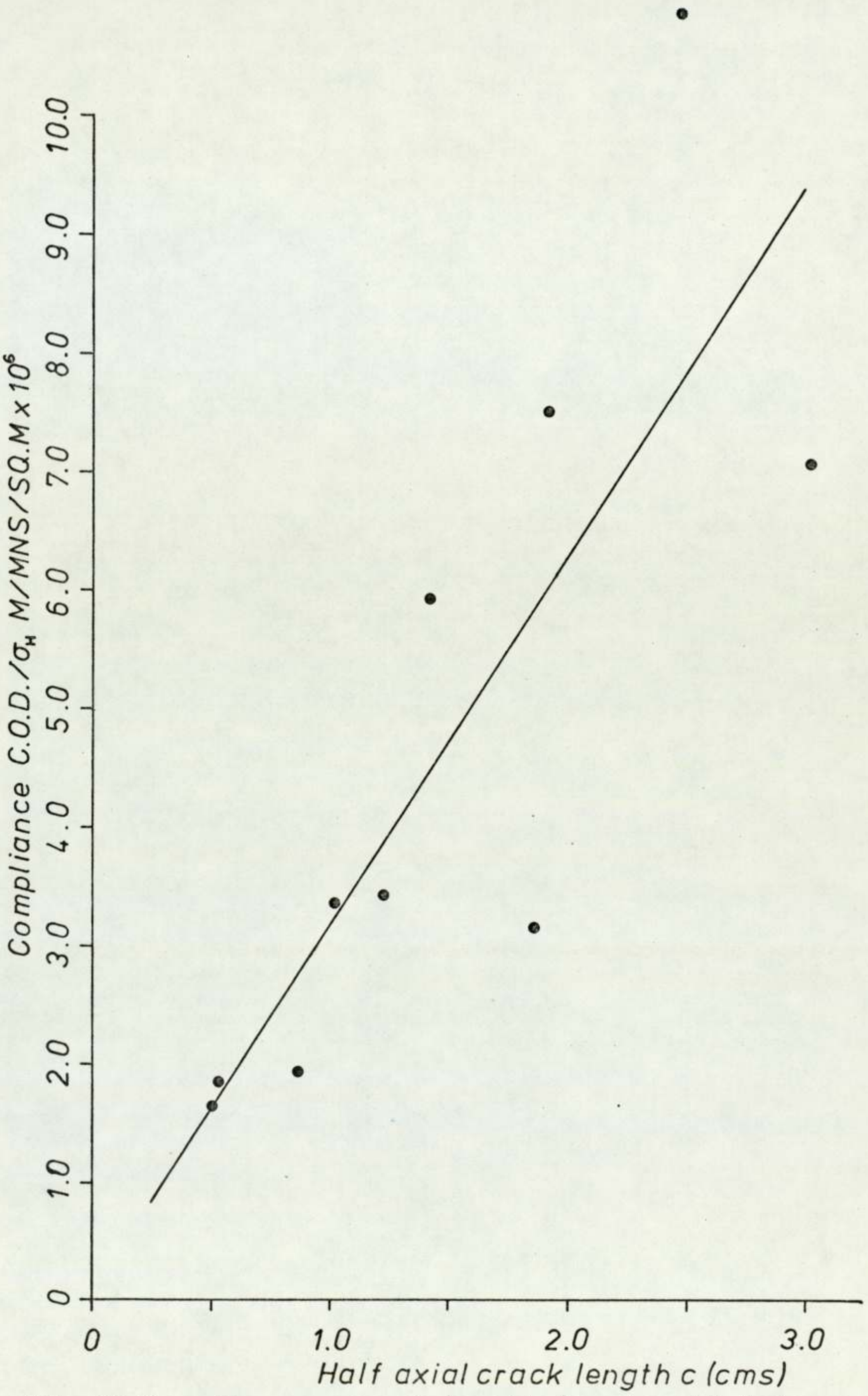

Fig.29. Compliance v. crack length for J and L tubes.

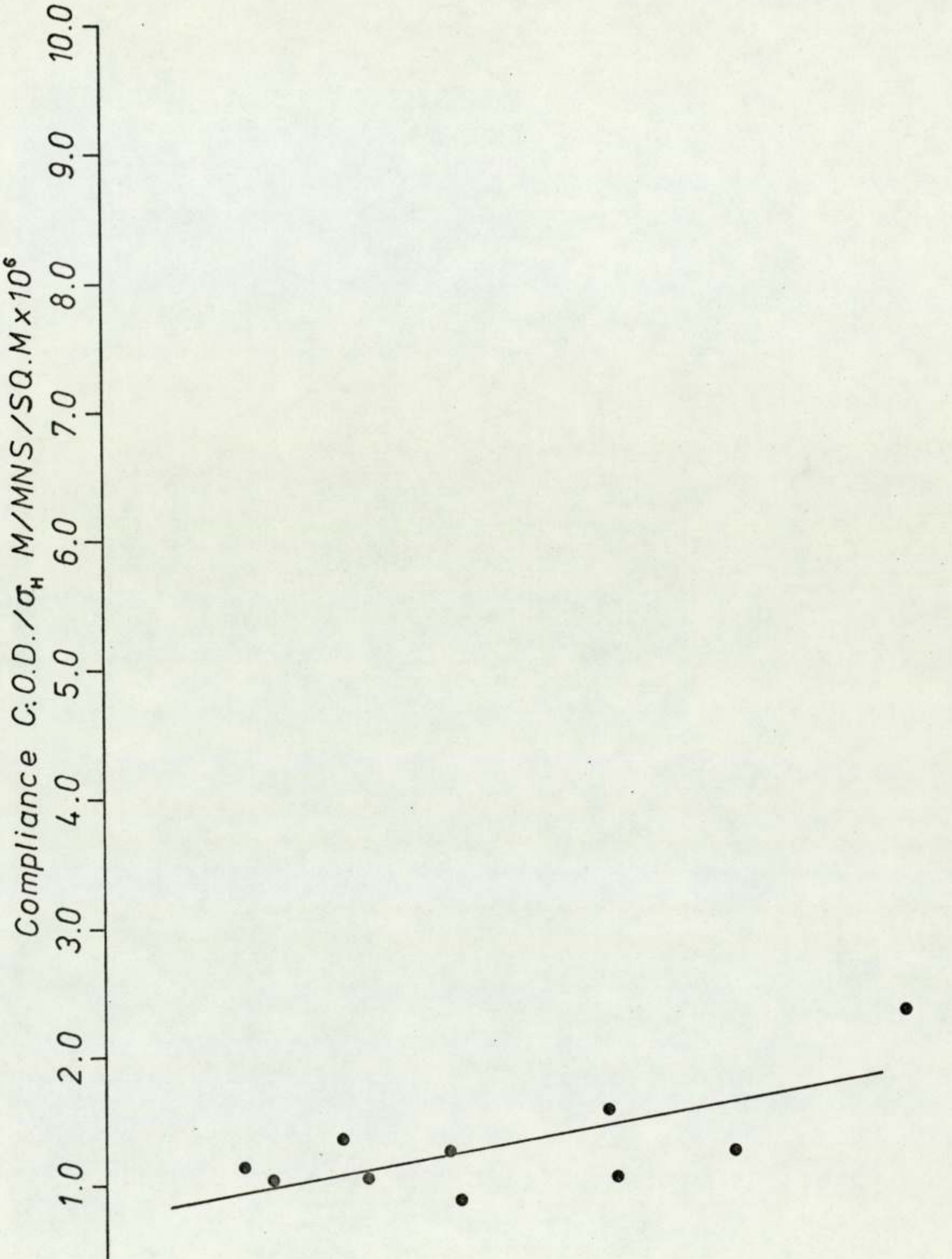

Fig. 30. Compliance v. crack length for C and G tubes.

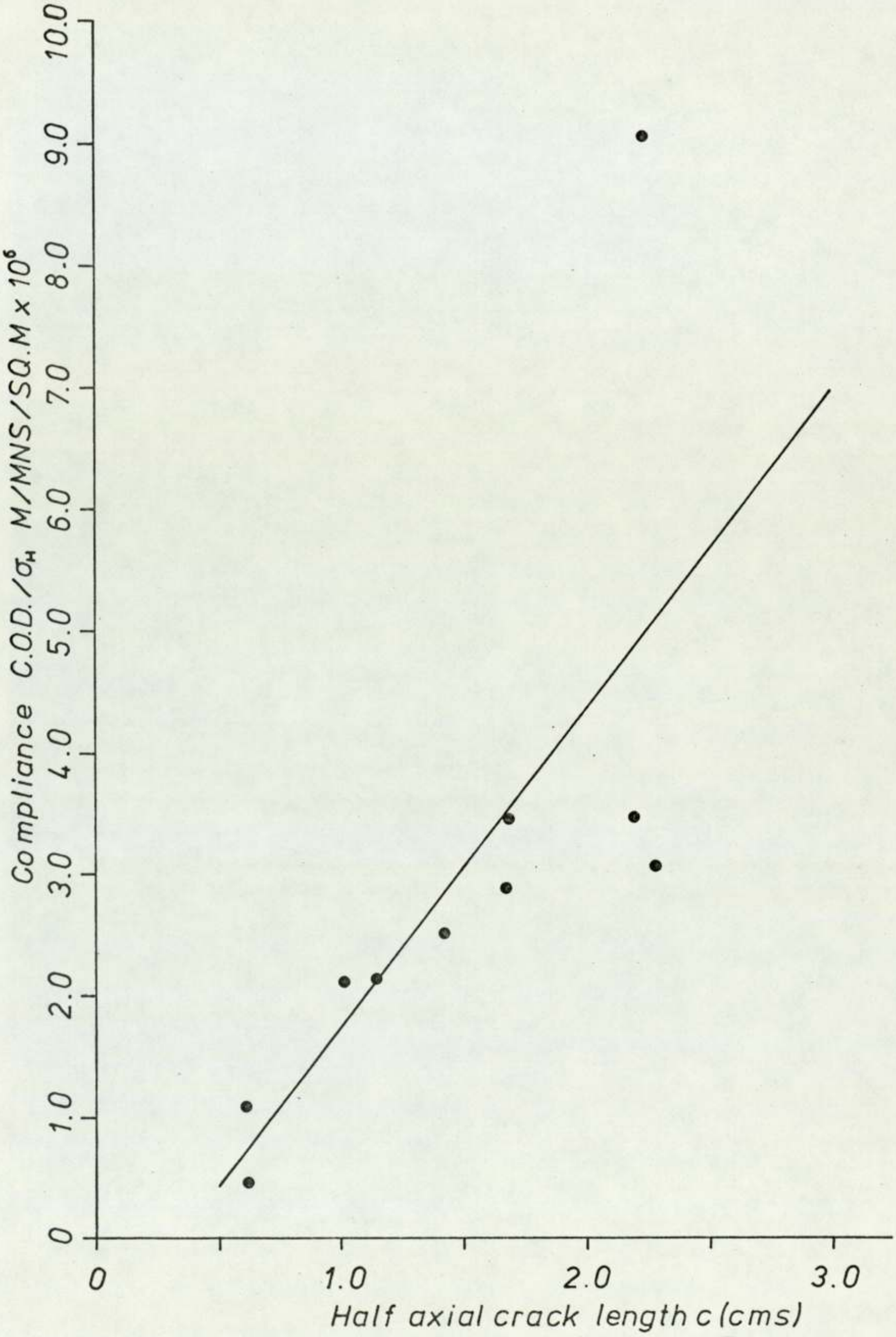

Fig. 31. Compliance v. crack length for B and F tubes.

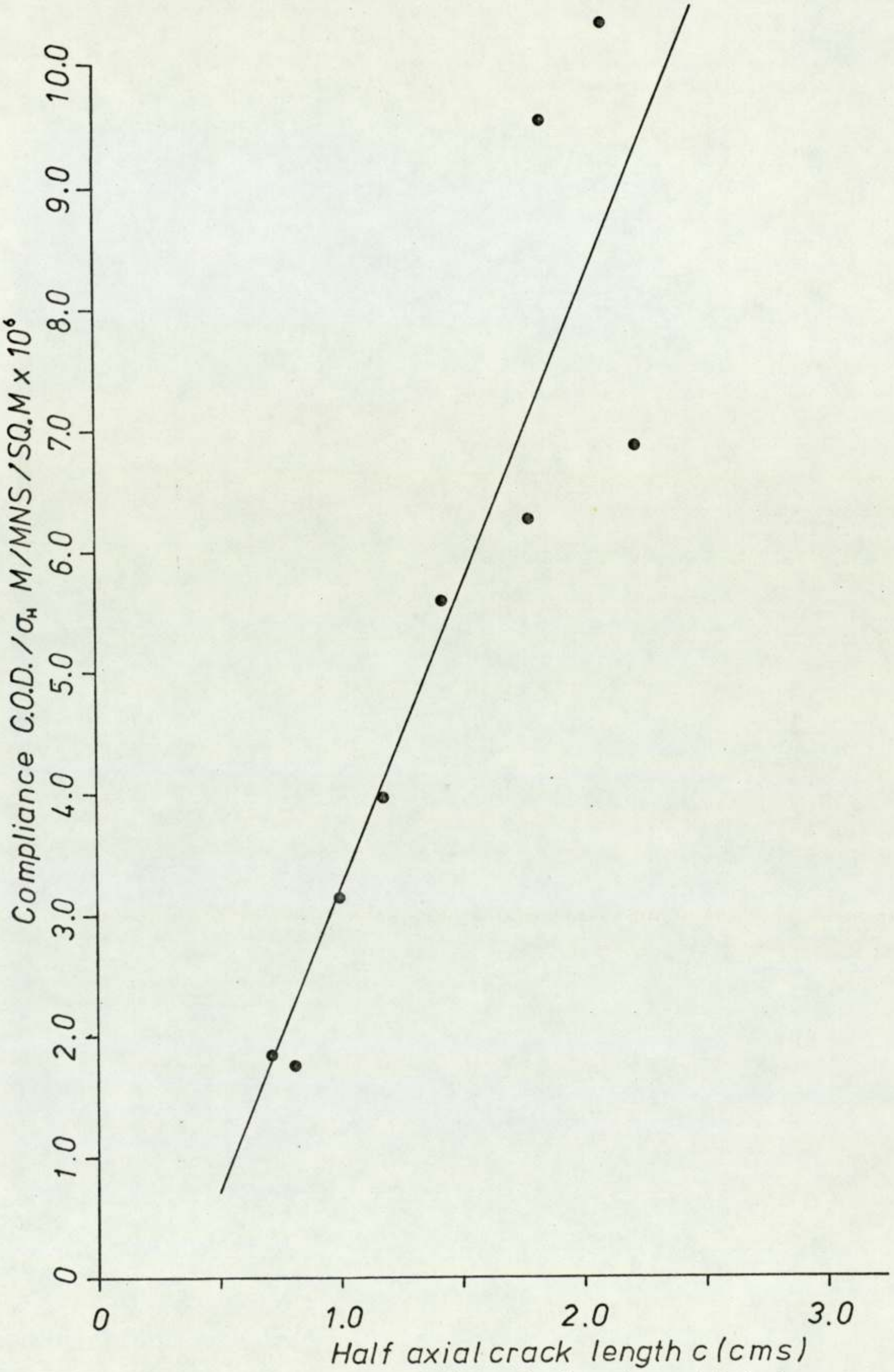

Fig. 32. Compliance v. crack length for A and D tubes.

Examination of the graphs revealed that, for each tube type, the compliance increased with increasing crack length. This was confirmed by the above regression analysis. The rate of change of compliance with crack length was clearly greater, the greater the slot depth. Scatter was shown around the regression lines and it is important to try and establish the source of this.

It may be assumed that no significant error was made in the measurement of the slot length, 2c. The slot length was accurately measured by means of a travelling microscope. The measurement of the crack opening displacement was accurate since it depended on a previously calibrated clip gauge. During calibration it was found that the output from the clip gauge was linear over all ranges and sensitive enough to measure the displacement to ± 0.02mm. Errors which may have arisen in the magnitude of the hoop stress depended upon three measurements. These were, the measurement of the wall thicknesses and inside diameters of the tubes and the pressure. The pressure was measured by means of a transducer and was accurate to ± 0.1%. The wall thickness and inside diameter were subject to local variations. During curing the Royalene lining was subject to local contractions and this, coupled with the method of manufacture of the tubes, caused variations in wall thickness and inside diameter of as much as 15%. For the quarter and half through wall slots, the accuracy of the compliance measurements was affected adversely and this was reflected in the correlation coefficients, which increased with slot depth. Taking all these deviations into account, the probable error on σ_H was estimated as ± 13%. Although this was a significant error, it was not enough to explain the scatter involved.

The scatter probably arose from local material variations in the tubes. The Young's modulus and Poisson's ratio measurements showed variations from tube to tube, and the volume fraction measurements were not constant. The superimposition of these factors on the compliance measurements may explain the scatter involved.

6. 2. 2. Volume change measurements.

The change in volume/unit length was calculated from the change in the perimeter due to elastic strain and the opening of the slot. The elastic strain was obtained from a knowledge of the hoop modulus, E_{22} and the hoop stress. This assumed that the tube deformed uniformly, despite the presence of the slot. The compliance was taken as the slope of the linear portion of the pressure versus volume change graph, obtained at the start of pressurising.

Figs. 33, 34, 35, 36 and 37 show the graphs of compliance versus half axial crack length for each tube type and defect depth. For similar reasons to those described in 6. 2. 1., the data was assumed to be representative of a linear function and was subjected to regression analysis with the following results:

	Intercept	Slope	Regression coefficient	Degrees of freedom
K and M tubes	7.1×10^{-6}	9.56×10^{-5}	0.862	9
J and L tubes	7.86×10^{-6}	1.68×10^{-4}	0.766	9
C and G tubes	4.91×10^{-6}	1.06×10^{-5}	0.857	9
B and F tubes	3.19×10^{-6}	2.14×10^{-4}	0.790	9
A and D tubes	2.89×10^{-6}	3.31×10^{-4}	0.942	8

In all cases the regression coefficients were significant at the 95% confidence level.

For each tube type the compliance increased with crack length and this increase was greater, the greater the slot depth.

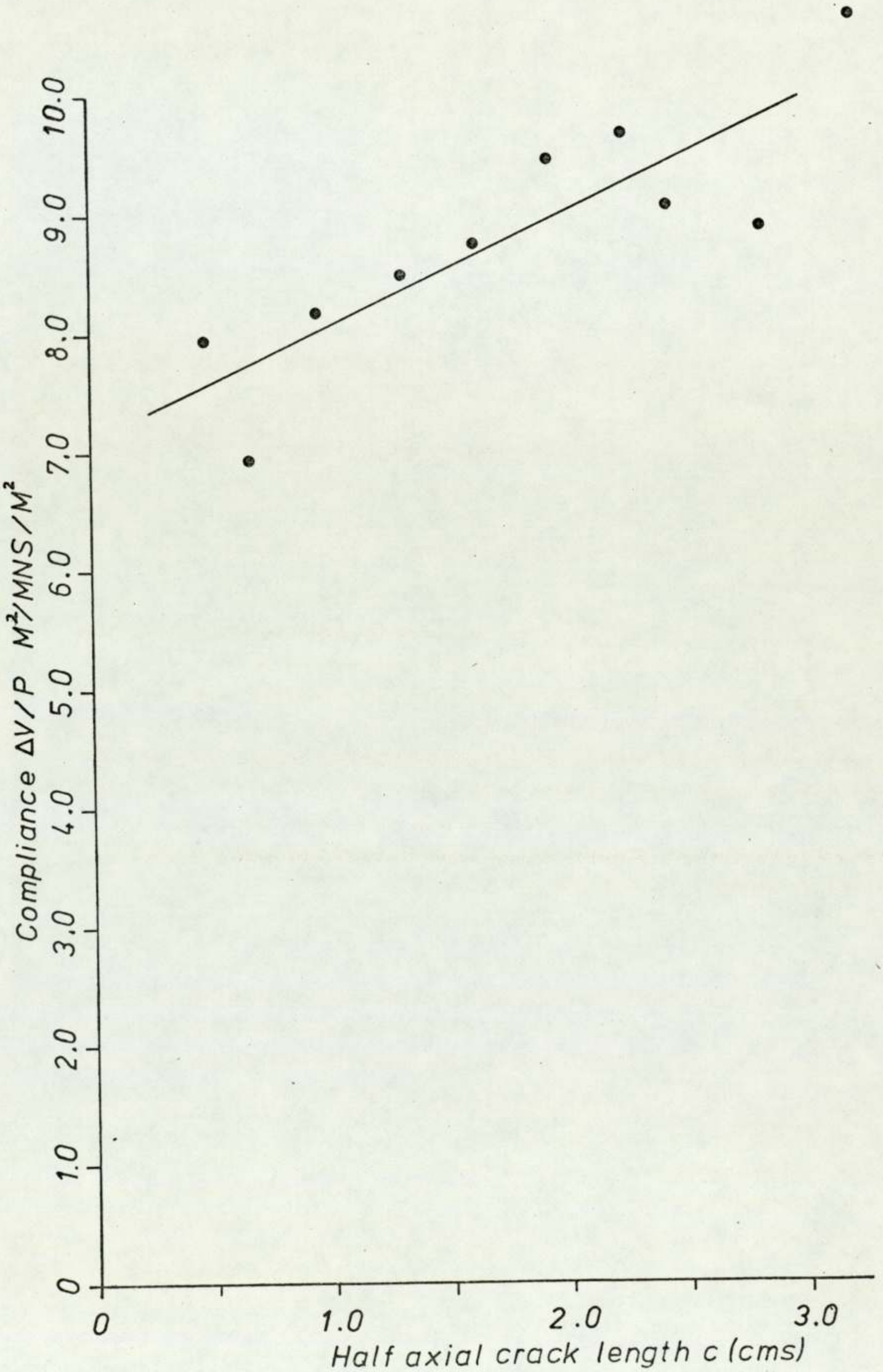

Fig. 33. Compliancev. crack length for K and M tubes.

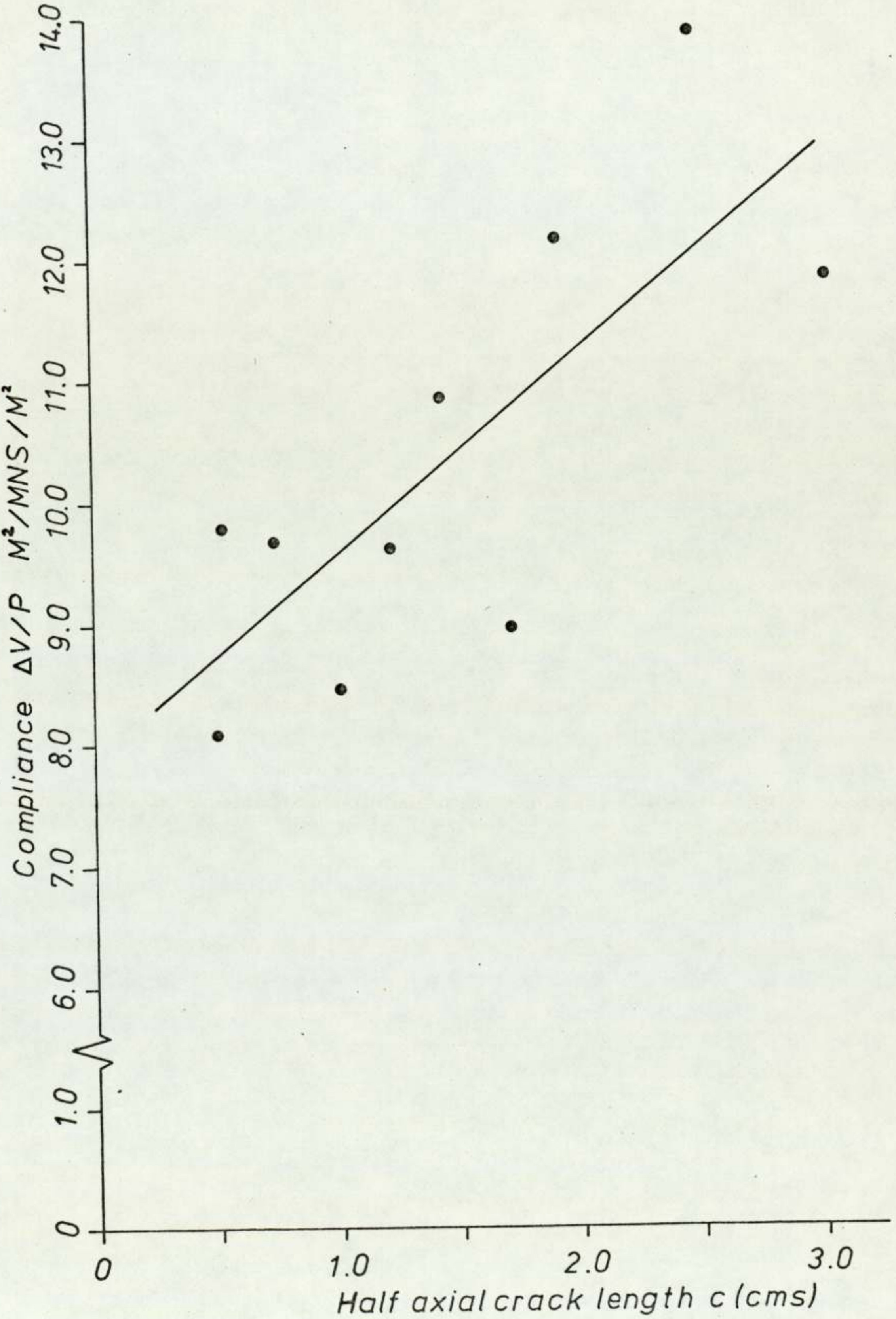

Fig. 34. Compliance v. crack length for J and L tubes.

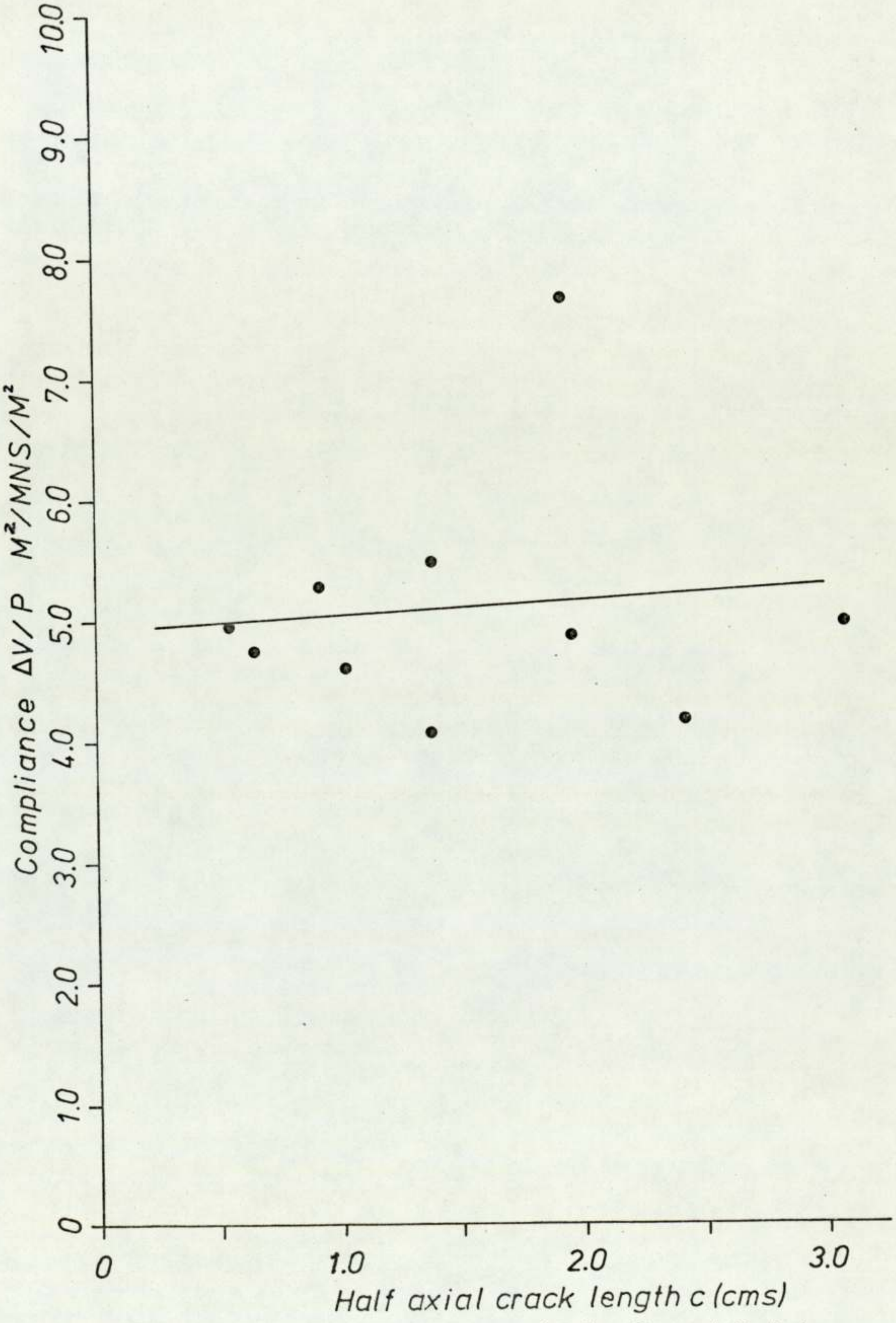

Fig. 35. Compliance v. crack length for C and G tubes.

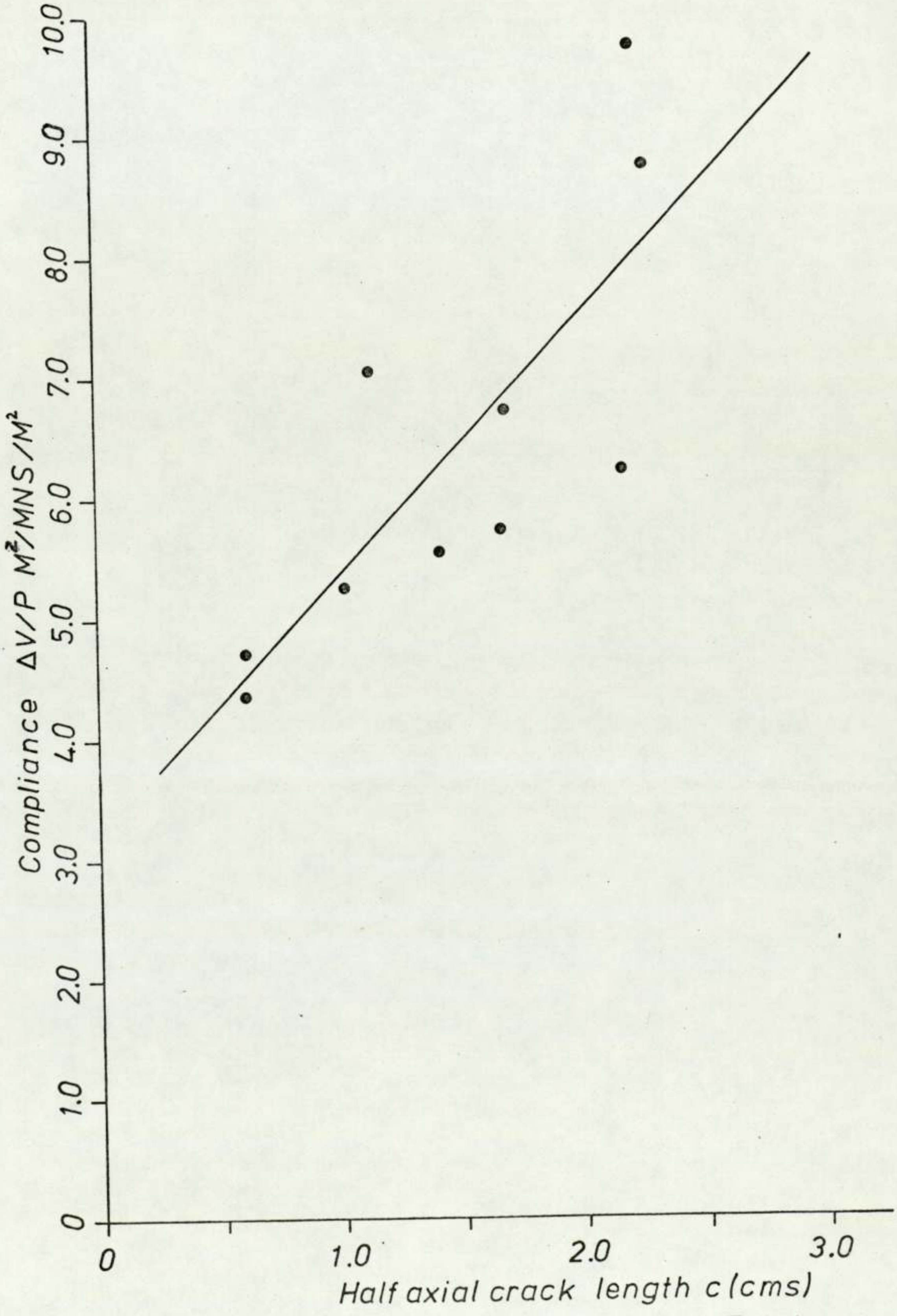

Fig. 36. Compliance v. crack length for B and F tubes.

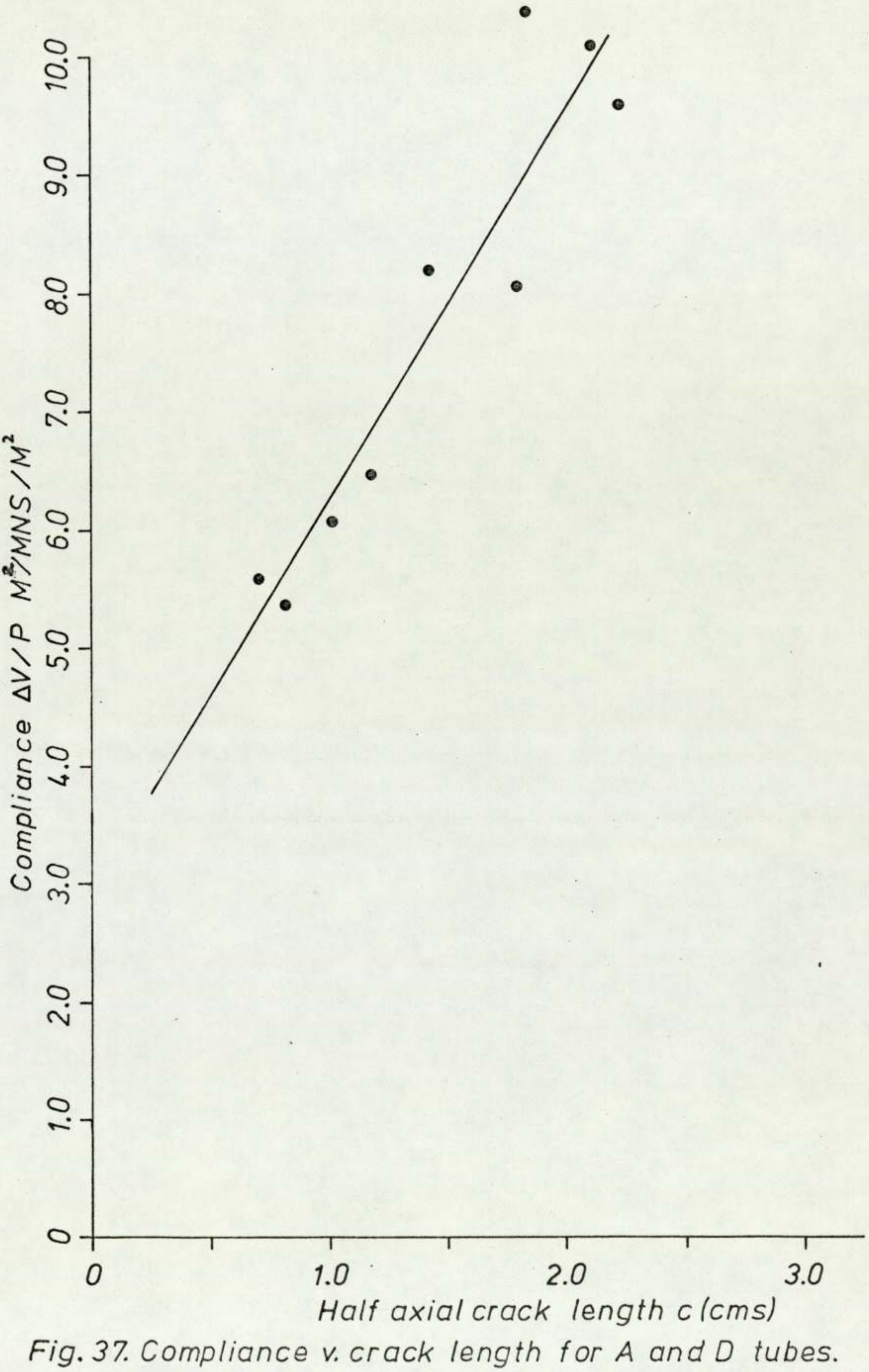

Fig. 37. Compliance v. crack length for A and D tubes.

The errors involved in the calculation of $\Delta V/P$ were not as large as those for the calculation of C.O.D./σ_H. The measurement of volume change involved the calculation of elastic strain which eliminated errors due to σ_H. The overall probable error on $\Delta V/P$ was determined as ± 1.0%. This confirms the premise that local material variations were responsible for the scatter of the results. The regression coefficients for the volume change method of compliance measurement were generally higher than for the crack opening displacement method. This is a reflection of the more accurate compliance measurement.

In conclusion it has been established that the compliance, measured in two different ways, increased with increasing crack length. The increase was greater, the greater the depth of the defect. In both cases, the measurements were subject to scatter which was probably due to local material variations in the tubes.

The variation of compliance with crack length can be used to determine K_c values of the material from a knowledge of the failure pressures and hoop stresses.

The two equations are:

1) Crack opening displacement

$$K_c = \sigma_H^{*} \left(\frac{EL}{2(1-\nu^2)} \frac{dC''}{dc} \right)^{\frac{1}{2}}$$

(see Appendix 1 for derivation)

2) Volume change

$$K_c = P^* \left(\frac{E}{2(1-\nu^2)} \frac{d(\Delta V/P)}{dc} \right)^{\frac{1}{2}}$$

(after Underwood et Al(45))

The comparison of K_c values obtained by each compliance method is shown in section 6. 4.

6. 3. Failure mechanisms of tubes subjected to internal pressure.

6. 3. 1. Tubes without artificial defects.

6. 3. 1. 1. Plain ± 30° helix angle tubes (H tubes).

Table 7 in section 5. 3. shows the failure pressures and hoop stresses sustained for five tubes (H1 - H5), each with a lay up of ± 30° helix angle. The average ultimate hoop stress was 66.6 MN/M^2 which corresponded to an ultimate internal pressure of 5.02 MN/M^2. The hoop stress versus hoop strain graph for each tube was linear at the start of pressurising, but, at about 50% of the ultimate pressure, became non-linear. This was probably due to a combination of two effects:

1) The fibres attempting to rotate,

2) The response of the resin becoming non-linear.

The rotation of the fibres, due to shear stresses, can be seen in plates 10 and 11.

Failure of the tubes was initiated at the reinforcement. An example of the sequence of events leading to failure of a typical tube (H3) is shown in plates 12 to 15. Plate 12 shows the tube prior to pressurising. At a hoop stress of 40 MN/M^2 a crack was initiated along and parallel to a band of fibres as shown in plate 13. Further stress caused the band to increase in width, as the crack propagated, and for other cracks to be initiated, as shown in plate 14. Further pressure caused the band width to continue to increase until failure as shown in plate 15. The initiation of the failure close to the reinforcement was due to

Plate 10.

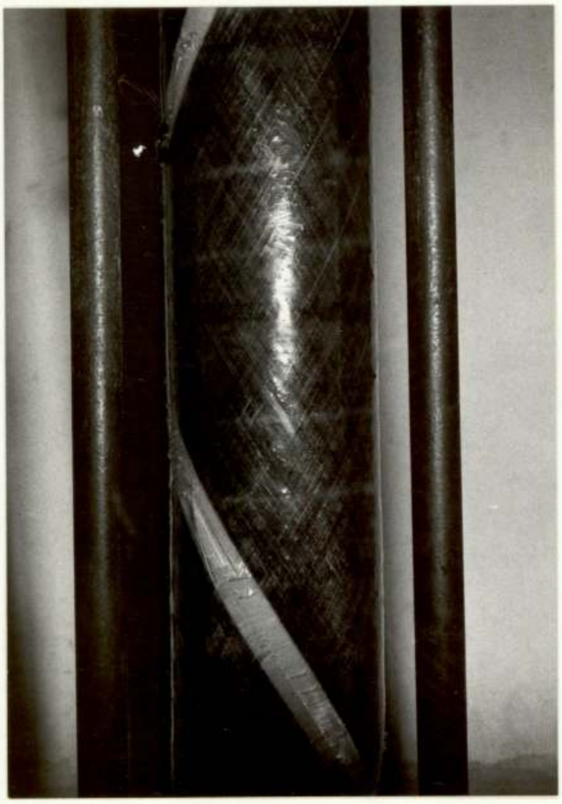

Plate 11.

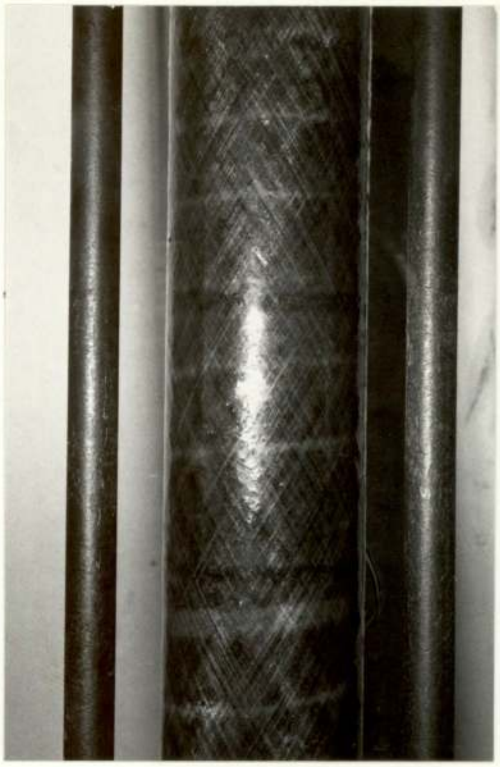

Plate 12.

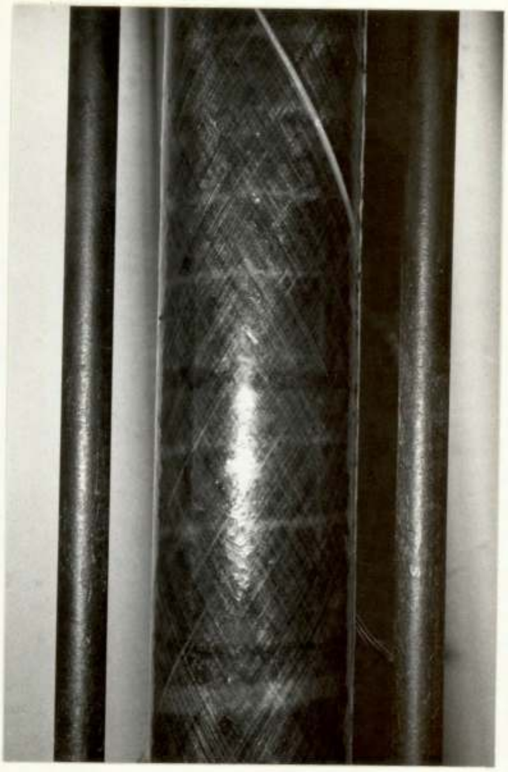

Plate 13.

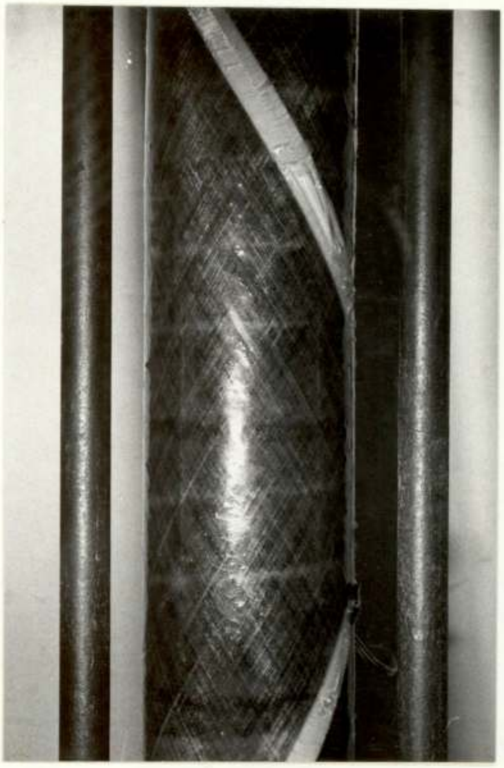

Plate 14.

Plate 15.

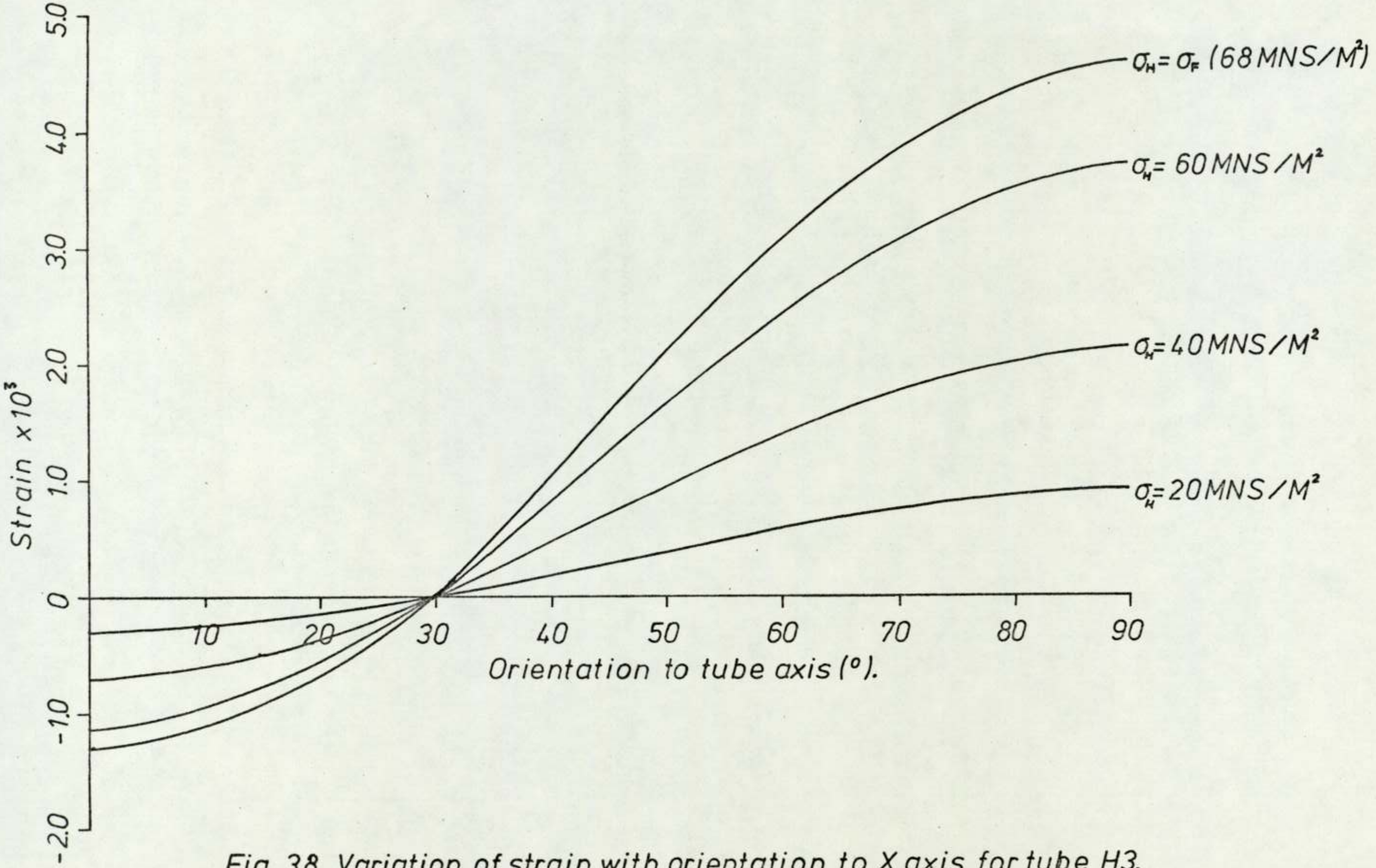

Fig. 38 Variation of strain with orientation to X axis for tube H3.

the presence of stress concentration due to the section change. It is possible to calculate a value of the stress concentration in this region, but the mathematics is complex and beyond the scope of this work.

Fig. 38 shows the variation of strain with angle to the X - axis for a typical tube H3. This was obtained from the output of the strain gauge rosette, in the usual way. The curve shows that the change-over from tensile to compressive strain occurred at 30° to the axis of the tube. The maximum hoop strain which the tube sustained was 4.6×10^{-3}.

6. 3. 1. 2. 50% ± 30° and 50% ± 90° tubes (A and E tubes).

Table 7 in section 5. 3. shows the failure pressures of six tubes (A1 and E1 - E5) with a lay up of 50% ± 30° and 50% ± 90° helix angles. The average ultimate hoop stress was 721.8 MN/M^2 which corresponded to an ultimate internal pressure of 49.4 MN/M^2. In all cases th hoop stress/hoop strain graphs were linear up to the point of failure of the tubes. Plates 16 to 19 show the sequence of events leading to the failure of a typical tube, E1. Plate 16 shows the tube before pressurising. At the relatively low pressure of 120 MN/M^2, voids were clearly visible between the fibre/matrix interface in the ± 30° layers, as shown in plate 17. Plate 18 illustrates that, at a higher pressure of 400 MN/M^2 , the voids were more clearly visible. Catastrophic failure, initiated at the ends of the tubes near the reinforcement, is shown in plate 19. The failure close to the

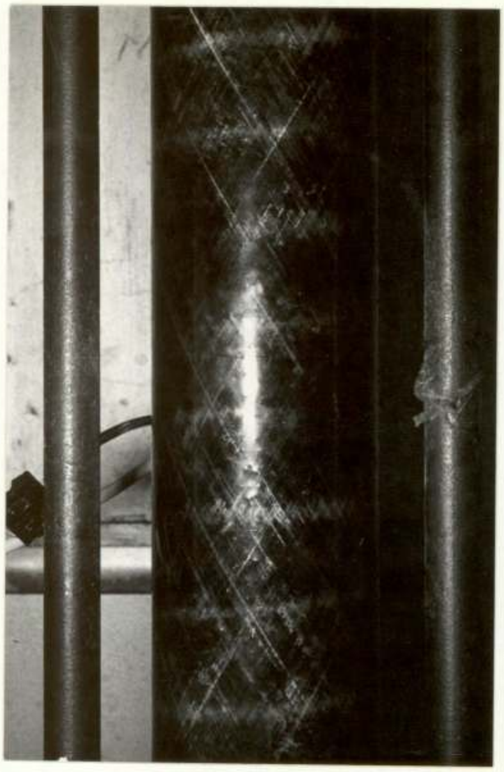

Plate 16.

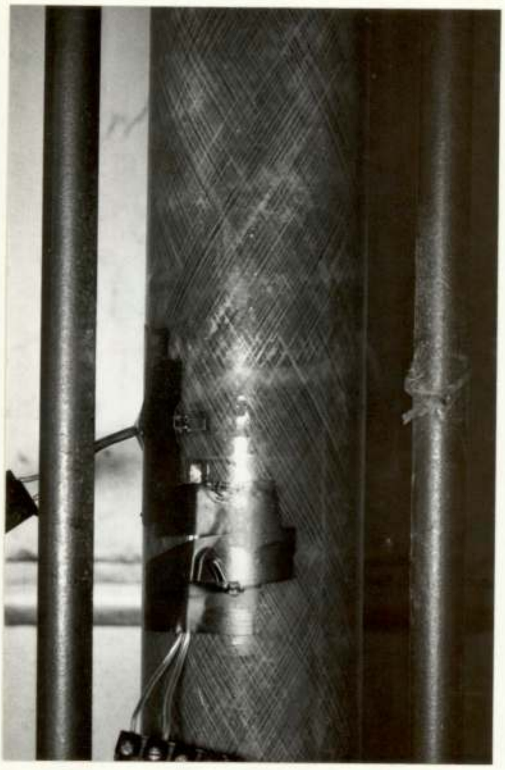

Plate 17.

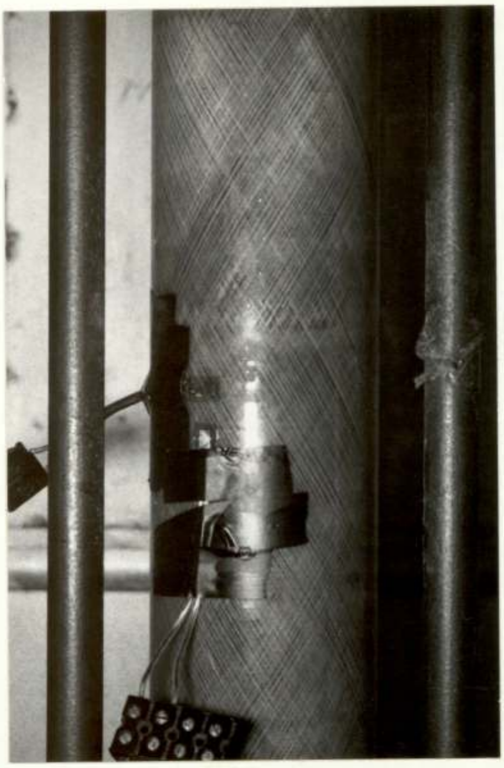

Plate 18.

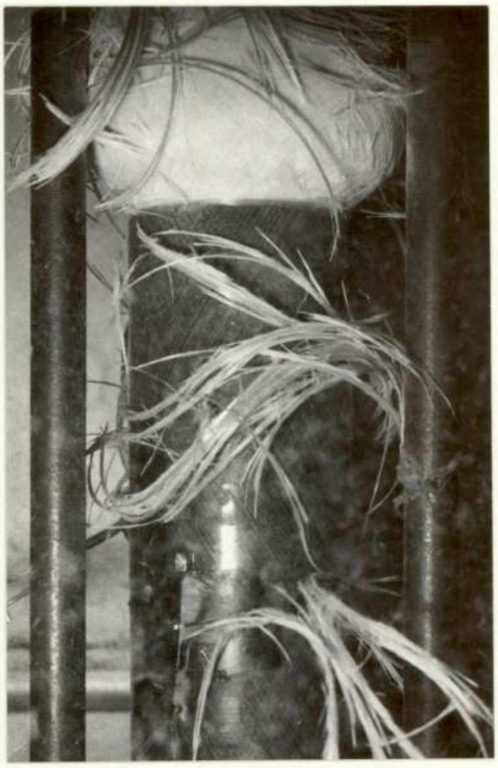

Plate 19.

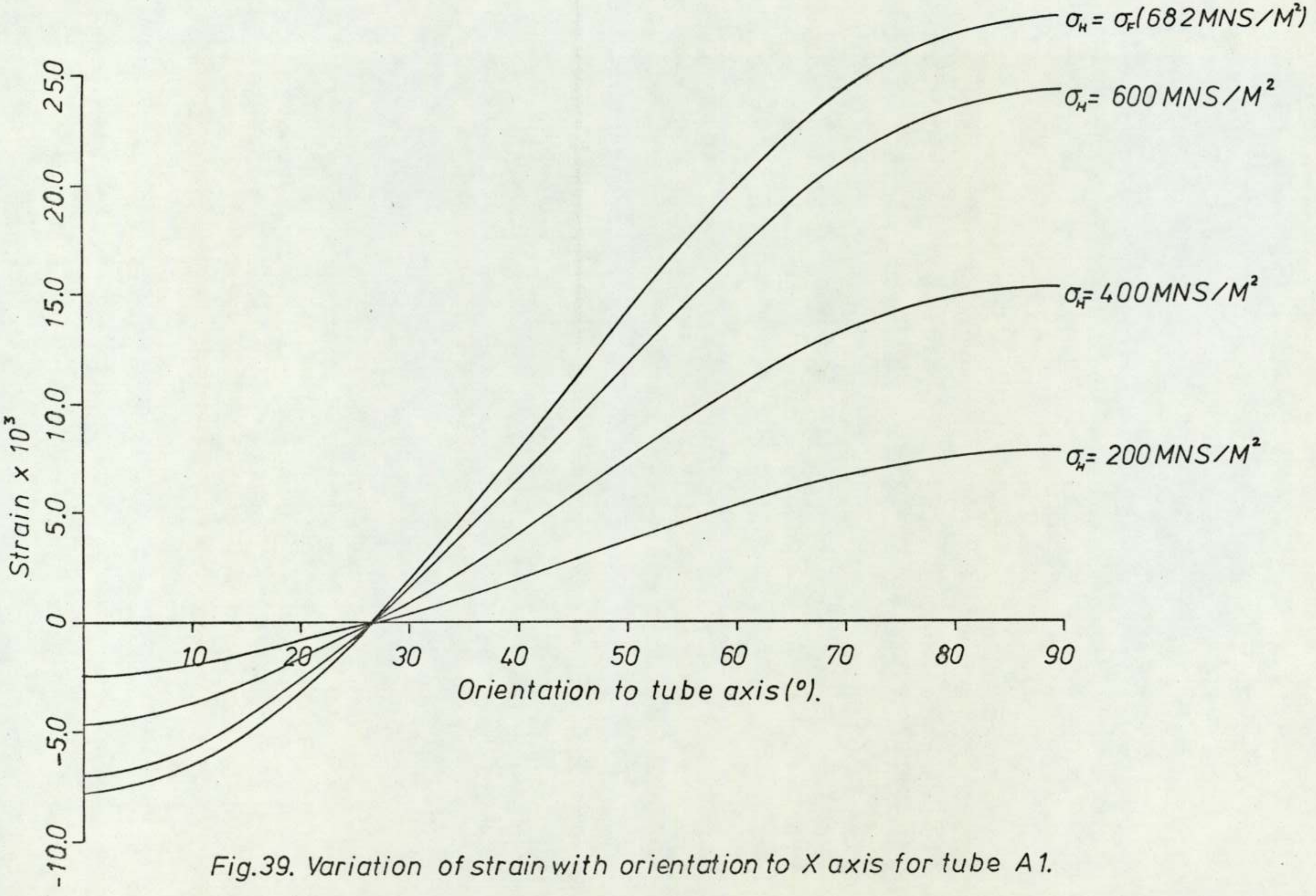

Fig.39. Variation of strain with orientation to X axis for tube A1.

reinforcement of the tubes was typical . This was due to the section change causing a stress concentration. As previously stated in section 6. 3. 1. 1., the calculation to obtain the magnitude of the stress concentration is beyond the scope of this thesis. The failure was accompanied by a loud report due to the release of a large amount of strain energy stored in the windings.

Fig. 39 shows the variation of strain with angle to the X - axis for a typical tube A1. At a relatively low stress level of 100 MN/M^2 the hoop strain was 5×10^{-3}, which was more than the maximum strain that the plain ± 30° tubes could sustain. This explains the large number of voids observed in the ± 30° layers at the low stress levels. The hoop windings restrained the ± 30° layers, but when these layers failed the ± 30° layers could instantly bulge out as shown in plate 19. The maximum hoop strain at failure was 27.5×10^{-3}. The change-over from tensile to compressive strain occurred at about 26° to the axis of the tube, which was lower than the plain tubes due to the presence of the hoop winding.

6. 3. 2. Tubes with artificial defects.

Table 7 in section 5. 3. lists the failure pressures and hoop stresses for the tubes which contained slots. The failure pressure, P^* was taken as the pressure at the point of intersection, of a line drawn at 95% of the slope of the pressure versus crack opening displacement graph. (see Fig. 40) The failure pressure, P^* obtained in this way was used to calculate the failure hoop stress, σ_H^*. This is an accepted means of obtaining failure stresses for isotropic materials, such as most metals. The increase in compliance due to crack extension causes the plot to become non-linear. The stress determined in this way is representative of the stress required to cause crack extension of 2%.

Section 6. 2. illustrated that the compliance increased with crack length for the tube types discussed here and justifies the use of the criteria normally used for isotropic materials. The slot did not always increase in length, but there was enough fibre and resin damage to increase the effective crack length; this caused the pressure/crack opening displacement plot to become non-linear.

Further justification, for considering the onset of failure to have occurred shortly after the graphs became non-linear, is shown in plates 20 to 23. The plates show a series of events which took place during the pressurising of tube G1. Fig. 40 shows the stress at which each photograph was taken and its position on the stress/crack opening displacement curve. The sequence shows that, shortly after the curve became non-linear,

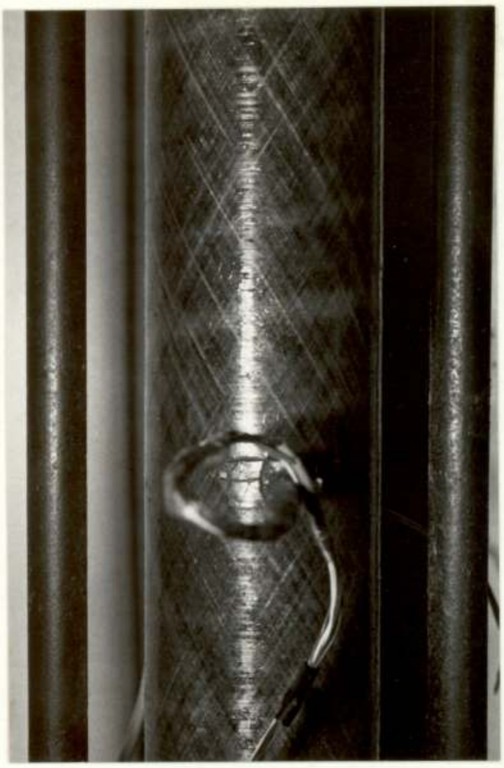

Plate 20.

Plate 21.

Plate 22.

Plate 23.

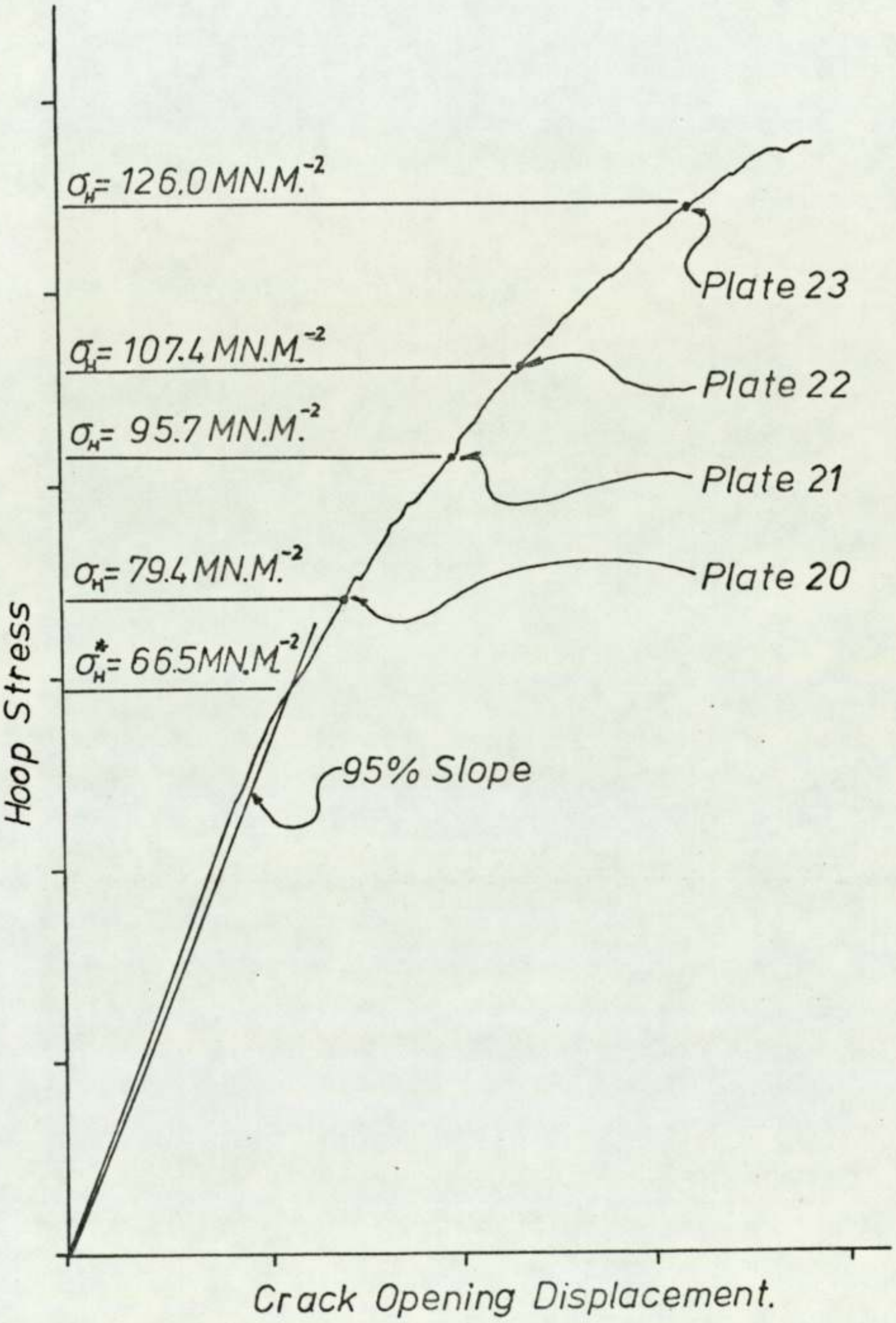

Fig. 40. Hoop stress v. crack opening displacement for tube G2.

the hoop winding began to break away from the tube. This was followed by catastrophic failure of the tube, illustrated in plate 23. The other tubes, for each category, showed this behaviour to lesser or greater degrees depending on the tube and defect types. They were consistent in that the onset of failure became clearly visible shortly after the curves became non-linear.

The data for the the five different categories are presented in two ways. Section 2. 2. 2., in the Literature Survey, illustrate two criteria for the interpretation of data obtained by subjecting cylindrical pressure vessels to internal pressure (Table 2). The two important equations are:

Equation 1

$$\sigma_H^* = \frac{K_c}{(\pi c)^{\frac{1}{2}}} \left(1 + S \frac{c^2}{Rt}\right)^{\frac{1}{2}}$$

Equation 2

$$\sigma_H^* = \frac{K_c}{(\pi c)^{\frac{1}{2}}} \left(1 + S \frac{c^2}{R^2} 50\tanh \frac{R}{50t}\right)^{\frac{1}{2}}$$

(The factor ϕ_3 was not included in these equations since it is a plastic zone correction factor, not expected to be relevant in the case of glass reinforced plastics)

The factor S was calculated from the equation:

$$S = 0.49(12(1 - \nu^2))^{\frac{1}{2}} \qquad \text{(Folias}^{(2)}\text{)}$$

A K_c value was determined for a tube which had a relatively short slot and failed at a high pressure, P^*. Variations of σ_H^* were then computed for increasing values of crack length, c,, for the two equations.

The second way of interpreting the data was similar to that presented in reference 3. Inspection of equations 1 and 2 reveals that $(\sigma_H^{*2} \pi c)^{-1}$ is a linear function of c^2/Rt and c^2/R^2 50tanhR/50t with K_c^{-2} and SK_c^{-2} the slope and intercept respectively. (this is fully discussed in reference 3 and in section 2. 2. 2.). Graphs of $(\sigma_H^{*2} \pi c)^{-1}$ versus c^2/Rt and c^2/R^2 50tanh R/50t were obtained and compared for different K_c values.

6. 3. 2. 1. Plain ± 30° helix angle tubes with full through wall defects (J and L tubes).

The average value of ν_{21} for tubes J and L was 0.230 which resulted in a value for S of 1.65. K_c values were calculated using the data obtained from tube L1 for equations 1 and 2. The two K_c values were 4.36 and 4.35 $MN.M.^{-\frac{3}{2}}$ for equations 1 and 2 respectively. Fig. 41 shows the variation of σ_H^* with crack length, c. The experimental vales of σ_H^* and c are also illustrated.

The two theoretical lines are almost identical and differ by about 0.4%. The values of σ_H^* predicted by equation 2 are slightly higher than those from equation 1. The value of the function c^2/R^2 50tanh R/50t is smaller than the function c^2/Rt for a given c. In order to preserve a constant K_c the value of σ_H^* for equation 2 must be greater than σ_H^* for equation 1. The experimental measurements of σ_H^* were subject to an error of ± 13% as discussed in 6. 2. 1. The scatter of the points could be due to this error. The experimental points agree reasonably well with the theoretical lines in view of the experimental errors and the errors encountered with this material due to local variations. The equations are useful in the prediction of failure hoop stresses for this type of tube containing a full through defect. For practical purposes equation 1 is as good as the more complex equation 2 for the prediction of failure pressures.

Figs. 42 and 43 show graphs of $(\sigma_H^{*\,2} \pi c)^{-1}$ versus c^2/Rt and c^2/R^2 50tanh R/50t for equations 1 and 2 respectively. The graphs are very similar and show scatter around the lines of

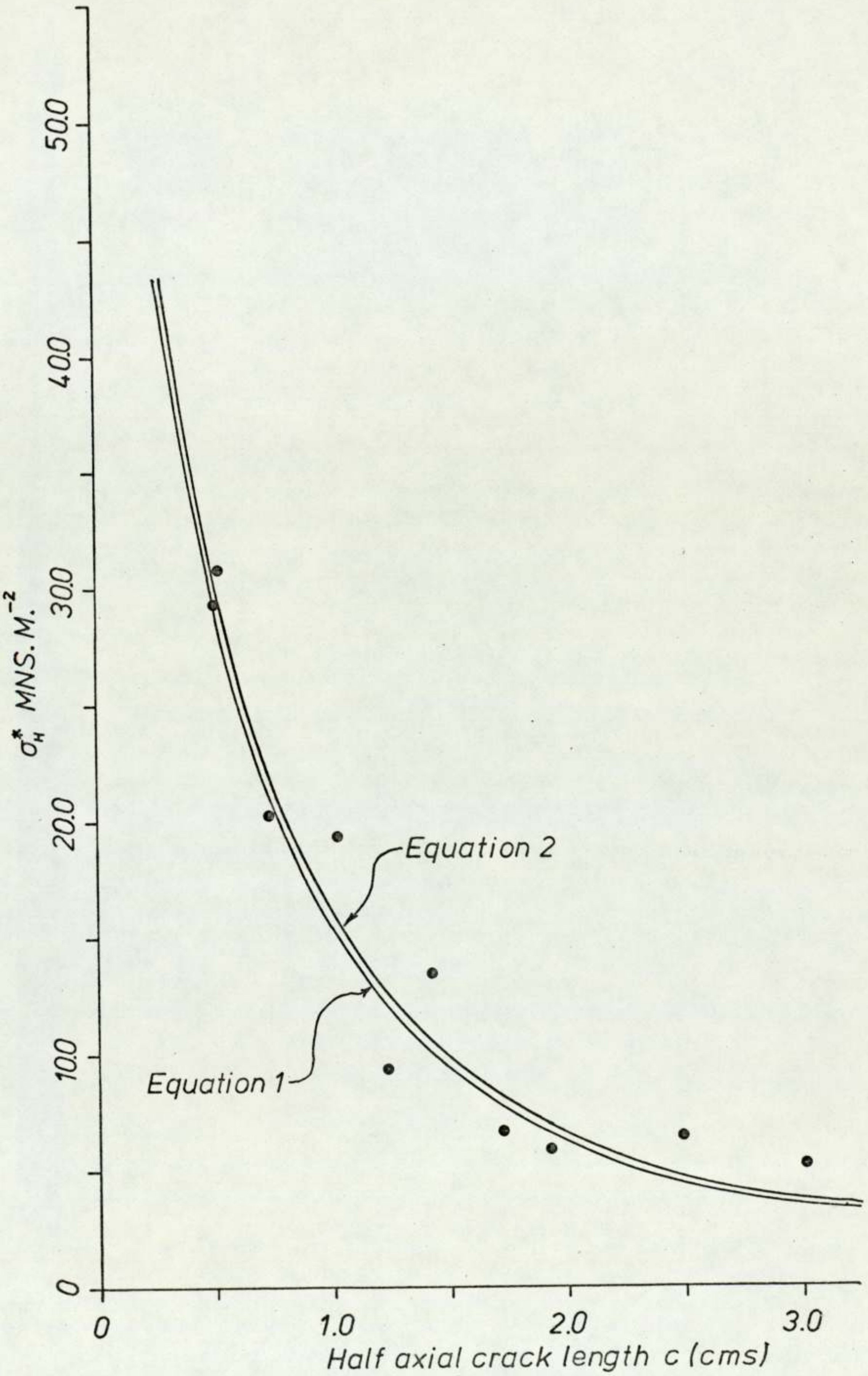

Fig. 41. σ_H^* v. crack length for J and L tubes.

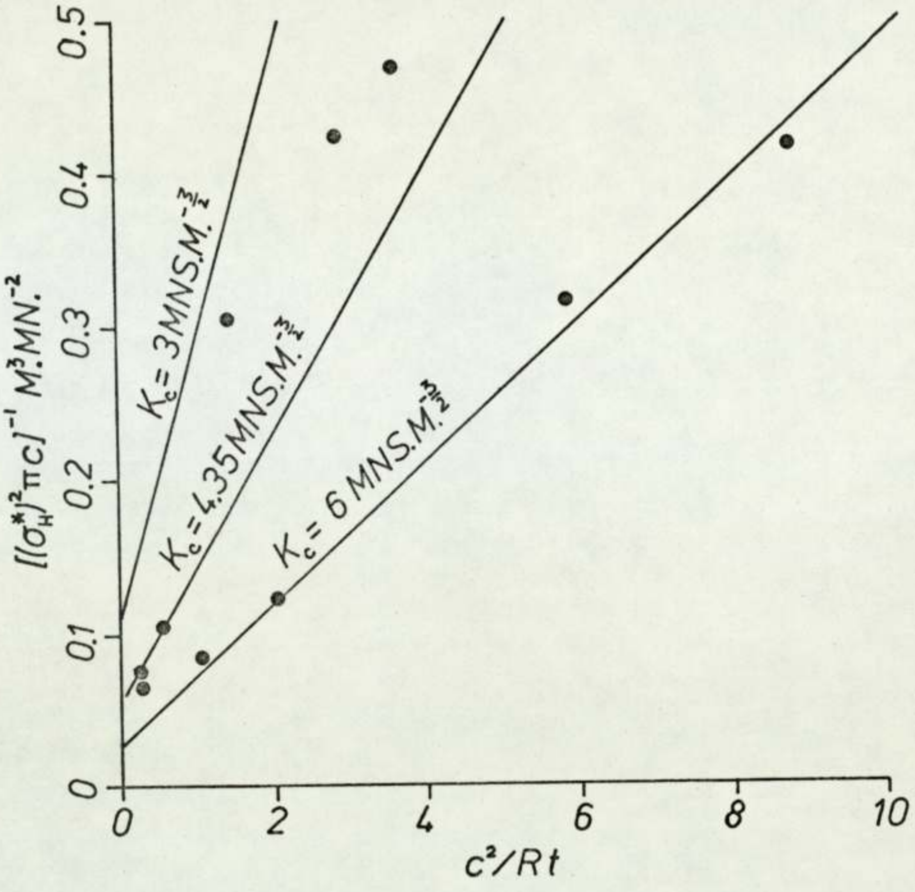

Fig.42. Equation 1 for J and L tubes.

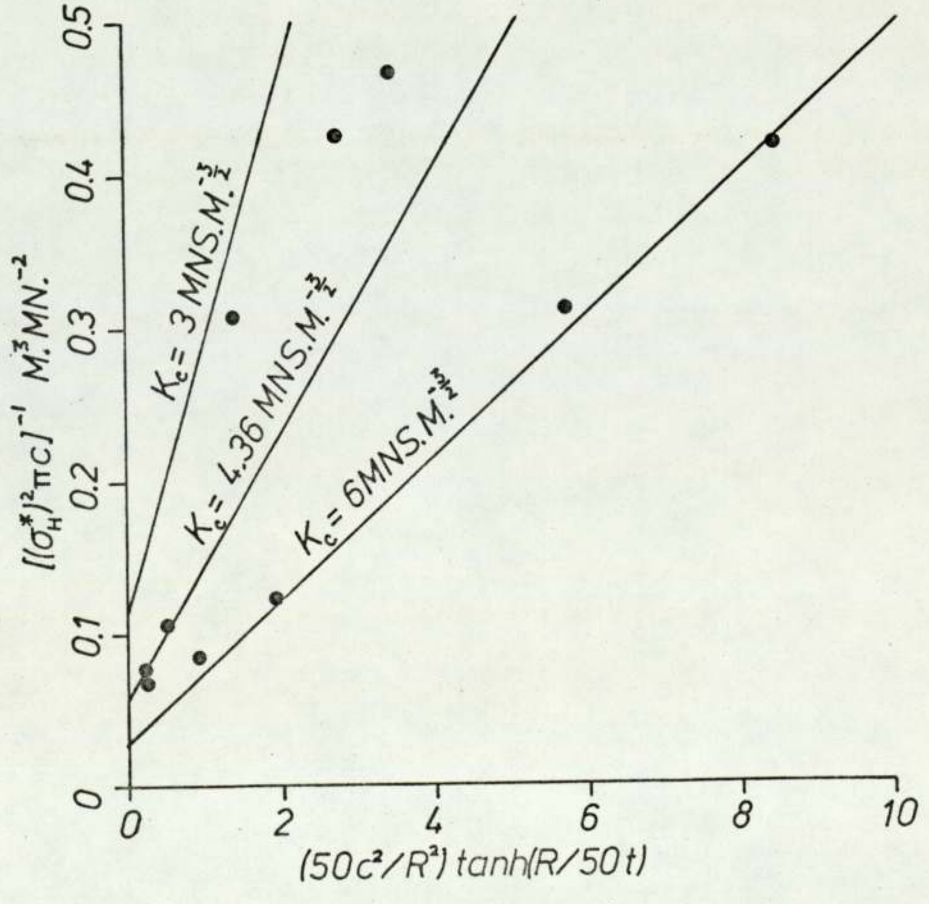

Fig.43. Equation 2 for J and L tubes.

$K_c = 4.36$ and $4.35 \text{ MN.M}^{-\frac{3}{2}}$. The discrepancies shown in the previous method of data presentation are highlighted by this method due to the form of the equations involved. The experimental points all lay within a band width of $K_c = 3$ and $K_c = 6 \text{ MN.M}^{-\frac{3}{2}}$. This illustrates clearly that for this material only a range of slot lengths will give a true representation of its behaviour. In this way a reliable, minimum value of K_c can be obtained for design purposes.

The tubes failed in a similar manner irrespective of slot length. Plates 24 to 27 show the progressive failure of tube L2, which was typical of the behaviour of the other tubes. Plate 24 shows the tube before pressurising. At a hoop stress of 22 MN/M^2, plate 25 shows the initiation and propagation at the ends of the slot, cracks between the fibre/matrix interface and parallel to the fibre direction. This is the normal propagation mechanism for the strong fibre/weak matrix systems. Plate 26 illustrates the crack propagation in a more advanced state, followed by failure as shown in plate 27. This was not the ultimate pressure which the tube could sustain, but the pressure at which leakage occurred due to the breakdown of the adhesive holding the thin copper sheet in place.

The series of plates shows that the onset of failure was similar, in some respects, to the tubes containing no defects, but the initiation was started at the ends of the slots. The stress concentration at the ends of the slots was evidently more severe than the stress concentration at the reinforced ends.

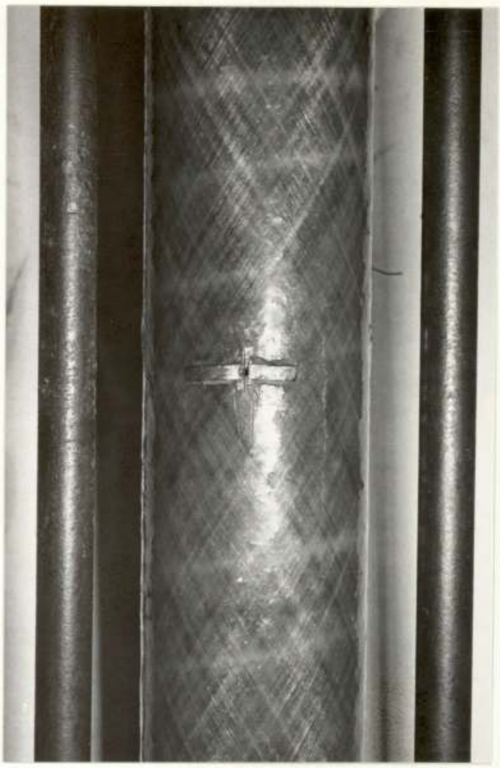

Plate 24.

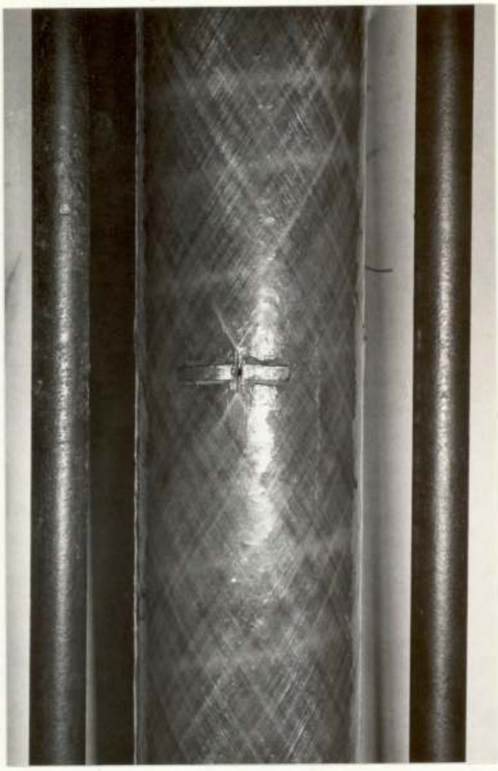

Plate 25.

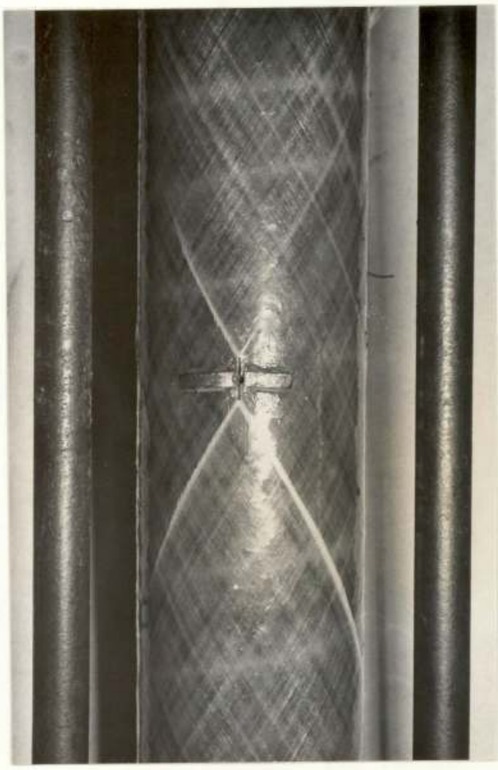

Plate 26.

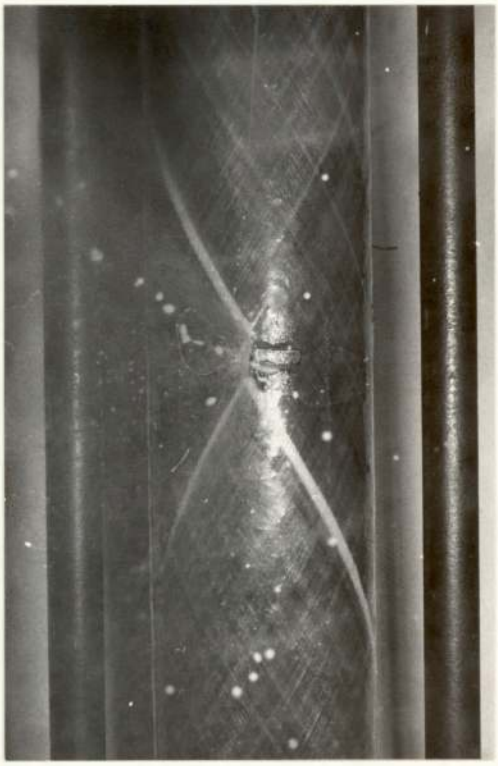

Plate 27.

6. 3. 2. 2. Plain ± 30° helix angle tubes with half through wall slots (K and M tubes).

The failure mechanism for the K and M series of tubes was interesting, since it was observed that the initiation of failure did not always take place in the vicinity of the ends of the slots. Very rapid initiation and growth of cracks sometimes took place, particularly for the tubes containing short slots, at the ends of the tubes, close to the reinforcement. When this occurred, small cracks were initiated at the ends of the slot, simultaneous to the growth of the previously initiated cracks. The initiation and growth of the cracks from the slot ends will be discussed first.

The average value of ν_{21} for these tubes was 0.304 which resulted in a value of S of 1.62, for equations 1 and 2. Another equation was considered for interpretation of the data for these tubes, equation 3. This did not contain a correction factor for crack mouth bulging.

Equation 3

$$\sigma_H^* = \frac{K_c}{(\pi c)^{\frac{1}{2}}}$$

Values of σ_H^* were computed using equations 1, 2 and 3 for increasing values of c and a fixed K_c value obtained from the test data of tube M1. The values of K_c were 5.13, 5.11 and 4.42 $\text{MN.M}^{-\frac{3}{2}}$ for equations 1, 2 and 3 respectively. Fig. 44 shows the variation of σ_H^* with c, for the three equations, and the experimental points.

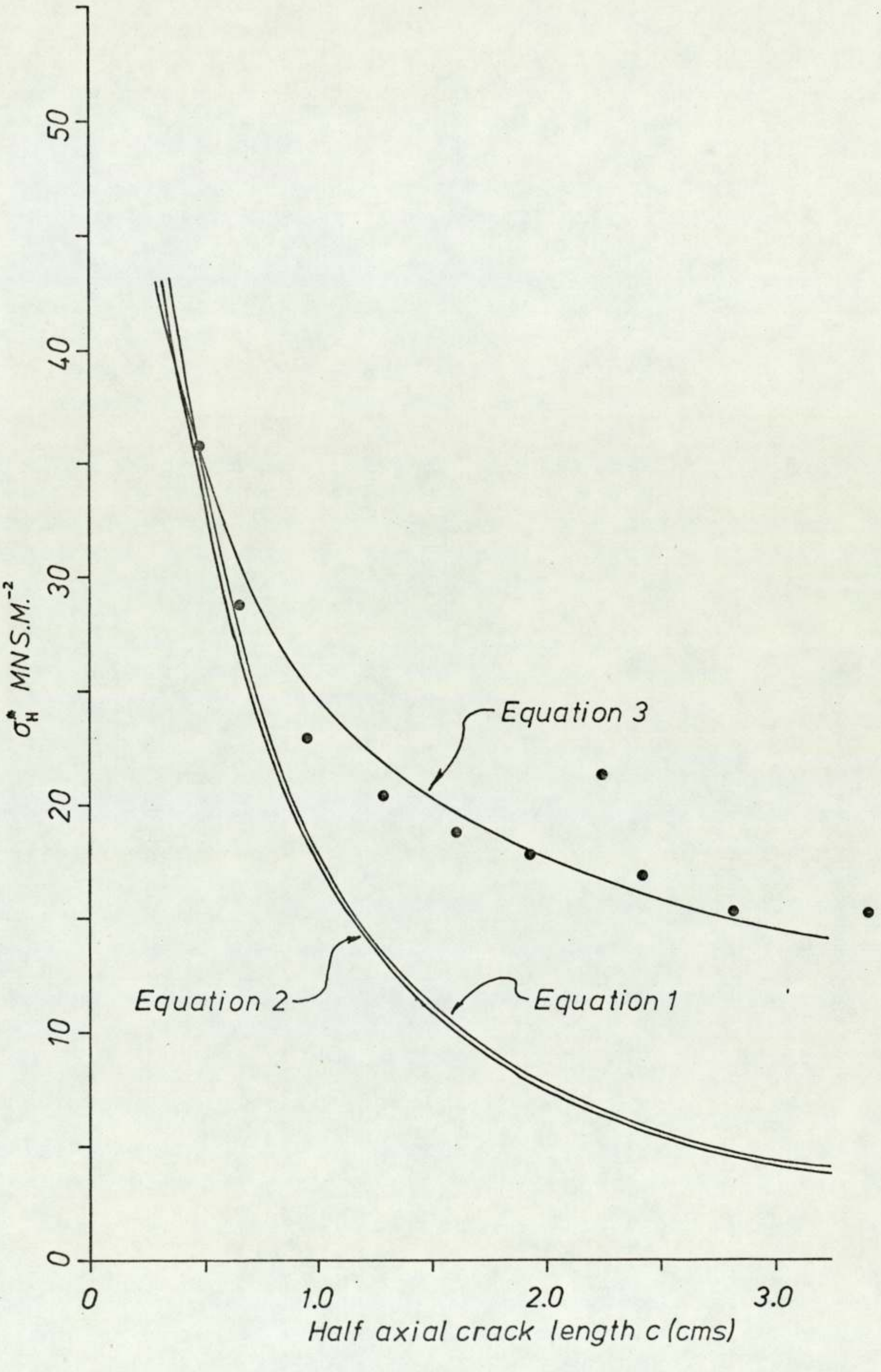

Fig.44. σ_H^* v. crack length for K and M tubes.

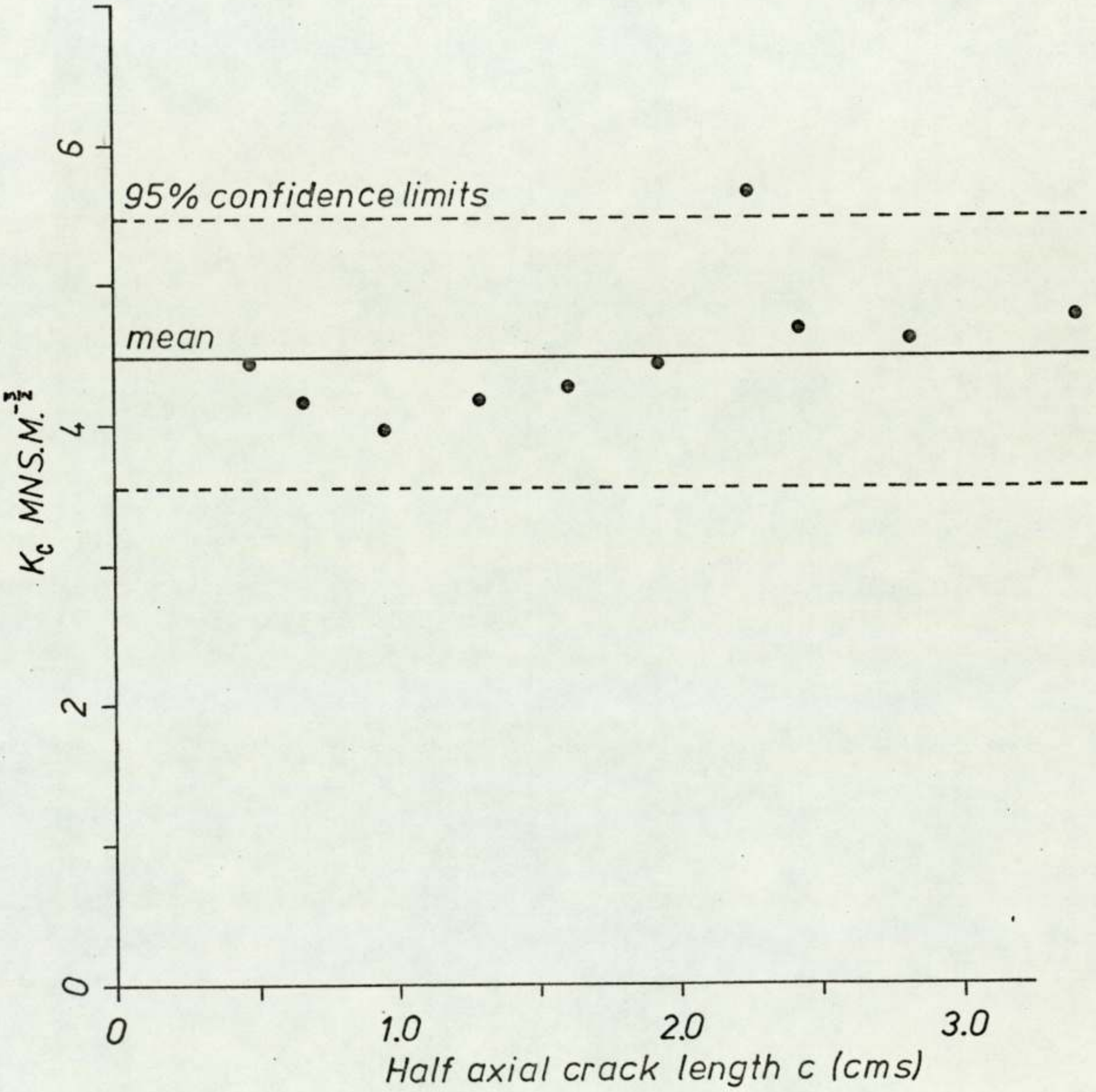

Fig. 45. Variation of K_c with crack length for tubes K and M using equation 3.

The theoretical lines for equations 1 and 2, while very similar to each other, did not lie near the experimental points. The line for equation 3 was a much better approximation to the data. It is apparent that, for this system, a correction factor for crack mouth bulging is not needed. The $\pm$ 13% probable error on σ_H^* could explain the scattering of the points except for the result from tube K4. Local thickening of the tube, in the slot region, may have caused the value of σ_H^* to be high. For practical purposes the use of equation 3 for the prediction of failure pressures is reasonably adequate.

The data could not be represented similarly to those of reference 3 since equation 3 was not of the required form. The K_c values obtained for each tube from equation 3 were plotted against crack length. This is illustrated in Fig. 45. The figure shows that the K_c values obtained using equation 3 were reasonably constant about a mean of 4.5 $\mathrm{MN.M}^{-\frac{3}{2}}$ and 95% confidence limits of 1.0 $\mathrm{MN.M}^{-\frac{3}{2}}$. This is further confirmation of the validity of the use of equation 3 for determination of K_c and subsequent prediction of failure pressures.

The above presents a useful means of prediction of the initiation and growth of cracks from a half through wall slot in a tube of this type. Its use is limited, since the initiation of failure of the tube as a whole can be governed by changes in section. The ultimate hoop stress for tubes containing relatively short slots was similar to the ultimate hoop stress for tubes without slots (H tubes). The failure hoop stresses were subjected to a statistical analysis, the results of which are presented below:

	mean ultimate hoop stress	variance
H tubes (no slot)	66.96 MN/M^2	1.86
K and M tubes (half through wall slot, $c < 1.5$cms)	63.92 MN/M^2	10.70

Ratio of the variances = 5.75

'F' ratio at the 95% confidence level = 6.59

The ratio of the variances indicates that, at the 95% confidence level, there was no significant difference between the ultimate hoop stresses for tubes with or without short slots, ($c < 1.5$cms). A similar analysis was carried out for tubes containing slots longer than this, $c > 1.5$cms < 3.5cms. The results were as follows:

	mean ultimate hoop stress	variance
K and M tubes (half through wall slot, c 1.5cm 3.5cm)	46.73 MN/M^2	131.61

Ratio of the variances = 70.76

'F' ratio at the 95% confidence level = 5.19

The ratio of the variances indicates that, at the 95% confidence level, there was a highly significant difference between the ultimate hoop stresses sustained by tubes containing long slots and those not containing slots.

The above illustrates that, if a short, half through wall slot ($c < 1.5$cms) was present, it did not have any significant effect on the ultimate hoop stress. If a longer slot ($c > 1.5$cms < 3.5cms) was present, then this had a deleterious effect on the ultimate hoop stress.

This was confirmed by observations of the mechanisms of failure. Plates 28 to 31 show the sequence of failure of tube K1, which had a half through wall slot of length, 2c = 1.318cm. Plate 28 shows the tube before pressurising. Plate 29 shows the initiation and growth of a crack from the end of the tube, near the reinforcement. At a higher pressure, plate 30 shows the growth of this crack and the initiation of a small crack from the end of the slot. Plate 31 shows that, at failure, the growth of the crack from the end of the slot was not extensive. The behaviour of this tube was typical of those tubes with very short slot lengths.

Plates 32 to 35 show the sequence of failure of tube K3, which had an intermediate slot of length, 2c = 3.238cms. Plate 32 shows the tube before pressurising. Plate 33 shows the initiation of cracks from the end of the slot as the tube is pressurised. At a higher pressure, plate 34 shows the growth of these cracks and the initiation of another crack, from the end of, and around the tube. At failure Fig 35 shows substantial growth of both cracks.

Plates 36 to 39 show the sequence of failure of tube M4, which had a long slot of length, 2c = 4.878cms. Plate 36 shows the tube before pressurising. Failure was initiated by cracks forming at the ends of the slot as shown in plate 37. At a higher pressure substantial growth of these cracks is shown in plate 38. The ultimate failure, shown in plate 39, shows

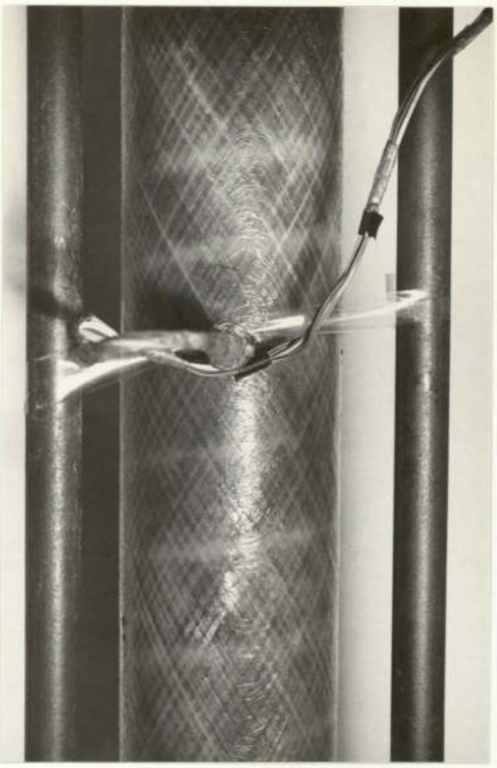

Plate 28.

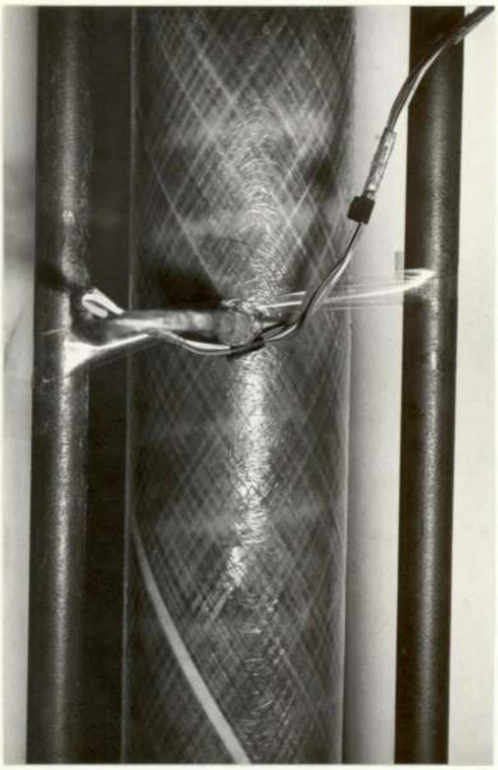

Plate 29.

Plate 30.

Plate 31.

Plate 32.

Plate 33.

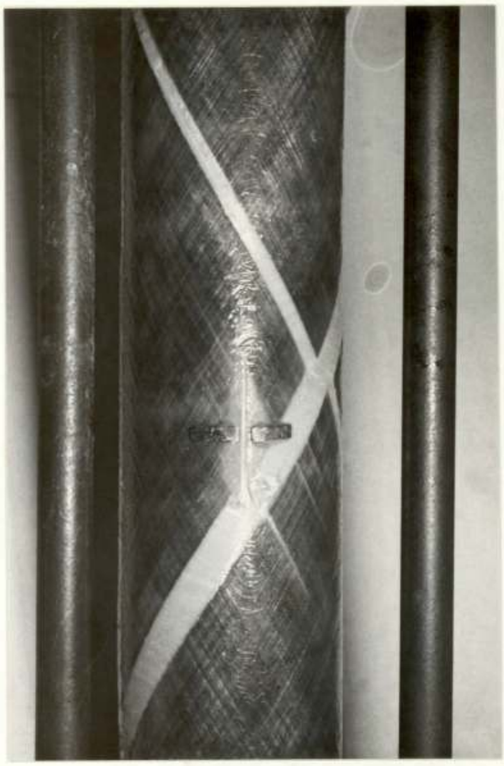

Plate 34.

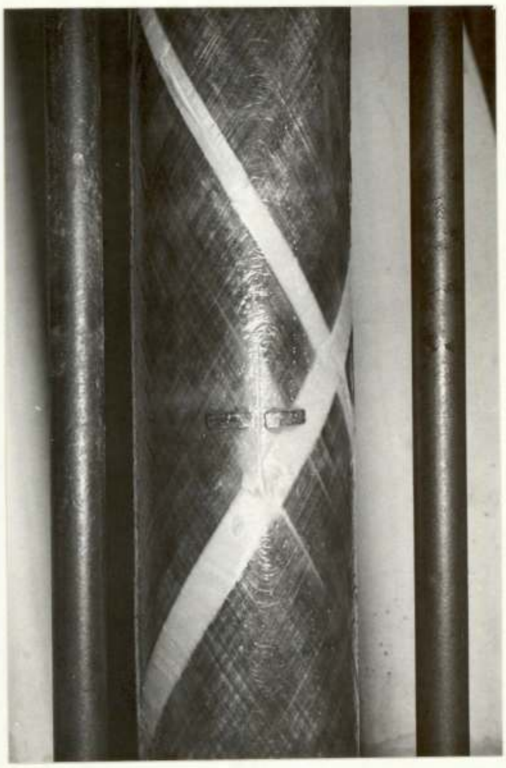

Plate 35.

Plate 36.

Plate 37.

Plate 38.

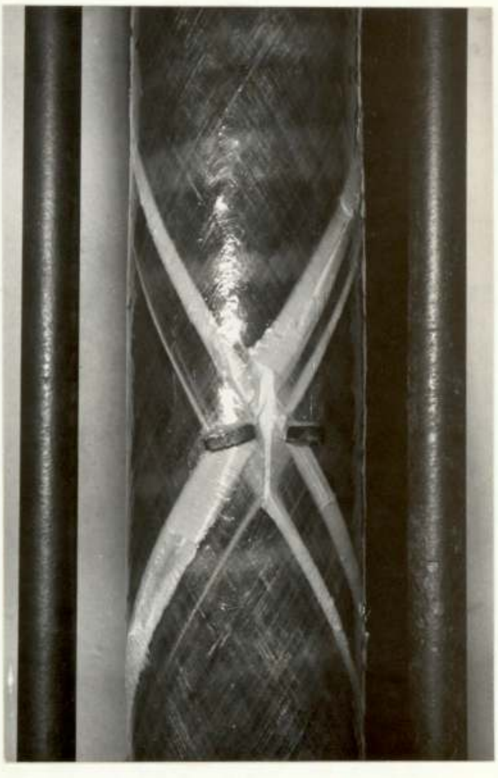

Plate 39.

that no cracks were initiated from the ends, near the reinforcement.

These series of plates illustrate that, for the K and M tubes containing half through wall slots:

1) For small slots failure was due, almost entirely, to cracks initiated at the ends of the tubes, close to the reinforcement.

2) For intermediate slots failure was due to cracks initiated, both at the slot tips and at the reinforcement.

3) For large slots failure was due, almost entirely, to cracks initiated at the slot tips.

For intermediate slots, the stress concentrations due to section change and presence of a slot appear to be of a similar magnitude. At the ends of the tube bending moments are set up as the tube distorts. It is possible to calculate the magnitude of the stresses in these areas, but this is beyond the scope of this thesis.

The behaviour of the tubes illustrates that the presence of even large defects may not be as important, for design purposes, as local stress concentrations due to section change. In most circumstances, defects of the size introduced into the tubes for these experiments, will not be present. Clearly, large section changes and small root radii must be avoided, wherever possible, in the design of pressure vessels with this type of lay up.

6. 3. 2. 3. 50% ± 30° and 50% ± 90° helix angle tubes with full through wall defects (A and D tubes).

The average value of ν_{21} for tubes A and D was 0.218, which resulted in a value for S of 1.66. K_c values were calculated, using the data for tube D2, for equations 1 and 2. The two K_c values were 10.56 and 10.50 $MN.M^{-\frac{3}{2}}$ for equations 1 and 2 respectively. Fig. 46 shows the variation of σ_H^* with crack length, c. The experimental values of σ_H^* and c are illustrated also.

The theoretical lines for the two equations are almost identical and agree well with the experimental points. In nearly all cases the actual failure hoop stresses were higher than those obtained from the equations. The discrepancies with the theoretical lines can nearly all be explained by the probable error on the measurement of σ_H^* of ± 13%. The experimental point for tube A5 shows the most discrepancy and may be due to a local thin part of the tube causing an underestimation of the value of σ_H^*. It is apparent that the equations may be used, with a reasonable degree of accuracy, for the prediction of failure pressures for tubes with this lay up and containing full through wall defects.

Figs. 47 and 48 show graphs of $(\sigma_H^{*\,2}\pi c)^{-1}$ versus c^2/Rt and c^2/R^2 50tanh R/50t for equations 1 and 2 respectively. The graphs are very similar and show that nearly all the experimental points lay below the $K_c = 10.50$ and $K_c = 10.56$ $MN.M^{-\frac{3}{2}}$ lines for the respective equations. The experimental point which lay

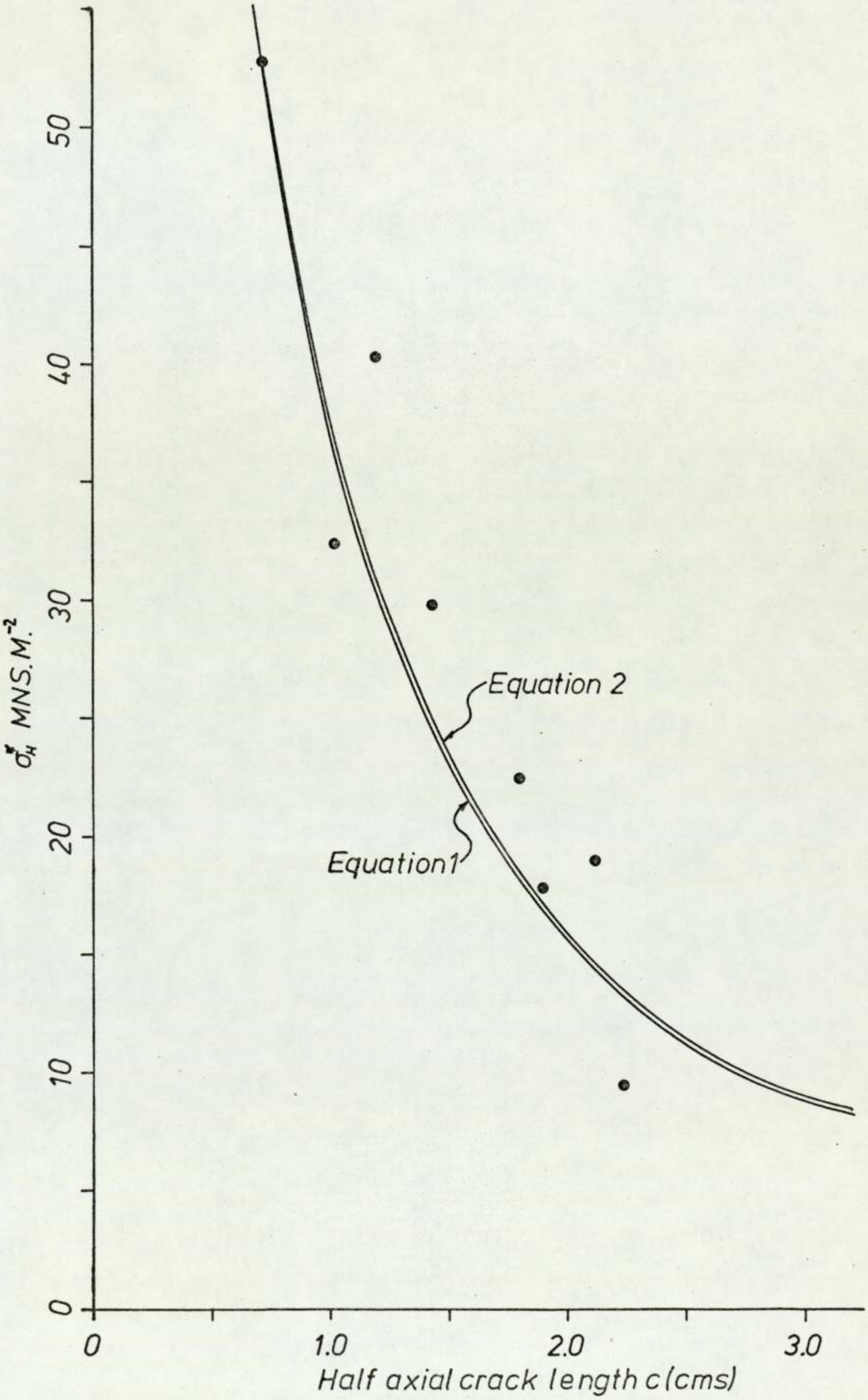

Fig.46. σ_H^* v. crack length for A and D tubes.

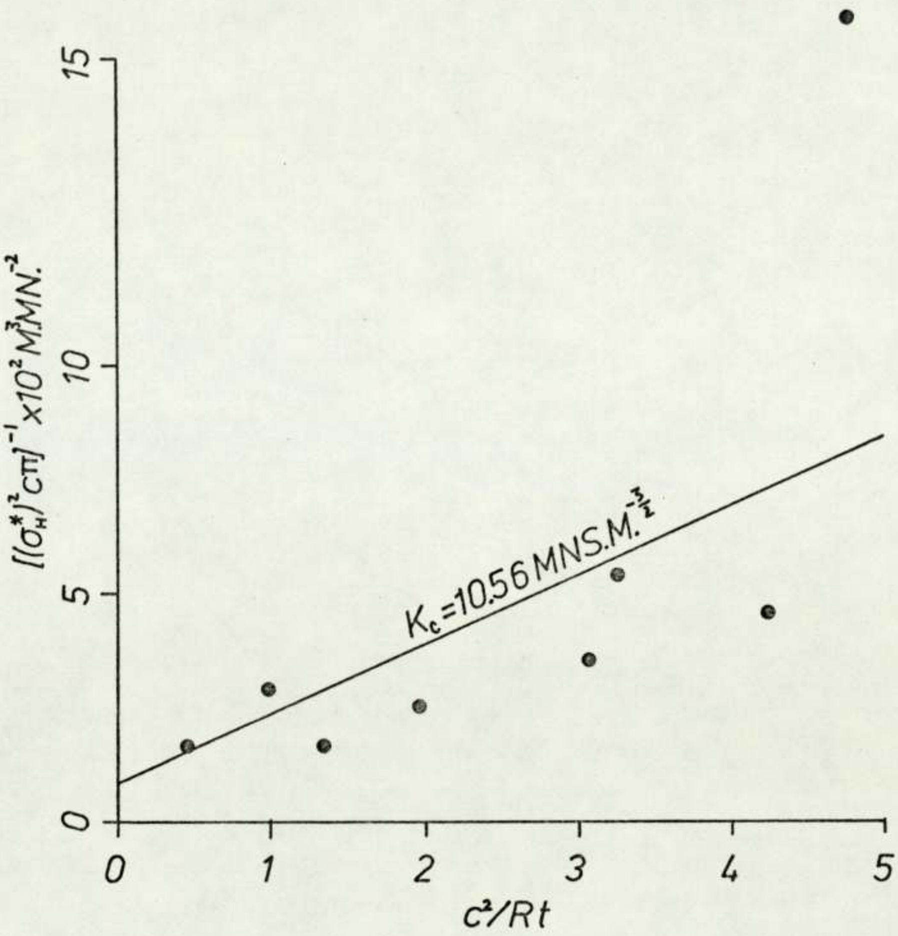

Fig.47. Equation 1.

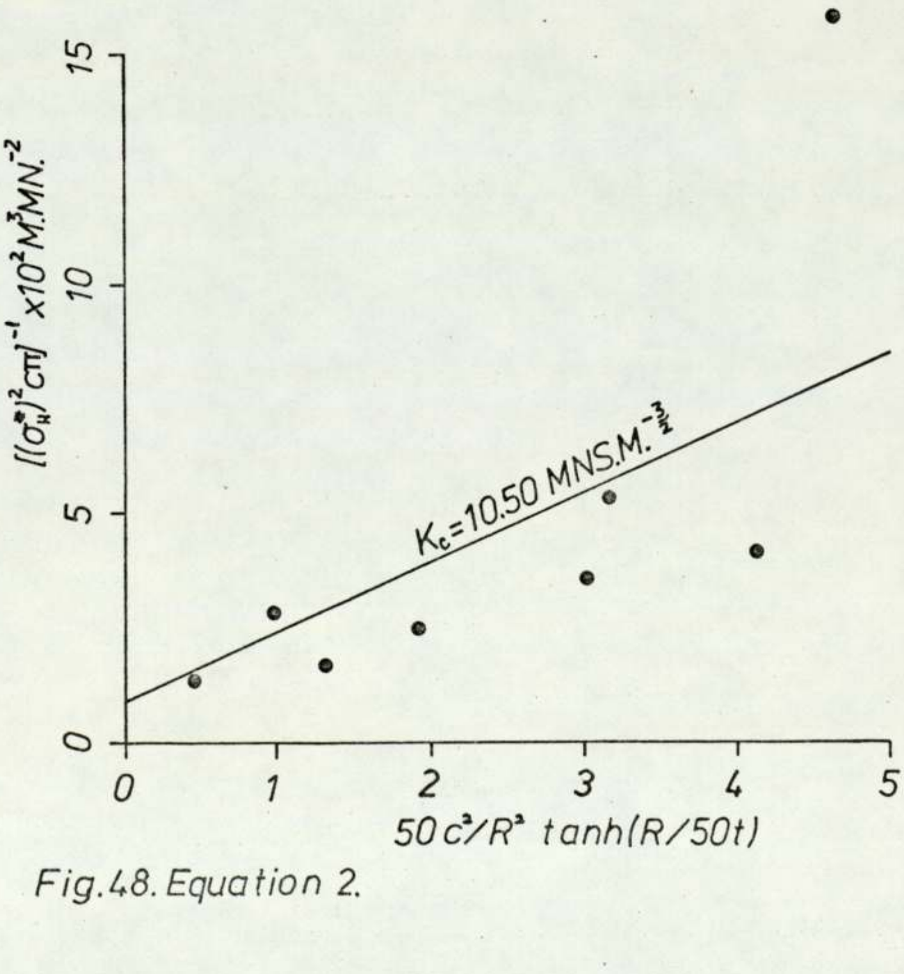

Fig.48. Equation 2.

away from the line was the one for tube A5. The discrepancy shown by this point in Fig. 46 is highlighted by this means of presentation. These figures give confirmation to the value of using the equations as a basis of design. Equation 1 is as useful as the more complex equation 2.

Plates 40 to 43 show the series of events leading to the failure of tube A3, which contained a relatively short slot of length, c = 0.821cms. An interesting failure mechanism for this system was noted. Plate 40 shows the tube before pressurising. The cut, hoop windings first started to break away from the $\pm 30^{\circ}$ layers. This was due to the inability of the interface to sustain the strain as the $\pm 30^{\circ}$ layers started to bulge. This is shown in plate 41. To contain the volume of liquid pumped into the tube, further deformation of the $\pm 30^{\circ}$ layers was necessary. To deform further these layers had to push against the layers of hoop winding which were still intact. This resulted in the cut, hoop winding section splitting away completely, as shown by plate 42. Since the defect was relatively short the layers had to deform a long way to contain the liquid. The bulge deformed to its minimum diameter, i. e. it became a bulge of semi-circular cross section. The stresses required to deform the bulge further were evidently greater than those required to break off the hoop windings. Further pressure resulted in the removal of hoop windings and failure as depicted by plate 43.

Plates 44 to 47 show the breakdown of the interlaminar interface of the hoop and $\pm 30^{\circ}$ layers around the slot present

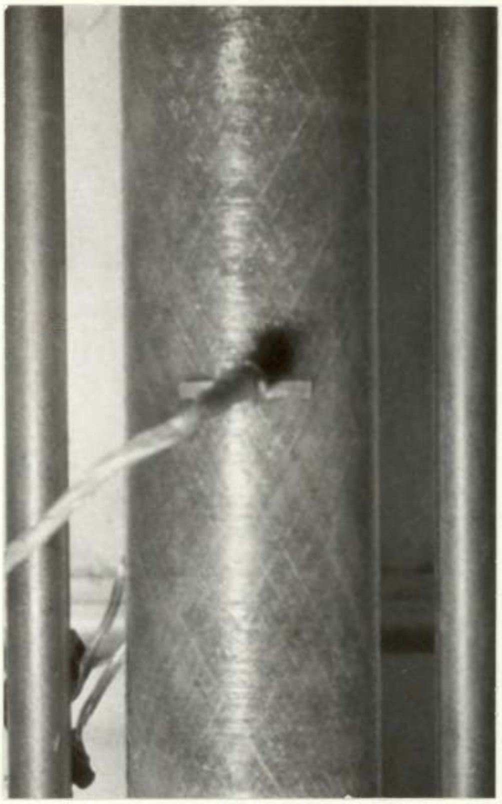

Plate 40.

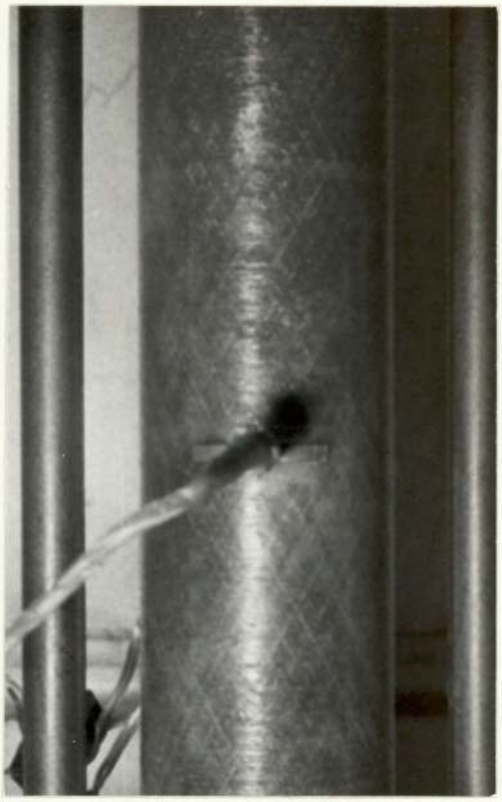

Plate 41.

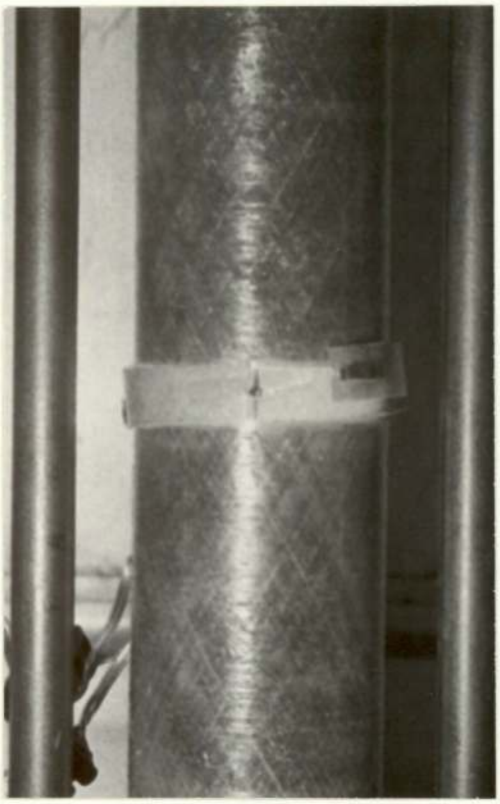

Plate 42.

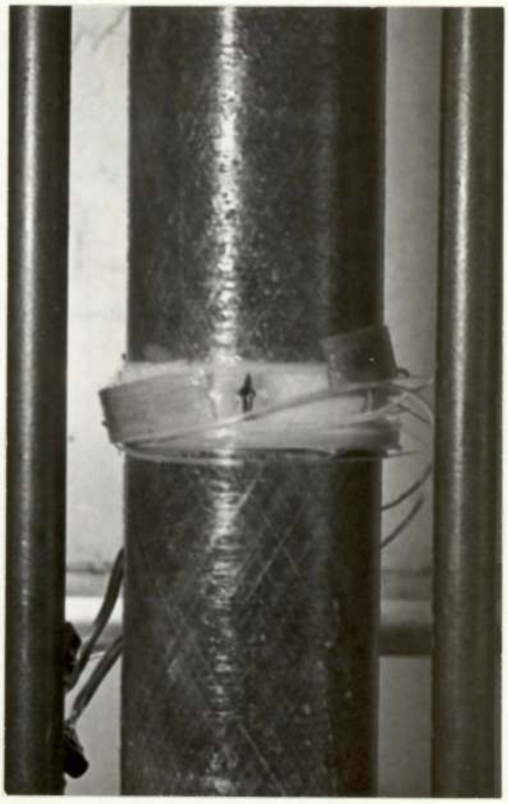

Plate 43.

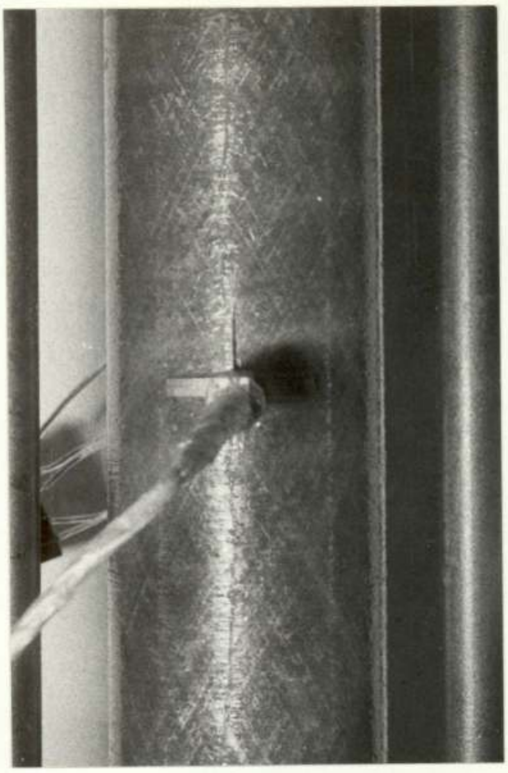

Plate 44.

Plate 45.

Plate 46.

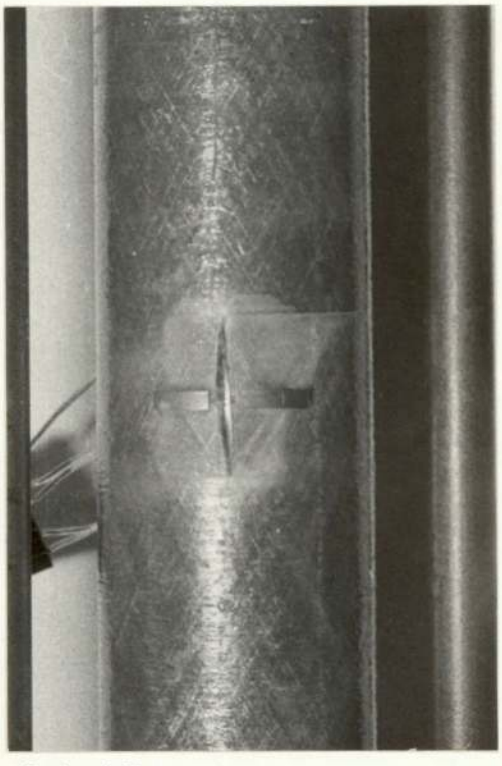

Plate 47.

in tube A5. The slot length, c was 2.232. Plate 44 shows the slot before the tube was pressurised. Plate 45 and 46 show the circular growth of the debonding of the interface as the tube is pressurised. The growth of the circles impinged and the whole broke away as shown in plate 47. Local stress concentrations existed, at the notch ends, as the ± 30° layers tried to deform outwards. This helps to explain the initiation of the debonding in the proximity of the slot tip, and its subsequent growth towards the centre of the slot.

Plates 48 to 51 show the sequence of events leading to the failure of tube A4, which contained a slot of length, c = 1.802cm. Plate 48 shows the tube before pressurising. Plate 49 illustrates that the hoop windings started to break away as the tube was pressurised. The ± 30° layers had to deform to contain the liquid which was being pumped into the tube. The shape of the bulge which was created by this is shown in plate 50. Since the slot length was relatively long the bulge did not reach the critical semi-circular cross section before failure, as shown by plate 51.

The failure hoop stresses, even for small slots, were low compared with the failure hoop stresses for this type of tube without slots, (approximately 10%). The cutting of the hoop windings had a very deleterious effect on the performance of the tubes and made them quite notch sensitive; the tubes containing no hoop winding only showed a lowering of failure hoop stress by about 50% for the short slots. Since the hoop windings are present on the outer layers, care must be taken in the handling of the tubes to avoid drastic decreases in performance of damaged tubes.

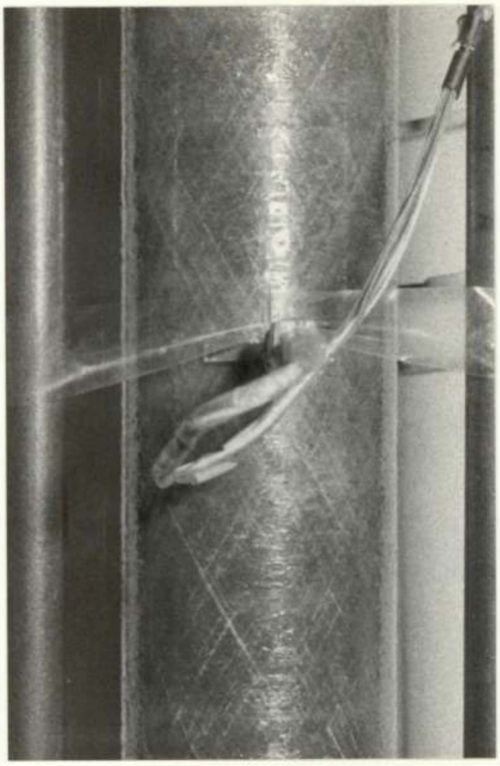

Plate 48.

Plate 49.

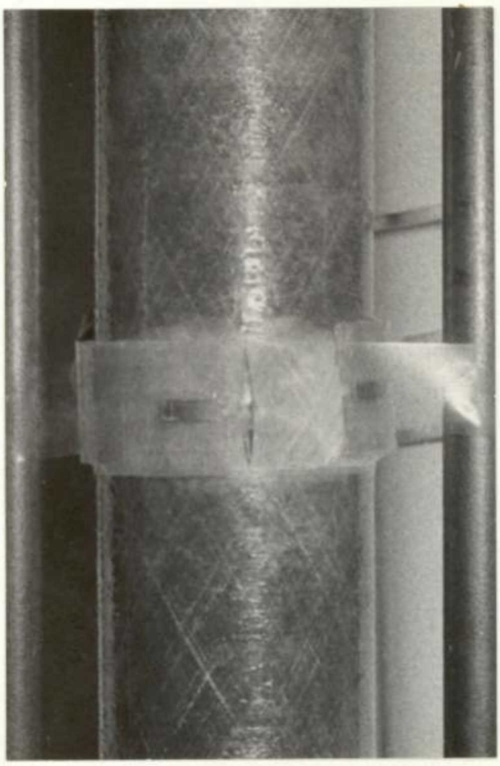

Plate 50.

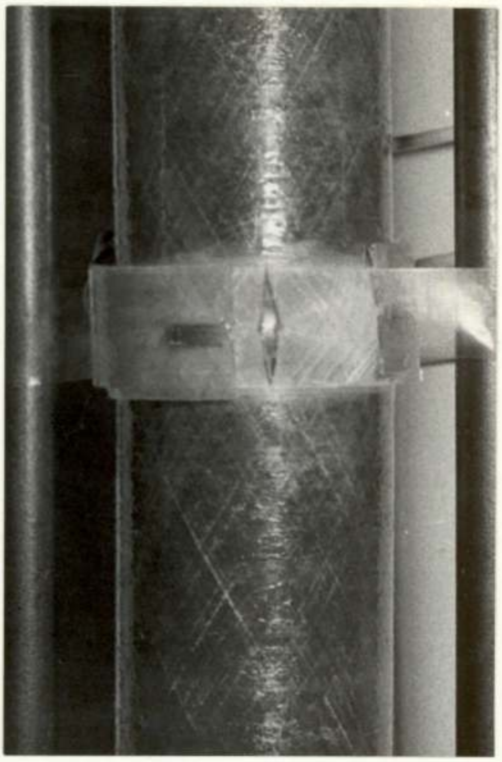

Plate 51.

6. 2. 3. 4. 50% ± 30° and 50% ± 90° helix angle tubes with half through wall slots (B and F tubes).

The average value of ν_{21} for tubes B and F was 0.211, which resulted in a value for S of 1.66. K_c values were calculated using the data obtained from tube B1 for equations 1 and 2. The two K_c values were 9.00 and 8.96 $MN.M^{-\frac{3}{2}}$ for equations 1 and 2 respectively. Fig. 49 shows the variation of σ_H^* with crack length, c. The experimental values of σ_H^* and c are also illustrated.

Similarly to previous discussions the theoretical lines for the two equations are almost identical and agree reasonably well with the experimental results. Nearly all the actual failure hoop stresses were higher than the ones obtained from the equations. The probable error estimate of $\pm$ 13% on σ_H^* could account for the discrepancies in all of the results, except those for tubes B3 and B5. It was necessary to estimate the depth of slot which would cut through all of the hoop layer. This was determined by measuring the hoop thickness in the walls of the tubes. Difficulty was encountered in obtaining an accurate depth of cut since the surface of the tube was slightly corrugated. Small inaccuracies in the slot depth could result in large errors in σ_H^*, particularly if the hoop winding was not completely cut. This may explain the high values of failure hoop stress measured for these tubes. The equations are useful for prediction of failure pressures for this type of tube and containing a half through wall defect.

Figs. 50 and 51 show variations of $(\sigma_H^{*2} \pi c)^{-1}$ with c^2/Rt

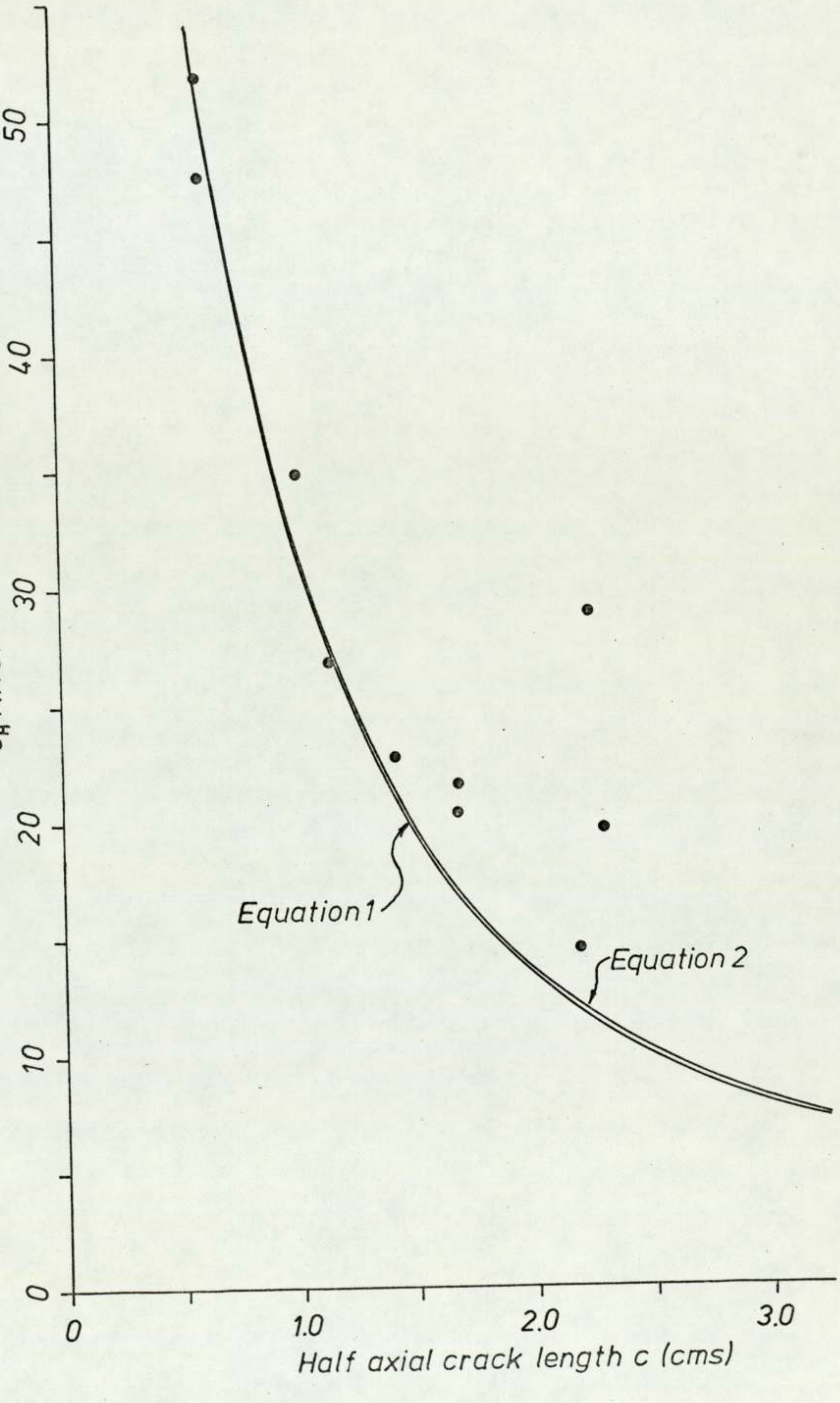

Fig. 49. σ_H^* v. crack length for B and F tubes.

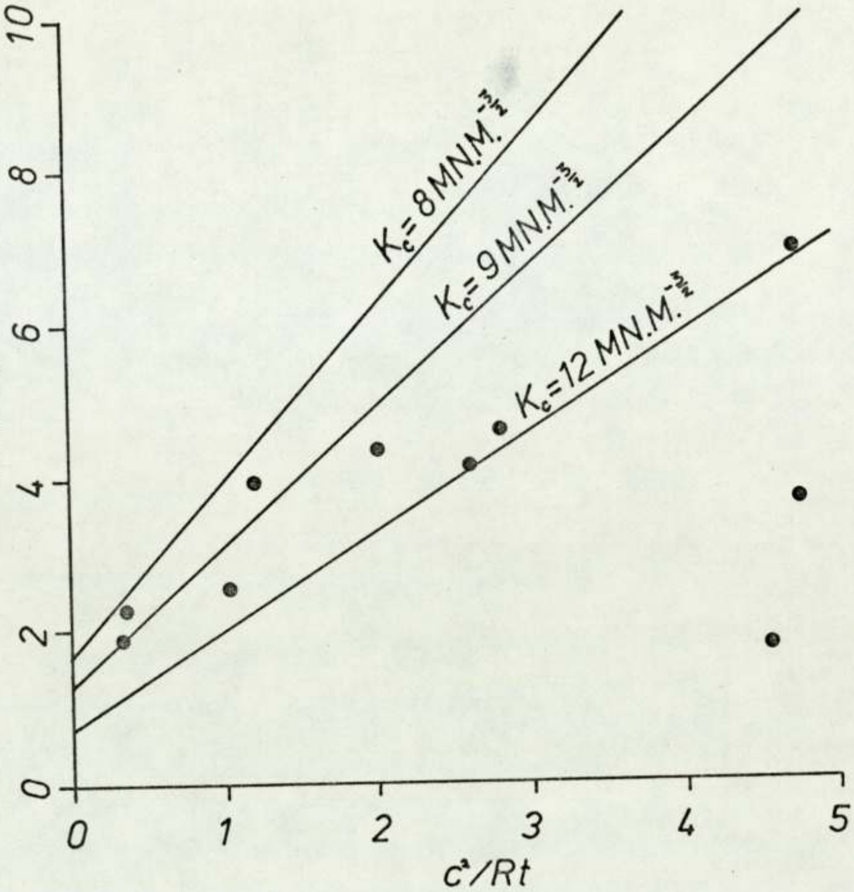

Fig.50. Equation 1.

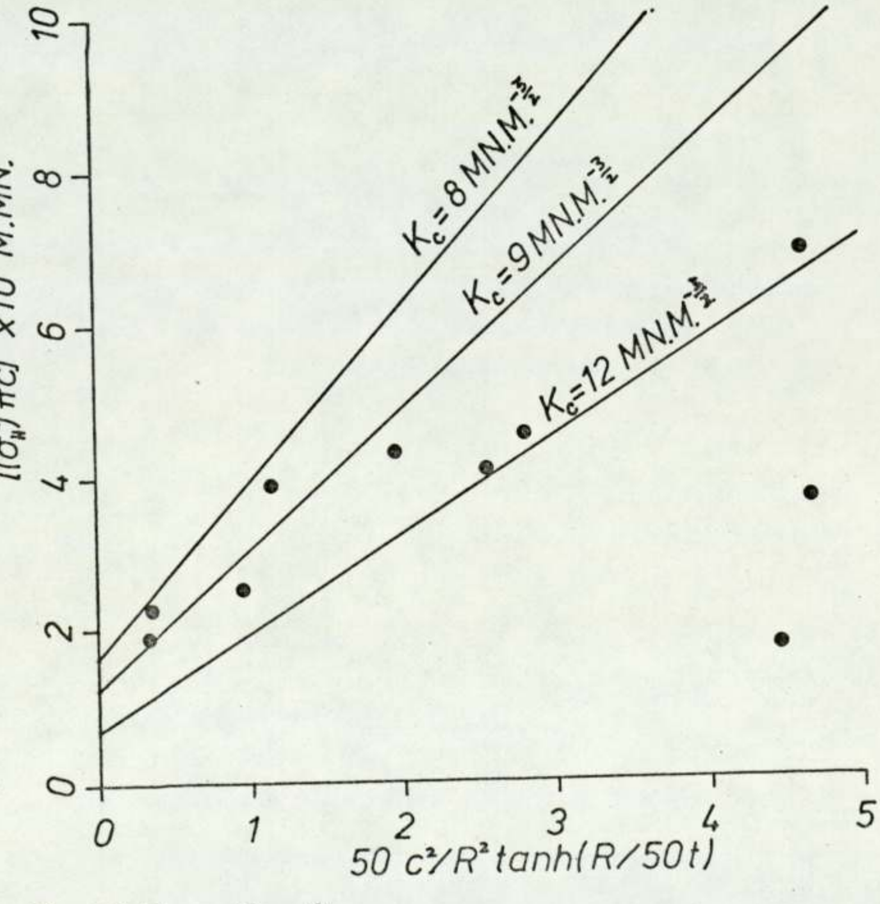

Fig.51. Equation 2.

and c^2/R^2 50tanh R/50t for equations 1 and 2 respectively. The graphs are very similar and show that all the points, except two for tubes B3 and B5, lie between a band width of $K_c = 8$ and $K_c = 12$ MN.M^{-2}. The figures confirm that equations 1 and 2 are useful for prediction of failure pressures. For design purposes, the line $K_c = 8$ MN.M^{-2} contains all the failures. Similarly to the A and D tubes, the cutting of the hoop windings has drastically reduced the pressure holding capabilities of these tubes.

The failure mechanism was slightly different for different slot lengths as shown by the A and D tubes. Plates 52 to 59 show the series of events leading to the failure of tube F1. This tube had a relatively short slot of length, 2c = 1.234cm. Plate 52 shows the tube before pressurising. As the tube was pressurised the interface between the cut, hoop layers and the $\pm 30^\circ$ layers was broken as the $\pm 30^\circ$ layers deformed. Plate 53 shows the cut, hoop layers after they had broken away. As further liquid was pumped into the tube the volume was taken up by bulging of the $\pm 30^\circ$ layers. The pressure remained fairly constant at this point. The deformation of the layers is shown in plate 54. More liquid caused the layers to bulge further, until the critical, semi-circular cross sectioned bulge was reached. This is shown in plate 55. The stress required to decrease the radius of the bulge was greater than that to remove some of the intact hoop windings. The removal of some of these windings, with the subsequent relief of stress, is shown in plate 56. As more liquid was pumped in the bulge reached its new critical semi-circular

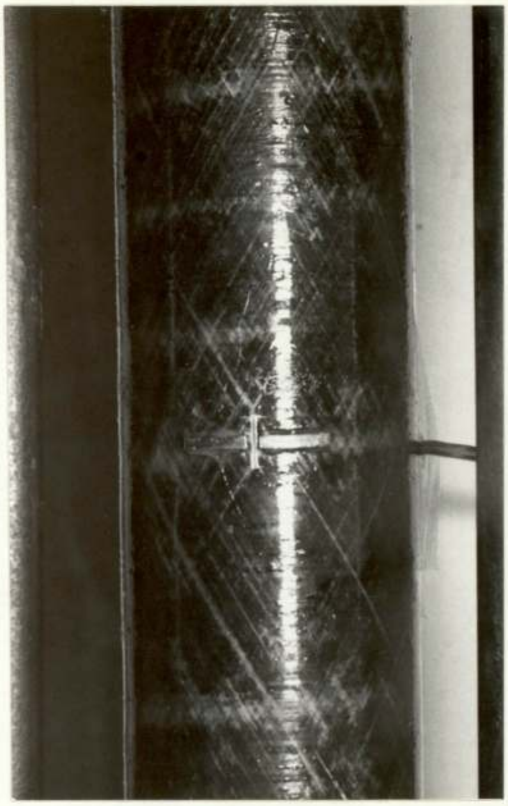

Plate 52.

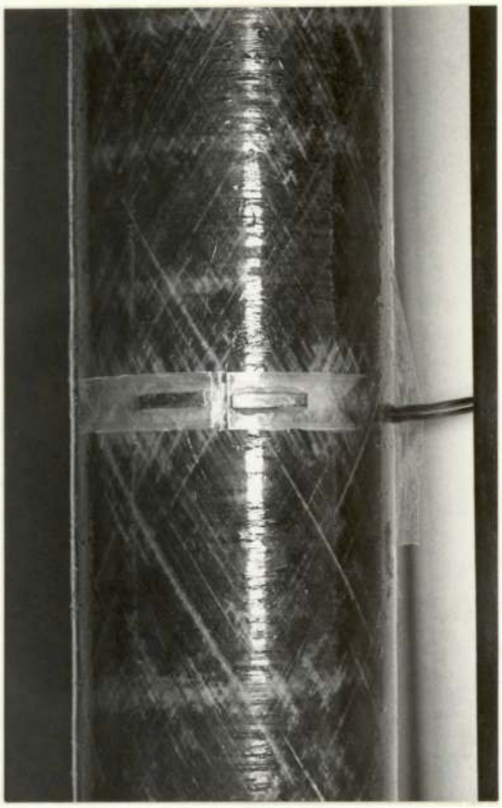

Plate 53.

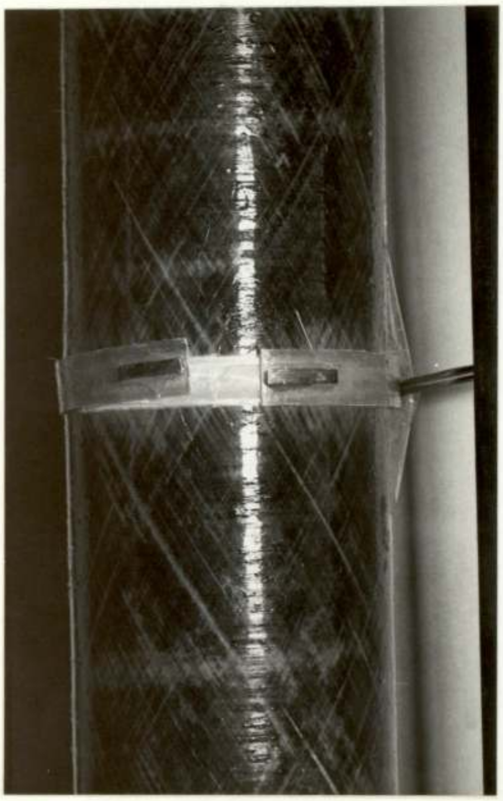

Plate 54.

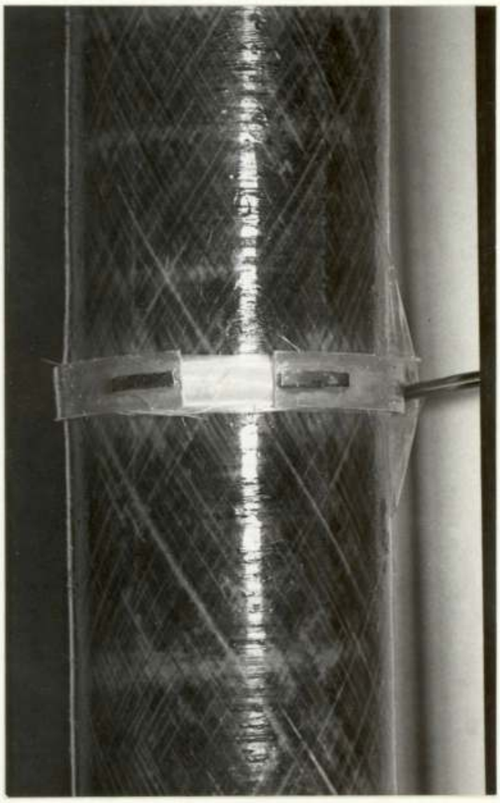

Plate 55.

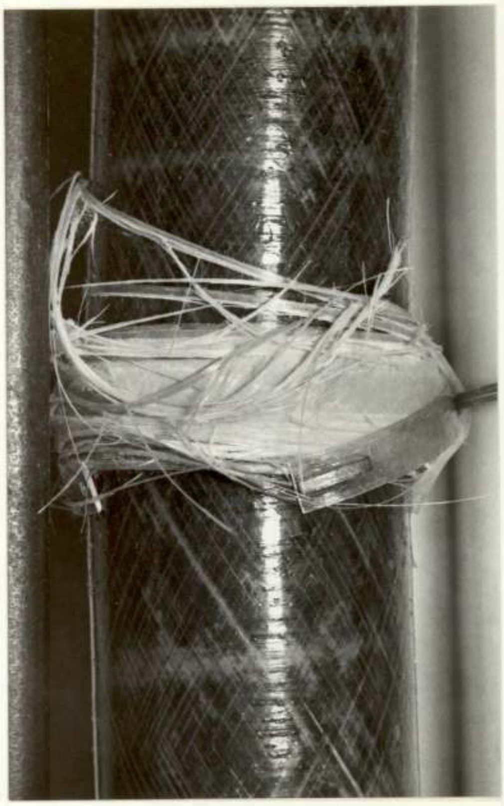

Plate 56.

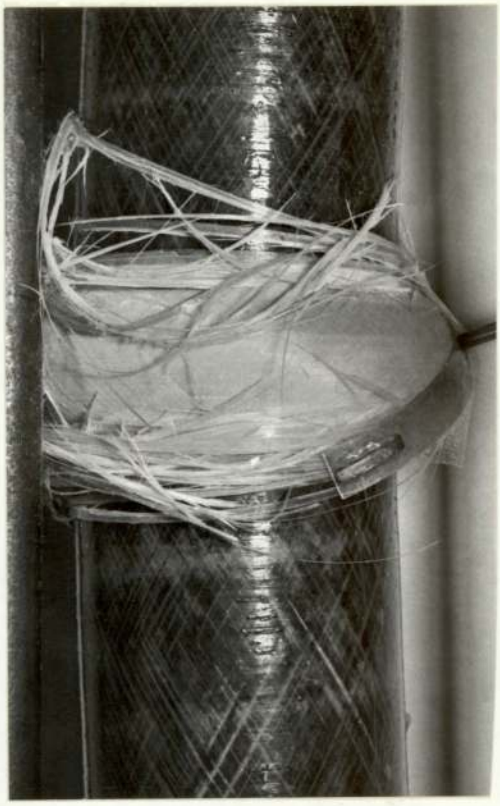

Plate 57.

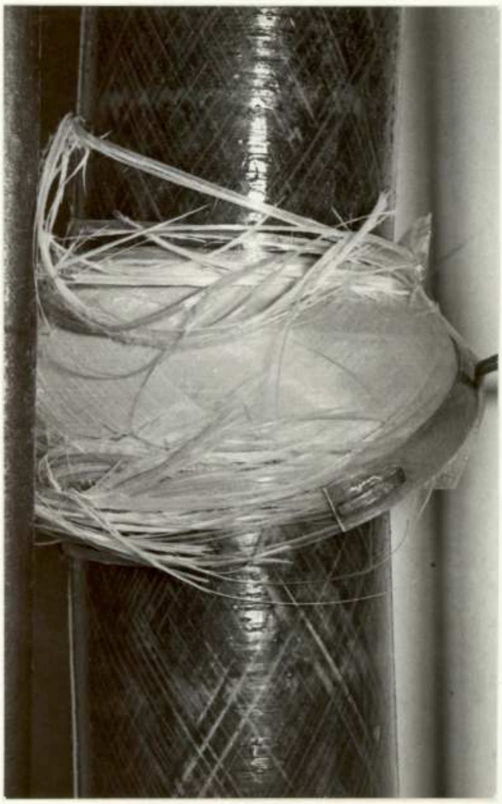

Plate 58.

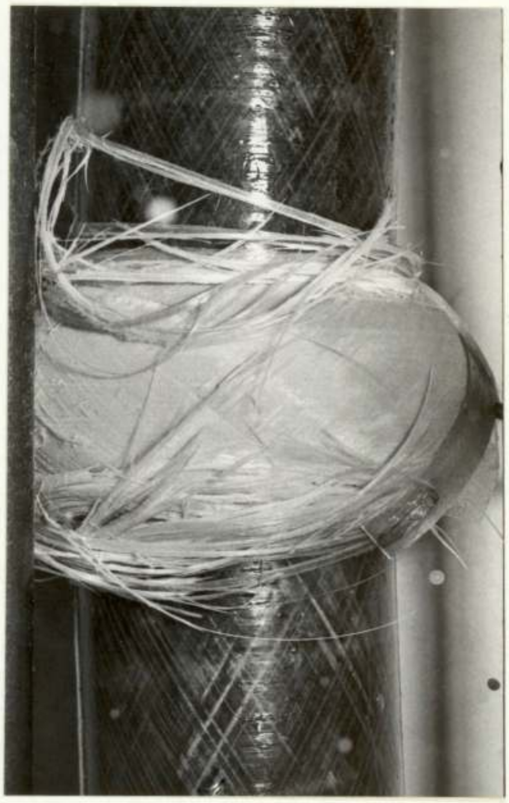

Plate 59.

cross section, shown in plate 57. Plate 58 illustrates that, more hoop windings were then stripped away. This process was repeated until failure occurred as shown in plate 59. This behaviour was typical for tubes containing short slots, ($2c < 2.0cm$).

The tubes with longer slots did not display this behaviour of splitting of hoop layers ahead of the slot. Plates 60 to 63 show the sequence of events leading to the failure of tube F3. This tube had a relatively long defect, $2c = 2.864cm$. Plate 60 shows the tube before pressurising. Similarly to the tubes with short slots, the pressure first caused the cut, hoop layers to be debonded and forced away from the $\pm 30^\circ$ layers as shown in plate 61. Plate 62 shows the $\pm 30^\circ$ layers beginning to bulge out and decrease the radius of cross section. The bulge did not reach the critical semi circular cross section before failure, depicted by plate 63.

Tube F1 had a shorter slot than tube F3, but after removal of hoop layers the tubes were similar. The hoop windings continued to be removed, even after the slot length was greater than that of tube F3. The $\pm 30^\circ$ layers were strained and weakened to allow the initial removal of hoop windings and deformed easily to the critical semi-circular cross section. This resulted in continual hoop winding removal and gross bulging at failure of the tube.

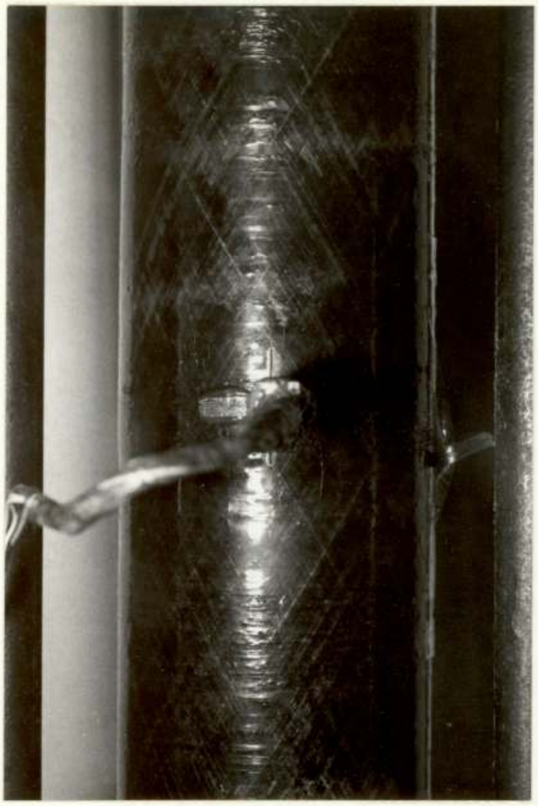

Plate 60.

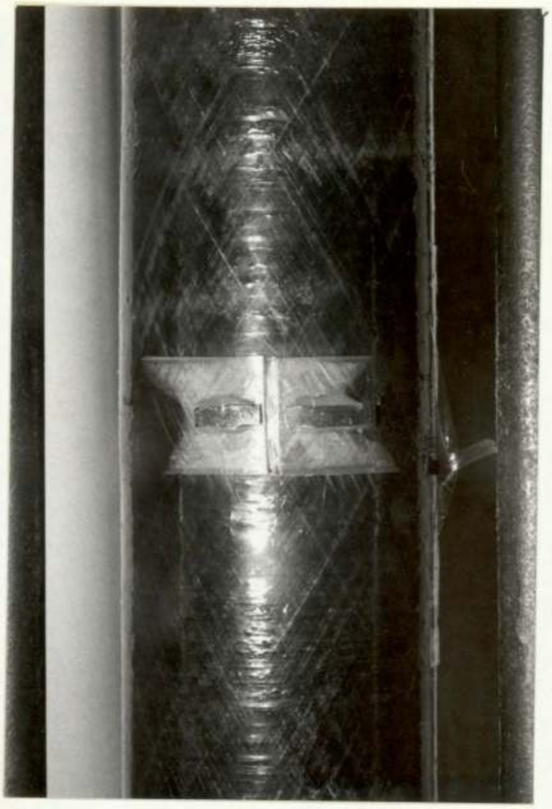

Plate 61.

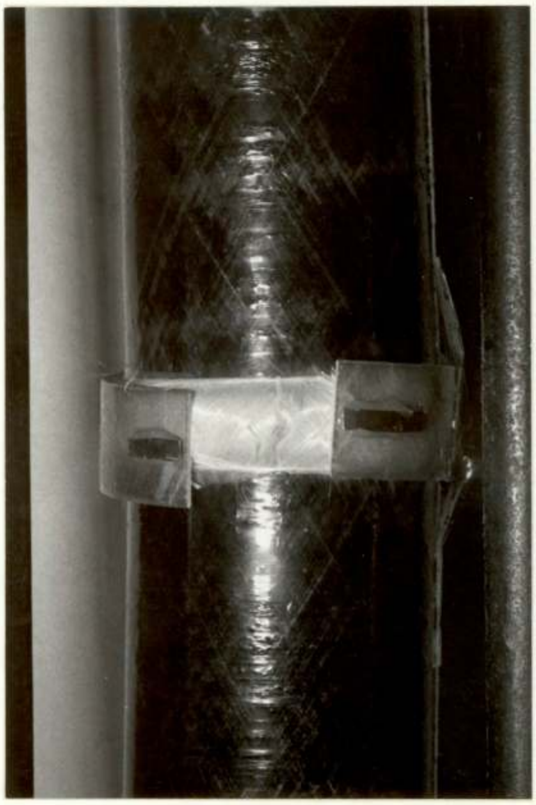

Plate 62.

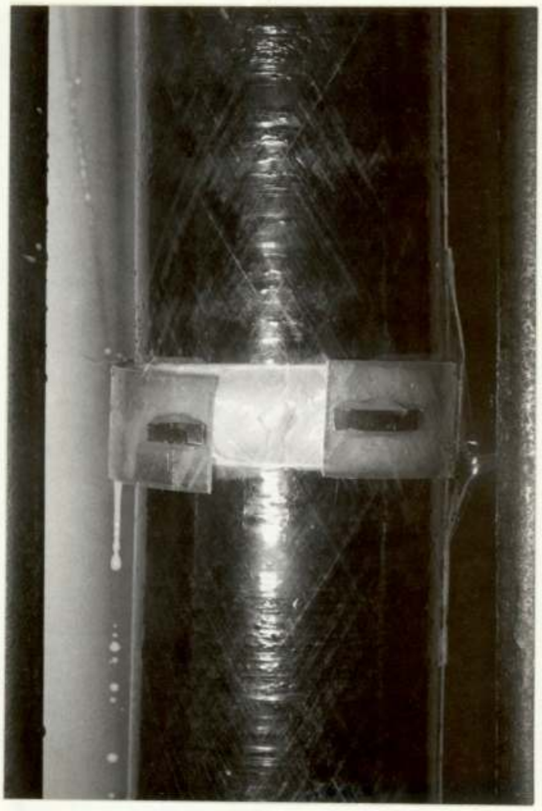

Plate 63.

6. 3. 2. 5. 50% ± 30° and 50% ± 90° helix angle tubes with quarter through wall defects (C and G tubes).

The average value of $_{21}$ for tubes C and G was 0.222, which resulted in a value of S of 1.66. Another equation was considered for the interpretation of the data for these tubes. This was equation 3 which did not contain a correction factor for crack mouth bulging. The equation was:

Equation 3

$$\sigma_H^* = \frac{K_c}{(\pi c)^{\frac{1}{2}}}$$

K_c values were calculated using the data from tube C4 for equations 1, 2 and 3. The K_c values were 13.25, 13.20 and 11.00 $\mathrm{MN.M}^{-\frac{3}{2}}$ for equations 1, 2 and 3, respectively. Fig. 52 shows the variation of σ_H^* with crack length, c for the equations. The experimental points are also illustrated.

The theoretical lines for equations 1 and 2 are almost identical, but underestimate the failure hoop stresses for tubes containing long defects. The line for equation 3 overestimates the failure hoop stresses for most tubes. For quarter through wall slots crack mouth bulging is not as pronounced and the correction factor, given by Folias, appears to be too large. The scatter of the results is probably due to the difficulty of obtaining a reproducable slot depth for these tubes. Small differences in slot depth have a pronounced effect on σ_H^*. Using equations 1 and 2 would underestimate the failure pressures which the tubes could sustain for these types of defect.

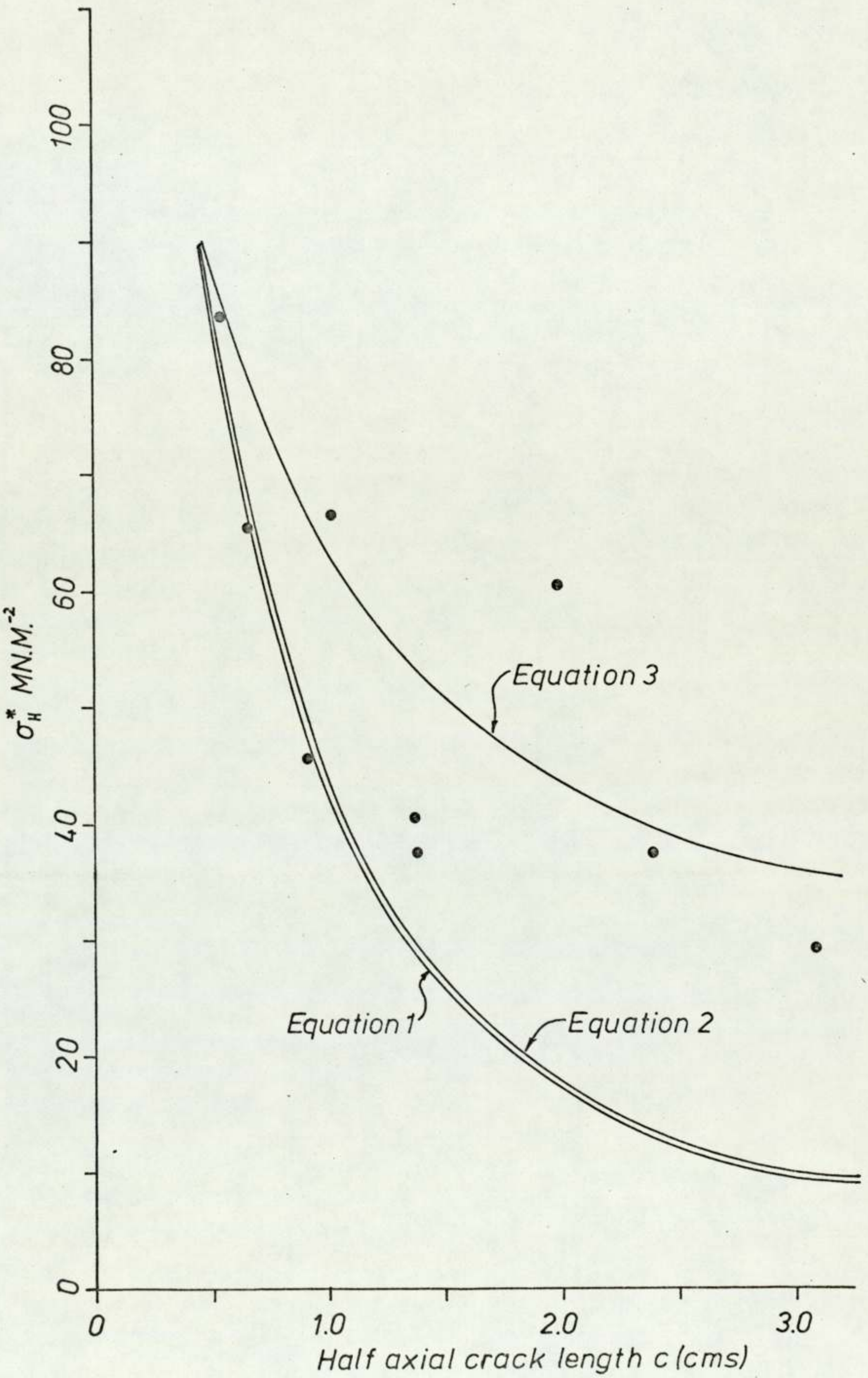

Fig. 52. σ_H^* v. crack length for C and G tubes.

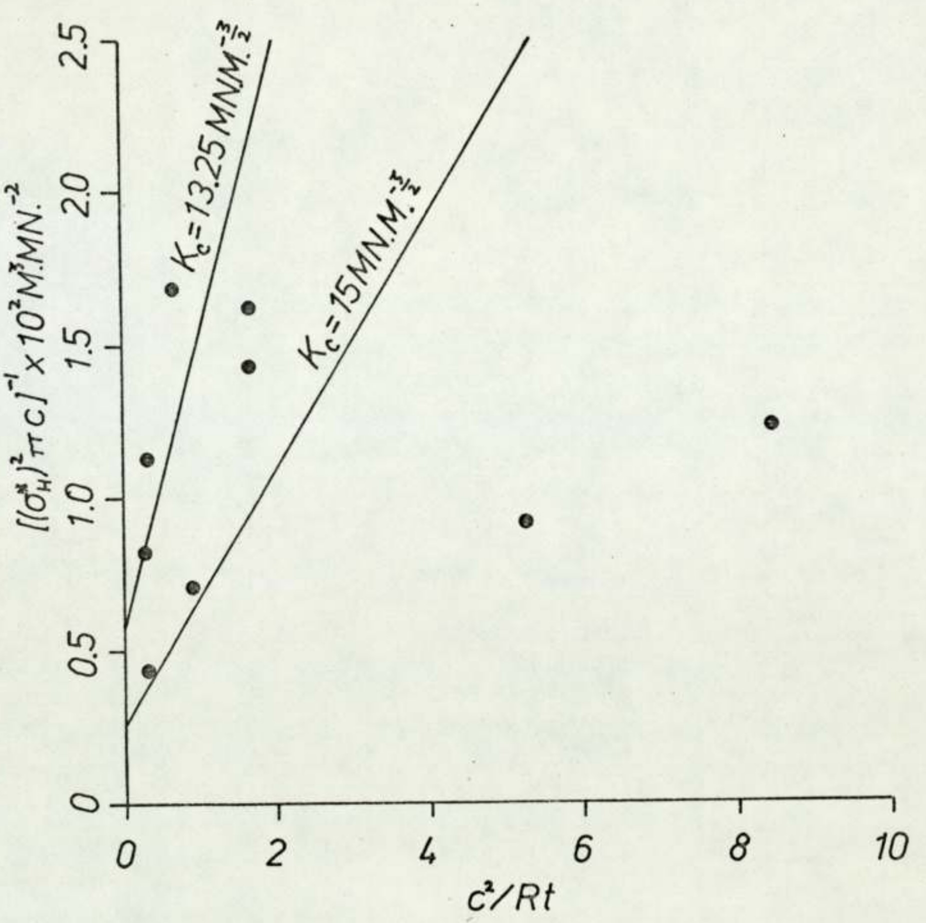

Fig.53. Equation 1.

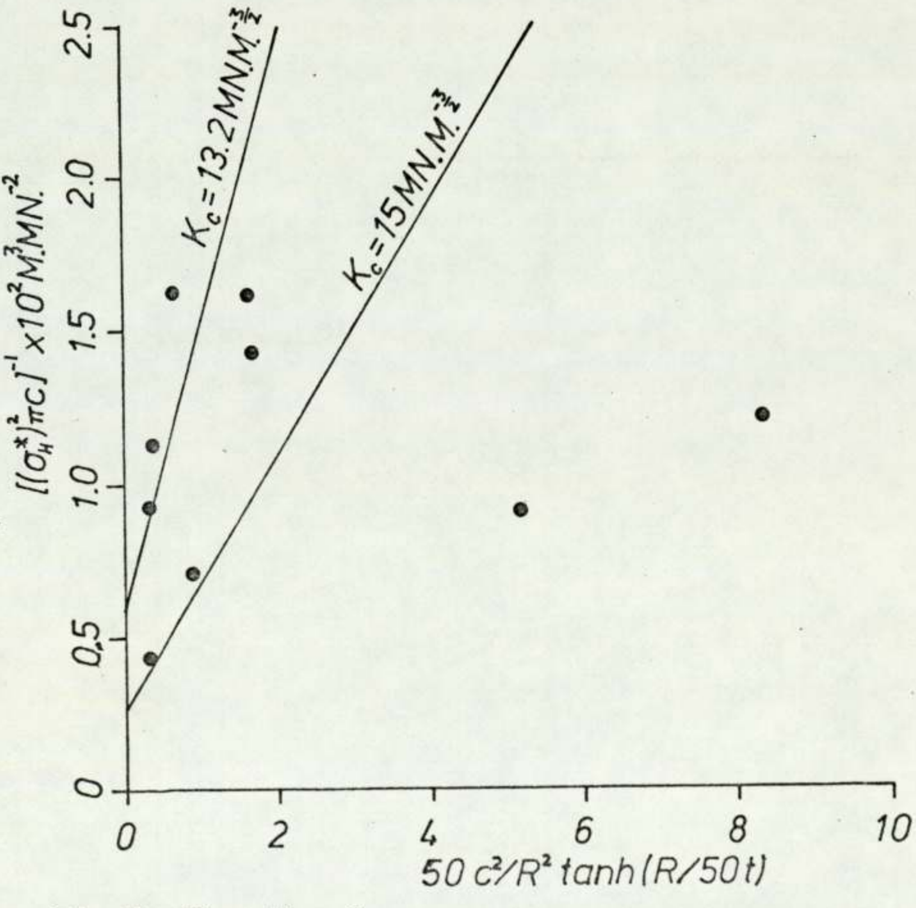

Fig. 54. Equation 2.

Figs. 53 and 54 show graphs of $(\sigma_H^{*2} \pi c)^{-1}$ versus c^2/Rt and c^2/R^2 50tanh R/50t for equations 1 and 2. The graphs are very similar and show that most of the points lie around the $K_c = 13$ and $K_c = 15$ $MN.M^{-\frac{3}{2}}$ lines. The method of presentation emphasises the scatter shown by the previous means of interpretation. The graphs illustrate that designing, using equations 1 and 2, would underestimate the usable strengths of the tubes. K_c values were calculated using equation 3 for the experimental data. This resulted in a mean K_c value of 10.14 $MN.M^{-\frac{3}{2}}$ with 95% confidence limits of ± 4.6 $MN.M^{-\frac{3}{2}}$. This equation is of little use for the prediction of failure pressures for this type of defect.

Plates 64 to 65 show the sequence of events leading to the failure of tube C4. This tube had a relatively short slot, 2c = 2.104cm. Plate 64 shows the tube before pressurising. Similarly to the other tubes containing a hoop winding, the failure mechanism began by debonding of the cut, hoop layers from the intact hoop layers. This is shown in plate 65. Voids in the $\pm 30^\circ$ layers are also shown. The layers were strained more than they could sustain, but were held by the hoop layers. When failure of the hoop layers occurred, the $\pm 30^\circ$ layers quickly deformed to the critical semi-circular cross section and began to remove hoop layers at either side as shown by plate 66. It is clear that this mechanism of hoop layer removal at either side of the bulge was promoted easily when the $\pm 30^\circ$ layers were strained well past their normal maximum level. This was confirmed by the similar mechanism shown for longer slots. Previous tubes containing long slots did not show this mechanism. The hoop layers were removed continuously

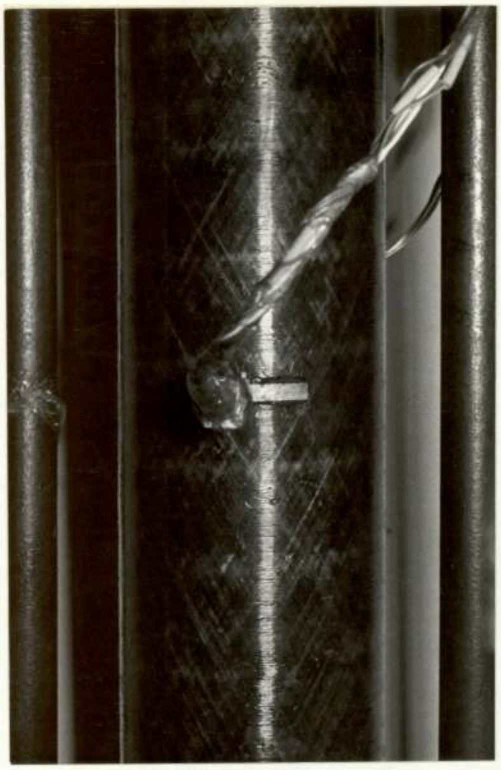

Plate 64.

Plate 65.

Plate 66.

Plate 67.

as the bulge grew until failure occurred as shown in plate 67.

Figs. 68 to 71 show the sequence of events leading to the failure of tube C2. This tube had a slot of length, $2c = 2.756$cm. Plate 68 shows the tube before pressurising. As before the pressure resulted in the breaking of the bond between the cut, hoop layers and the intact, hoop layers. The tube was capable of sustaining a pressure high enough to severely strain the $\pm 30^\circ$ layers. Plate 69 shows the voids in these layers. When the pressure was high enough to break the hoop layers, the $\pm 30^\circ$ layers could deform quickly to the semi-circular cross section necessary to remove hoop layers. This is shown in plate 70. This plate was taken at the moment when the hoop layers failed. Almost simultaneously, the $\pm 30^\circ$ layers deformed and stripped hoop layers at either side. The bulge continued to grow, with the removal of hoop layers, until ultimate failure occurred as shown in plate 71.

The failure mechanisms illustrated by the tubes containing hoop windings, clearly illustrated that the hoop layers should not be damaged before a tube is put into service. Protection of the hoop layers is warranted if drastic reductions in the pressure holding capabilities of these tubes are to be avoided.

Plate 68.

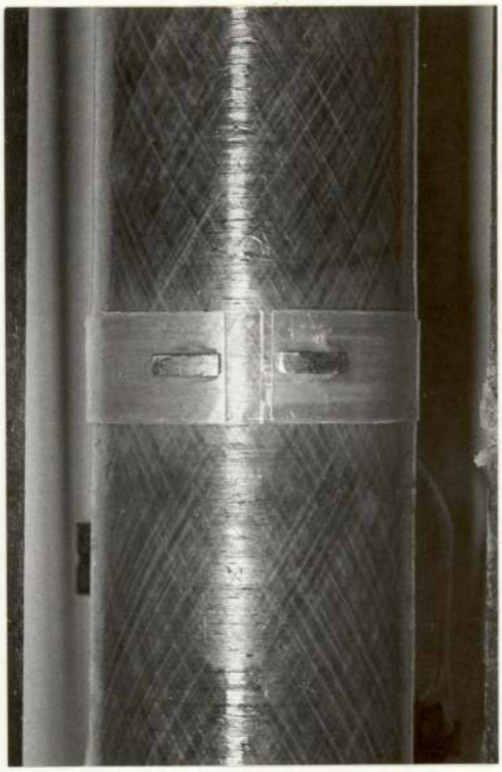

Plate 69.

Plate 70.

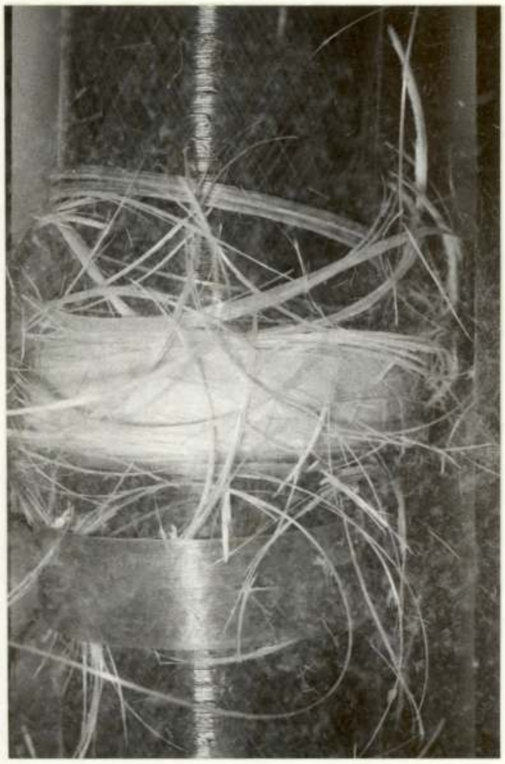

Plate 71.

6. 4. Obtaining K_c values from the compliance testing.

Section 6. 3. illustrates there was strong experimental evidence that constant K_c values could be obtained for the materials which were the subject of this work. The K_c values were obtained from similar equations to those used for metals. The expression

$$K_c = \sigma_H^* (\pi c)^{\frac{1}{2}} (1 + S\, c^2/Rt)^{\frac{1}{2}} \qquad \ldots\ldots(1)$$

could be used to give reasonably constant values of K_c for most of the tube systems. This expression is similar to that used for metal pipes containing axial cracks of length, 2c:

$$K_c = \sigma_H^* (Y)\, c^{\frac{1}{2}} \qquad \ldots\ldots(2)$$

The constant Y is given by:

$$Y = 1.77(1 - 0.1(2c/L) + (2c/L)^2)(1 + S\, c^2/Rt)^{\frac{1}{2}} \qquad \ldots\ldots(3)$$

and includes the Folias correction factor. For very long pipe lengths the value of Y can be approximated to, $(\pi)^{\frac{1}{2}} (1 + S\, c^2/Rt)^{\frac{1}{2}}$, which is consistent with equation (1). The compliance measurements carried out here could be used to obtain K_c values for the two expressions:

$$K_c = \sigma_H^* (c)^{\frac{1}{2}} \left(\frac{EL}{2c(1-\nu^2)} \frac{dC''}{dc} \right)^{\frac{1}{2}} \qquad \ldots\ldots(4)$$

(see Appendix 1)

$$K_c = \sigma_H^* (c)^{\frac{1}{2}} \left(\frac{2Et^2}{cD^2(1-\nu^2)} \frac{d(\Delta V/P)}{dc} \right)^{\frac{1}{2}} \qquad \ldots\ldots(5)$$

(after Underwood et Al(45))

It is convenient to discuss the use of each equation separately.

6. 4. 1. Crack opening displacement measurements.

Equations (2) and (4) can be equated to each other by assuming that the expression (3) will hold for the tubes pressurised here. This results in:

$$1.77(1-0.1(2c/L)+(2c/L)^2)(1+S\ c^2/Rt)^{\frac{1}{2}}$$

$$= \left(\frac{EL}{2c(1-\nu^2)} \frac{dC''}{dc} \right)^{\frac{1}{2}}$$

By algebra and integration an expression for C'' is obtained:

$$C'' = (1+S\ c^2/Rt)^{\frac{1}{2}} \frac{2(1-\nu^2)}{E} (3.17c^2-1.71c^3+51.93c^4 -16.70c^5+281.22c^6)$$

Using average values for the constants in the above equation for tubes with and without hoop windings, two graphs of C'' versus crack length, c were obtained. These are shown in Figs. 55 and 56. The experimental values of compliance for the individual tubes are illustrated also.

The figures show that, in the range, c = 0 to 5cms, the rate of change of compliance with crack length is very small. The experimental values were slightly higher than the theoretical ones. The determination of rates of change of compliance for this range of crack lengths is difficult.

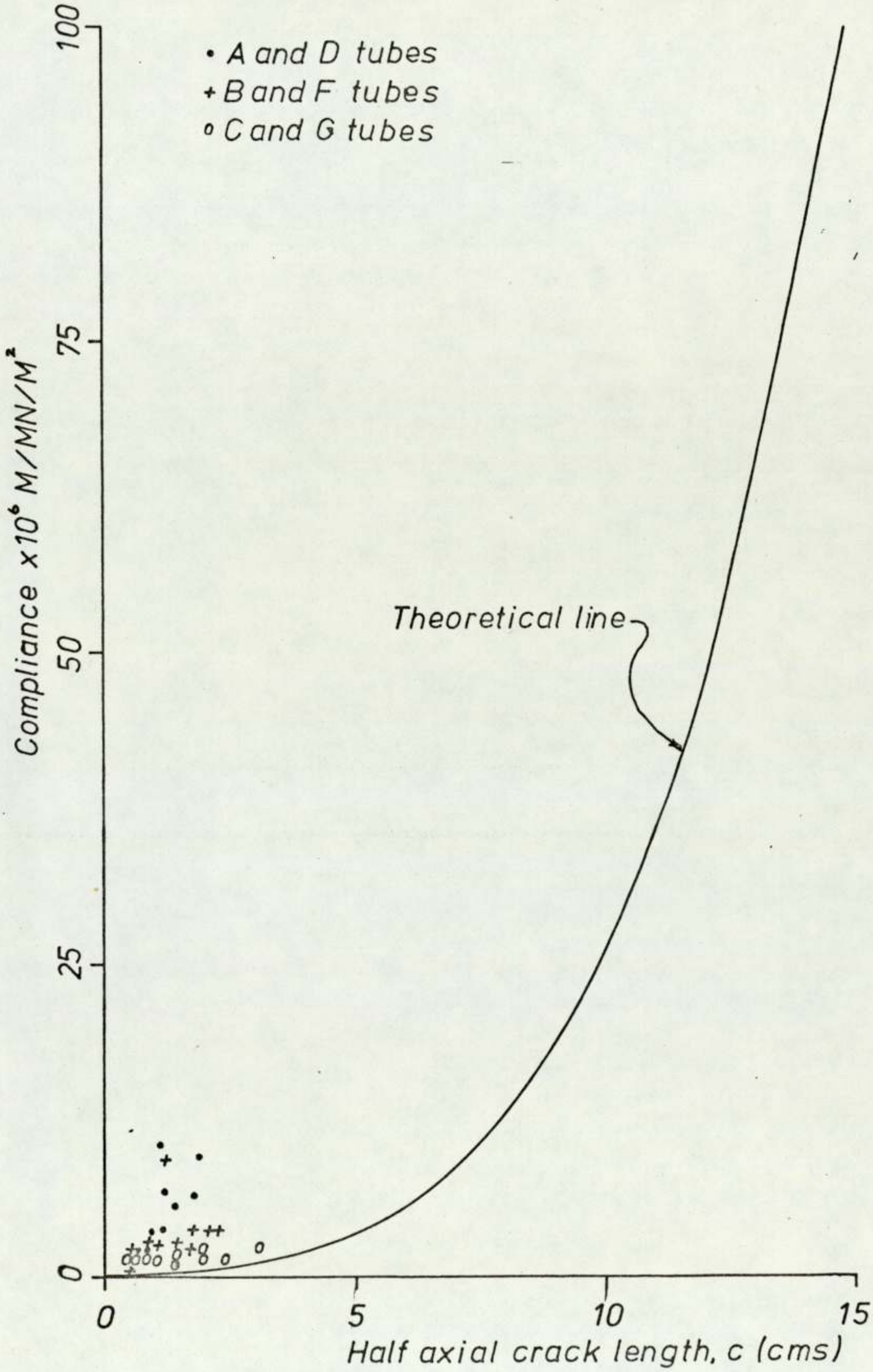

Fig55 Variation of compliance with crack length for tubes with hoop windings.

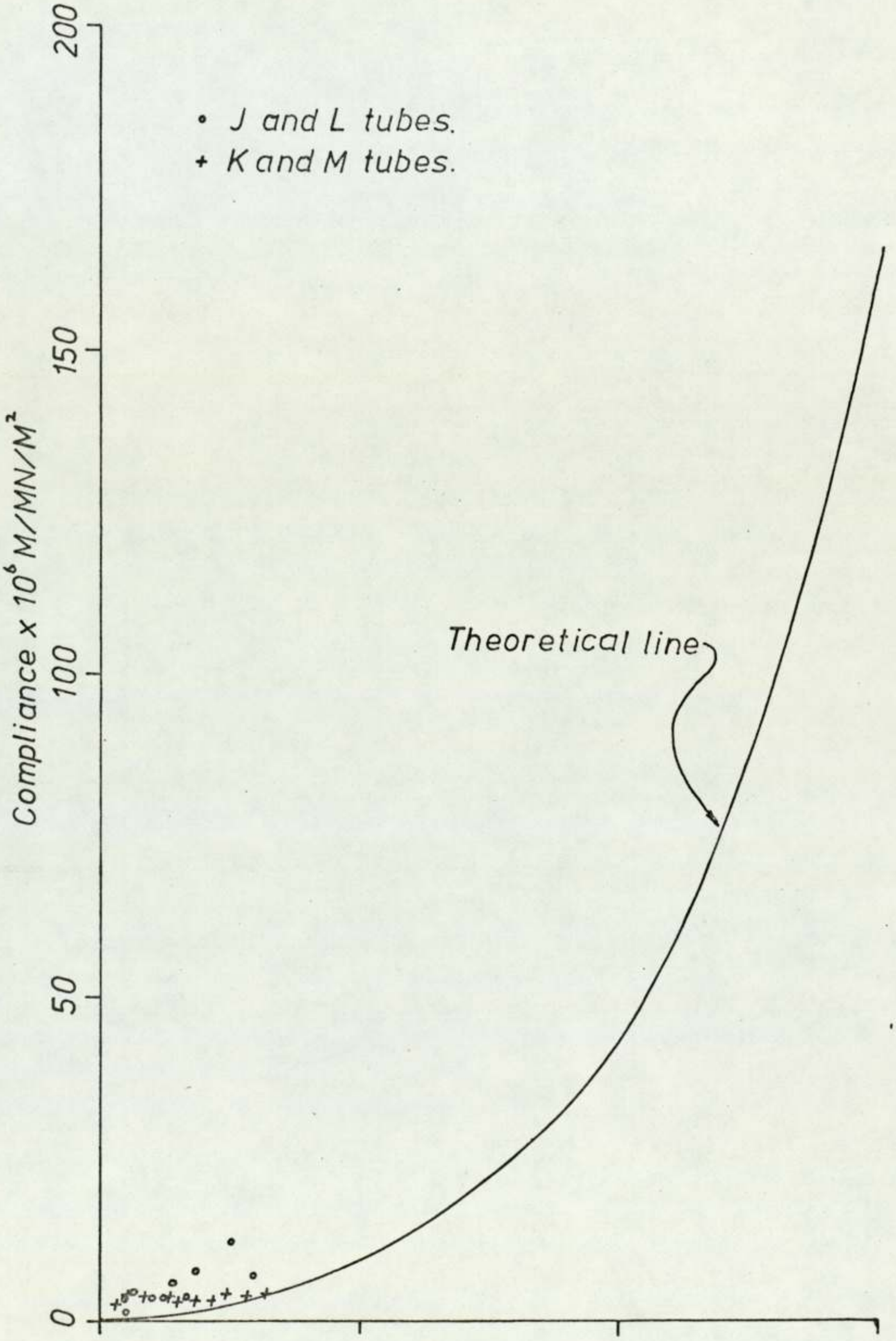

Fig56 Variation of compliance with crack length for tubes without hoop windings.

6. 4. 2. Volume change measurements.

Equations (2) and (5) can be equated to each other, by assuming that the expression (3) holds for the tubes which are the subject of this work. This gives:

$$1.77(1-0.1(2c/L)+(2c/L)^2)(1 + S\ c^2/Rt)^{\frac{1}{2}} = \left(\frac{2\,Et^2}{(1-\nu^2)cD^2} \ \frac{d(\Delta V/P)}{dc} \right)^{\frac{1}{2}}$$

By algebra and integration an expression for V/P is obtained:

$$\Delta V/P = (1+S\ c^2/Rt)^{\frac{1}{2}} \frac{(1-\nu^2)D^2}{2Et^2} (1.57c^2-0.84c^3+25.70c^4 -8.27c^5+139.20c^6)$$

Using average values for the constants in the above equation, for tubes with and without hoop windings, two graphs of $\Delta V/P$ versus crack length, c were obtained. These are shown in Figs. 57 and 58. The experimental values of $\Delta V/P$ are illustrated also.

In the range of, c = 0 to 5 cms, the rate of change of $\Delta V/P$ with crack length is very small. The experimental values agree with the theoretical line reasonably well, but it must be remembered that the scale of the Y axis is large compared to these. To determine the rate of change of compliance with crack length is seen to be very difficult for this range of c values, since it is so small.

Agreement between the theoretical lines appears to be better for volume change measurements than the displacement method. The volume change increments are larger than the displacement increments and may serve to reduce overall errors.

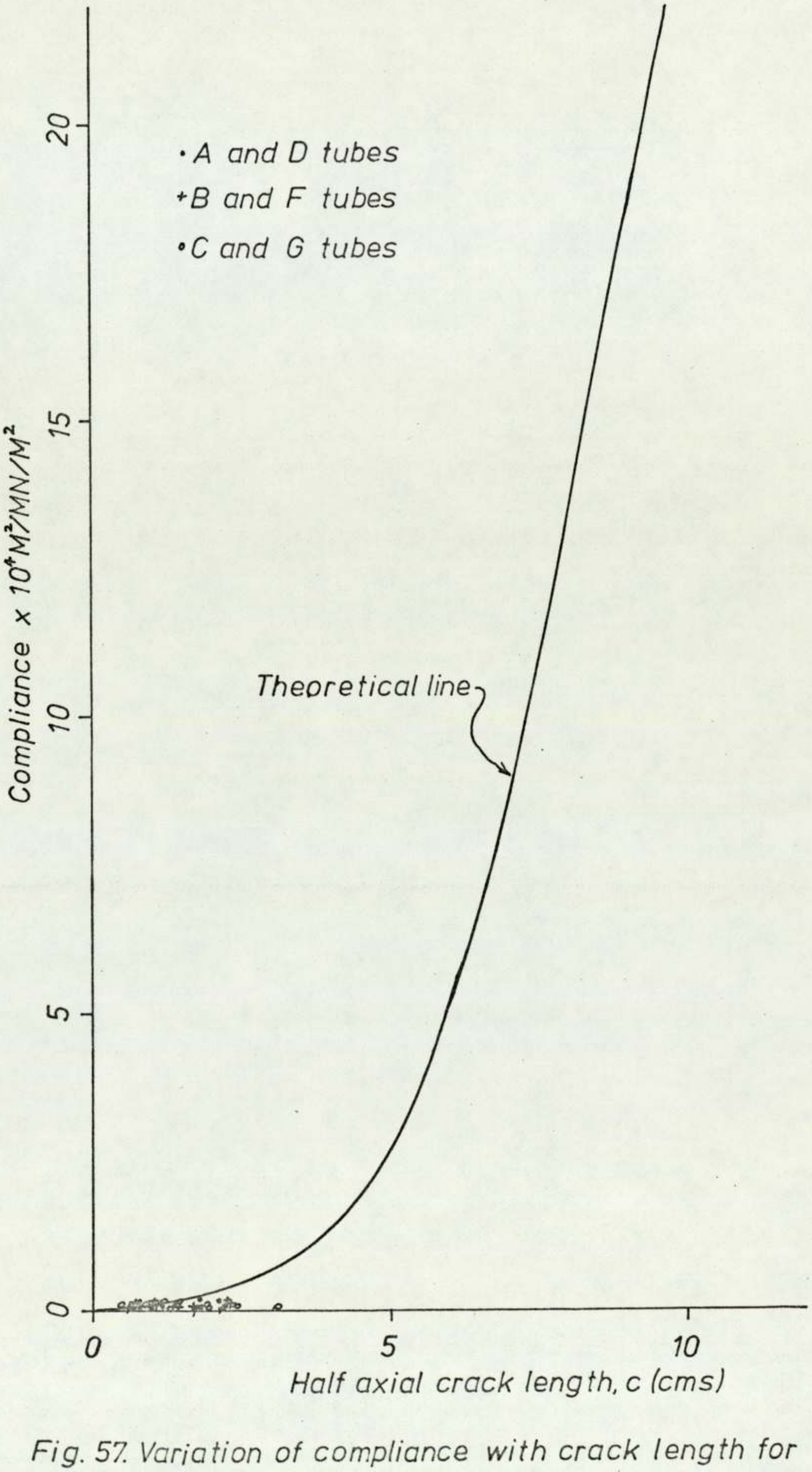

Fig. 57. Variation of compliance with crack length for tubes with hoop windings.

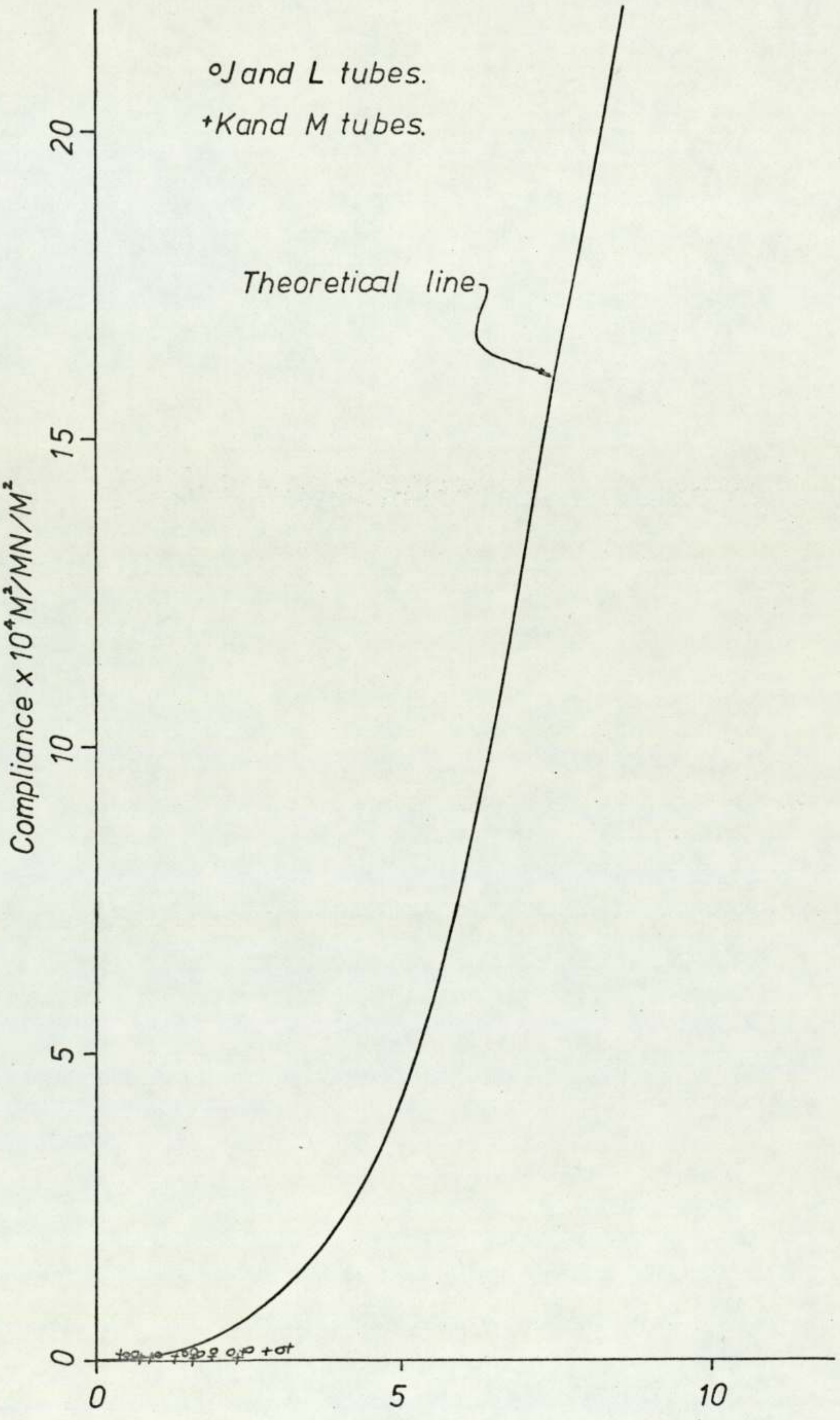

Fig. 58. Variation of compliance with crack length for tubes without hoop windings.

7. Conclusions.

7. 1. Young's Modulus and Poisson's ratio.

The use of the two theories presented by Wallis and Tsai was found to be limited. Neither theory was significantly better for the predictions and both were found to be poor for Poisson's ratio predictions. In general the predictions of Young's moduli were lower than the actual moduli for both theories. Estimates of the modulus for both theories were conservative and components could be overdesigned.

7. 2. Compliance measurements.

Both methods of estimating the compliance relied on several assumptions and this must be remembered when reaching the following conclusions. The compliance of the tubes was found to increase with increasing slot length for both measurements. The rate of change of compliance was greater, the greater the depth of the slot.

7. 3. Pressure testing of the tubes.

When designing pipework for the conveyance of liquids under pressure the engineer needs to know what defect size levels are tolerable and when section changes are critical. Section changes are inevitable in such places as junctions between one pipe and another. This is normally carried out by the use of flanges which are bolted together.

This work has shown that section changes can have an important influence on the failure of glass reinforced plastic tubes. Both the plain helical and the mixture of helical and hoop wound tubes failed at the ends near to the reinforcement. Indeed it was found that for a plain helically wound tube containing a half through wall defect, the stress concentration due to section change could be more important than the presence of the slot. Defects arising due to mechanical damage may be similar to the part through wall defects introduced into the tubes.

The failure strength of a tube containing no artificial defects was found to be increased by a factor of ten by the incorporation of 50% hoop windings. This is to be expected since there was no longitudinal stress present because the ends of the tubes were allowed to slide on the seals. The axis of the hoop windings was in the direction of the hoop stress. Damage of the hoop windings is critical because of this and when testing tubes with artificial defects present the failure hoop stress decreased markedly.

Defects are always present in structural materials and are expected in glass reinforced plastic tubes due to the method of manufacture and curing. For isotropic materials linear elastic fracture mechanics has been successfully applied for the prediction of failure of plates and pipes containing defects. It has been found that the equations can be used for the tubes which were the subject of this work for most of the defect types. Deviations from these equations were found when the defects were only part through the wall of the tube. This was probably because these defects were treated as though they were full through defects. The design of pipes which contain part through defects would be conservative. The equations, which contained Folias correction factors for crack mouth bulging, are useful to the engineer for designing pipe systems. It must be remembered that a change in the helix angle or lay up may affect the response of the tubes and invalidate the use of the equations.

All the tubes tested here had no longitudinal stress present due to the free ends. Whilst this applies in many circumstances it must be remembered that pipes could be subjected to biaxial stresses due to restraints. These restraints may derive from the jointing systems and supports or the tubes may be buried. It is important that the method of loading is taken into consideration when designing the pipe system.

A further test for the validity of the use of the equations was made by attempting to obtain the geometrical factor, Y for this material. It was found that the range of crack lengths studied here was too small for the rate of change of compliance with crack length to be measured accurately. Y calibration curves could only be determined by testing tubes in the range $c = 5$ to $c = 30$ cms(i.e. $c/W = 0.1$ to $c/W = 0.6$).

8. Suggestions for further work.

8. 1. Compliance Testing.

Compliance tests should be carried out on tubes with larger slots than those in the work presented here. Y calibration charts, determined in this way, could be compared with those obtained from equation (3) in 6.4. It is suggested that the variation of compliance obtained from a range of slot lengths from $c = 5$ to $c = 30$cm be investigated.

8. 2. Subjecting tubes to internal pressure.

The investigation into the effects of various types of defects on the two types of tube has been fairly exhaustive. The effects of the presence of these types of defects on tubes of other lay ups should be determined. Since the cutting of the hoop windings has been found to have a marked deleterious effect on the failure pressures of the tubes, it is suggested that various hoop lay ups be investigated. Damage to the tubes is far more likely on the outside and it is important to find a glass lay up which does not incorporate 100% of the hoop windings there.

A similar test programme to the one presented here should be created for tubes containing mixtures of carbon and glass fibres at various helix angles. It may be found that a thinner carbon fibre hoop winding inside the tube could replace much of the glass hoop layer on the outside and thus produce a less damage sensitive tube. Pressure tests should be carried out on tubes with carefully designed lay ups of the two fibres in order that an optimum be found.

References.

1. E. S. Folias, Int. J. Fract. Mechs., 1, (1965), p. 20.

2. E. S. Folias, Int. J. Fract. Mechs., 1, (1965), p. 104.

3. G. T. Hahn, M. Sarrate and A. R. Rosenfield, Int. J. Fract. Mechs., 5, (1969), p. 187.

4. D. M. Schuster and E. Scala, AIAA/ASME, 8th. Structures, Structural Dynamics and Materials Conference, March 29 - 31, (1967).

5. H. L. Cox, Brit. J. Appl. Phys., 3, (1952), p. 72.

6. J. O. Antwater, Mod. Plastics, 33, (1), (1956), p. 156.

7. N. F. Dow, General Electrics Co. Rep. No. R63/SD61, (1963).

8. B. W. Rosen, Mechs, of Comp. Strengthening, Fiber Composite Materials, American Society of Metals, Metals Park, Ohio, (1965), p. 37.

9. A. Kelly, Strong Solids, Oxford University Press, (1966).

10. I. M. Allison and L. C. Holloway, Plastics Inst. Conf. Research Projects in Reinforced Plastics, 20th. March, (1968).

11. F. R. Wallis, Summerfield Research Station Tech. Report No. 70/26, November 1970, I.M.I. Ltd., Kidderminster, Worcs.

12. V. C. Cutler, Society of Plastics Industry, Inc., 16th. Annual Tech. Manag. Conf., Reinforced Plastics Div., 1961.

13. S. W. Tsai, Structural Behaviour of Composite Materials, NASA CR-71, 1964.

14. L. B. Greszczuk, Report No. SM-45849, Missile and Space Systems Division, Douglas Aircraft Co.,Inc., January 1965.

15. A. H. Puppo and A. H. Evenson, J. Comp. Mats., 4, 1970, p.204.

16. R. Byron Pipes and N. J. Pagano, J. Comp. Mats., 4, (1970), p. 538.

17. N. J. Pagano and R. Byron Pipes, Inst. J. Mech. Sci., Permagon Press, 15, (1973), p. 679.

18. N. J. Pagano, J. Comp. Mats., 8, (1974), p. 65.

19. J. M. Whitney and C. T. Sun, J. Sound and Vibration, 30, (1), (1973), p. 85.

20. N. J. Pagano and R. Byron Pipes, J. Comp. Mats., 5, (1971), p. 50.

21. R. L. Foye and D. J. Baker, "Design of Orthotropic Laminates", 11th Annual AIAA Structures, Structural Dynamics and Materials Conference, Denver, Colorado, April 1970.

22. N. J. Pagano, J. C. Halpin and J. M. Whitney, J. Comp. Mats., 2, (2), (1968), p. 154.

23. N. J. Pagano and J. M. Whitney, J. Comp. Mats., 4, (1970), p. 360.

24. A. A. Griffith, Phil. Trans. Roy. Soc., A221, (1913), p. 163.

25. C. E. Inglis, Trans. Inst. Naval. Arch., 1, (1913), p. 219.

26. E. Orowan, Rep. Prog. Phys., 12, (1948-49), p. 185.

27. G. R. Irwin, U. S. Naval Research Lab., Report N. R. L. 4763, (1956).

28. R. W. Peters and P Kuhn, NACA TN3993, (1957).

29. R. B. Anderson and T. L. Sullivan, NACA TND3252, (1966).

30. R. W. Nichols, W. H. Irvine, A. Quirk and E. Bevitt, Proc. First Int. Conf. on Fracture, Sendai, Japan, 1673, (1966).

31. H. Kihara, K. Ikeda and H. Iwanga, Document X-371-66, Presented at Int. Inst. Welding, Delft, (1966).

32. W. J. Chrichlow and R. H. Wells, ASTM STP 415, 25, (1967).

33. A. R. Duffy et Al, Symposium on Line Pipe Research, American Gas Assoc., New York, (1965).

34. D. L. Getz, W. S. Pierce and H. Calvert, Correlation of Uniaxial Notch Tensile Data with Pressure Vessel Fracture Characteristics, ASME, (1964).

35. J. T. Barnby and B. Spencer, to be published in J. Mats. Sci.

36. R. J. Sanford and F. R. Stonesifer, U. S. Naval Research Lab., Report NRL 7112, June, (1970).

37. M. E. Waddups, J. R. Eisenmann and B. E. Kaminski, J. Comp. Mats., 5, (1971), p. 446.

38. P. W. R. Beaumont and D. C. Phillips, J. Comp. Mats., 6, (1972), p. 32.

39. J. E. Zimmer, J. Comp. Mats., 6, (1972), p. 312.

40. M. J. Owen and P. T. Bishop, J. Comp. Mats., 7, (1973), p. 146.

41. G. R. Irwin, Seventh Sagamore Ordnance Materials Research Conference, Aug., (1960).

42. W. F. Brown and J. E. Srawley, ASTM Spec. Tech. Pub., No. 410, (1967).

43. R. R. Wilson, Rev. Sci. Instruments, 12, Feb.,(1941), p. 91.

44. Formulae for Stress and Strain, Raymond J. Raork.

45. J. H. Underwood, R. R. Lasselle, R. D. Scanlon and M. A. Hussain, Eng. Fract. Mechs., 4, (1972), p. 231.

46. M. F. Card, NASA Technical Note D-3110.

47. A. W. Holdsworth, M. J. Owen and S. Morris, J. Comp. Mats., 8, (1974), p. 117.

48. E. M. Wu, 'Composite Materials Workshop', Editor S. W. Tsai, Technomic Pub. Co., Stanford, U.S.A., 1968.

Appendix 1.

Derivation of the equation to give K_c from crack opening displacement measurements.

Consider an infinite cylindrical pressure vessel containing an axial slot of length, 2c. The slot can increase in length when the rate of change of energy with crack length, dE/dc is equal to the rate of release of elastic energy. i. e.

$$\frac{dE}{dc} = Gt \qquad \ldots\ldots(1)$$

where G is the rate of release of elastic stored energy per unit area of crack advance, and

t is the wall thickness of the vessel.

or,

$$\frac{dE}{dc} = \tfrac{1}{2}F^2 \, dC/dc \qquad \ldots\ldots(2)$$

where dC/dc is the rate of change of compliance with crack length, and F is the hoop force applied to the pipe of length, L.

i. e.

$$F = \sigma_H L t \qquad \ldots\ldots(3)$$

Defining compliance, C as u/F; where u is the displacement resulting from the applied force F,

$$C = u/F \qquad \ldots\ldots(4)$$

Combining (3) and (4) we obtain:

$$C = \frac{u}{\sigma_H L t} \qquad \ldots\ldots(5)$$

Let $C' = C L$ ......(6)

then

$$C' = \frac{u}{\sigma_H t} \qquad \ldots\ldots(7)$$

Combining (1), (2), (3) and (7) we obtain:

$$Gt = \tfrac{1}{2}(\sigma_H t)^2 L\, dC'/dc \qquad \ldots\ldots(8)$$

but,

$$G = \frac{K^2(1-\nu^2)}{E} \qquad \ldots\ldots(9)$$

where K is the stress intensity factor.

substituting (9) for G in (8) we obtain:

$$\frac{K^2(1-\nu^2)t}{E} = \tfrac{1}{2}(\sigma_H t)^2 L\, dC'/dc \qquad \ldots\ldots(10)$$

or,

$$K = \left(\frac{E(\sigma_H t)^2 L}{2t(1-\nu^2)}\ \frac{dC'}{dc}\right)^{\frac{1}{2}} \qquad \ldots\ldots(11)$$

$$\text{Let } C'' = C't \qquad \ldots\ldots(12)$$

$$\text{Then } \frac{dC''}{dc} = \frac{t\,dC'}{dc} \qquad \ldots\ldots(13)$$

substituting dC''/dc for tdC'/dc in (11) gives:

$$K = \left(\frac{E\sigma_H L}{2(1-\nu^2)}\ \frac{dC''}{dc}\right)^{\frac{1}{2}}$$

or,

$$K_c = \sigma_H^{*}\left(\frac{EL}{2(1-\nu^2)}\ \frac{dC''}{dc}\right)^{\frac{1}{2}}$$

where dC''/dc is the rate of change of compliance at crack length, c. The compliance C'' is the slope of the line obtained on the plot of σ_H versus crack opening displacement.